CONF-9405143
ORNL/FMP-94/1

PROCEEDINGS OF THE EIGHTH ANNUAL CONFERENCE ON FOSSIL ENERGY MATERIALS

May 10-12, 1994
Oak Ridge, Tennessee

Compiled by
N. C. Cole and R. R. Judkins

Date Published: August 1994

Prepared by the
Department of Energy
Fossil Energy Office of Advanced Research
and
Oak Ridge Operations Office
AA 15 10 10 0

Prepared by the
OAK RIDGE NATIONAL LABORATORY
Oak Ridge, Tennessee 37831-6285
managed by
MARTIN MARIETTA ENERGY SYSTEMS, INC.
for the
U.S. DEPARTMENT OF ENERGY
under Contract DE-AC05-84OR21400

PREFACE

The Eighth Annual Conference on Fossil Energy Materials was held in Oak Ridge, Tennessee, on May 10-12, 1994. The meeting was sponsored by the U.S. Department of Energy's (DOE) Office of Fossil Energy through the Advanced Research and Technology Development (AR&TD) Materials Program, and ASM International. The objective of the AR&TD Materials Program is to conduct research and development on materials for longer-term fossil energy applications as well as for generic needs of various fossil fuel technologies. The management of the program has been decentralized to the DOE Oak Ridge Operations Office with Oak Ridge National Laboratory (ORNL) as the technical support contractor. The research is performed by staff members at ORNL and by researchers at other national laboratories, universities, and in private industry. The work is divided into the following categories: (1) ceramics, (2) new alloys, (3) corrosion research, and (4) technology assessment and technology transfer.

This conference is held each year to review the work on all of the projects of the Program. The final program for the meeting is given in Appendix A, and a list of attendees is presented in Appendix B.

These proceedings have been published from camera-ready masters supplied by the authors. All of the contributions have been checked for errors but have not been subjected to peer reviews. However, most of the papers had already undergone technical review within the individual organizations before submission to the Program Office.

The successful completion of the conference and publication of the proceedings has required help from several people. The organizers wish to thank Judy Fair for her superb coordination work; Gloria Donaldson for her assistance with preparations for the conference; Judy and Gloria for their excellent work at the registration desk; the ORNL Conference Office for their help in the many arrangements; and the numerous staff and support personnel associated with the conference. ASM International cosponsored the conference, for which we are especially grateful. Finally, we express our sincere appreciation to the authors whose efforts are the very basis of the conference.

TABLE OF CONTENTS

SESSION I - CERAMICS

FABRICATION OF FIBER-REINFORCED COMPOSITES BY CHEMICAL VAPOR INFILTRATION

D. P. Stinton, O. J. Schwarz, and J. C. McLaughlin
Oak Ridge National Laboratory
Oak Ridge, Tennessee 37831

ABSTRACT

Fiber-reinforced SiC-matrix composites of thick-walled tubular geometry have been fabricated by forced chemical vapor infiltration (CVI). Densification of fibrous preforms required very long times (greater than 150 hours) using the initial equipment configuration. After numerous modifications to the processing equipment that altered the temperature gradient, infiltration times were reduced to less than 40 hours. This paper will discuss the modifications to the processing equipment that successfully reduced the densification times.

INTRODUCTION

In advanced indirectly fired combustion systems, such as those considered in the Combustion 2000 program and externally fired combined cycle (EFCC) concepts, ceramic heat exchangers are required to transfer heat from the hot combustion gases to the clean air that drives the gas turbines. For high efficiencies, the temperature of the turbine inlet needs to exceed 1100°C and preferably be about 1260°C. The heat exchangers will operate under pressure and experience thermal and mechanical stresses during heating and cooling, and some transients will be severe under upset conditions. SiC-matrix composites appear promising for such applications because of their high strength at elevated temperature, light weight, thermal shock resistance, damage tolerance, and oxidation and corrosion resistance.

Fiber-reinforced ceramic composites are generally anisotropic because of the directional dependence of the continuous fibers. Therefore, mechanical properties of typical flexure specimens or C-ring specimens are not representative of the properties of tubular composites because the continuous fibers are severed. If structural members for coal-fired power plants are to be successfully designed with composite materials, the directional properties must be measured so that structural analysis programs may be used to establish the correct stress states and, subsequently, the correct sizes and shapes of the structural components. Although quite complex, all the elastic material constants can be determined from a single tubular specimen by applying a variety of combinations of tension, compression, and shear stresses and taking multiple readings of strains. Fiber-reinforced composite tubes of several fiber architectures were fabricated by forced chemical vapor infiltration (CVI), characterized, and the results were reported at the

Seventh Annual Conference on Fossil Energy Materials. Unfortunately, long times ($\approx$150 hours) were required to thoroughly densify the tubes. The objective of the current investigation was to optimize the forced CVI process so that composite tubes could be fabricated in much shorter times.

EXPERIMENTAL PROCEDURE

Fibrous Preforms

Fibrous preforms were prepared by tightly wrapping strips of Nicalon cloth (20 cm wide by 220 cm long) onto 2.54 cm diameter graphite mandrels to form tubes with fiber contents of about 32 vol%. Higher fiber loading was certainly desired, however, it was not possible to wrap the cloth any tighter by hand. Cloth wrapping of the preforms was selected because the preforms were easy and inexpensive to fabricate and simulate components that require comparable strengths in both the hoop and axial directions. Filament wound preforms were undesirable because of their increased cost and very low axial strengths.[1] Three dimensionally braided preforms were also of less interest because of the high cost of braiding the preform. The Nicalon+ cloth utilized for the fabrication of these preforms is a SiC-based polymer-derived fiber that is microcrystalline/amorphous in nature and contains significant amounts of silica.[2,3]

CVI Processing

Forced chemical vapor infiltration (CVI) as developed at the Oak Ridge National Laboratory has been used to fabricate composites of thick-walled tubular geometry. Details of the forced-CVI process have been reported in numerous publications.[4-7] Briefly, fibrous preforms are constrained by special fixturing such that reactants are forced through the walls of the preform (Fig. 1). Gaseous reactants enter the furnace through tubing that runs within the water cooling passage of the stainless steel injector. Reactants flow from the tubing in the cooling passage into a graphite gas distributor and are dispersed along the length of the preform through parallel slots in the distributor. Reactants then proceed uniformly through holes in the graphite mandrel into the preform. A temperature gradient is established through the preform wall such that decomposition of the methyltrichlorosilane (CH_3SiCl_3 or MTS) and deposition of SiC occurs in the presence of hydrogen as the gases approach the higher temperature regions of the preform. As the density and thermal conductivity of the preform increases, deposition moves progressively toward the inner diameter of the tube. The duration of infiltration is therefore controlled by the temperature gradient throughout the preform.

+ Nippon Carbon, Co., Tokyo, Japan

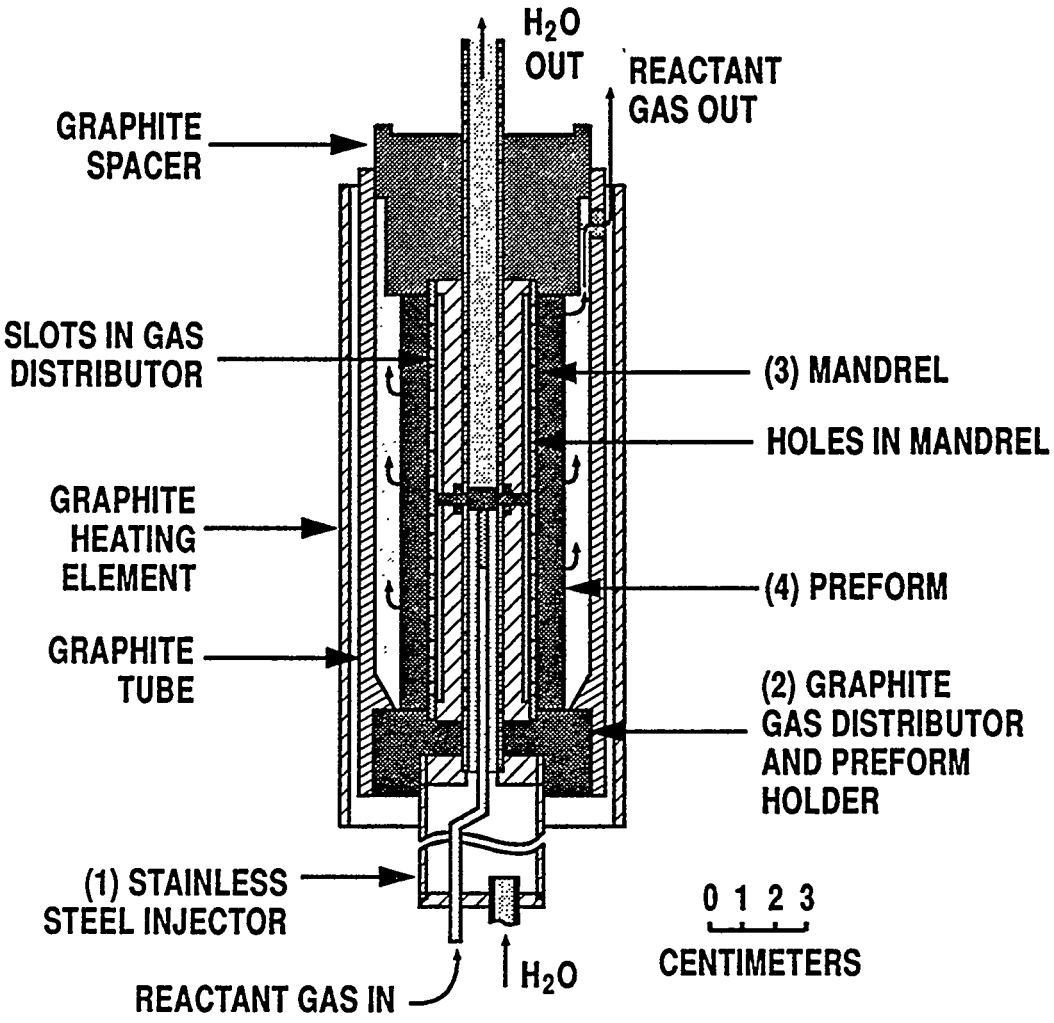

Fig. 1 Schematic of the equipment used to infiltrate tubular preforms.

RESULTS AND DISCUSSION

Densification of tubular preforms (2.5 cm ID by 0.6 cm wall thickness by ≈20 cm long) using the initial equipment required infiltration times of approximately 150 hours. Infiltration times were excessively long because of the steep temperature gradient through the preform (varied from ≈1200°C on the outside of the preform to about 500°C on the inside of the preform). A magnified view of the equipment with appropriate temperatures shown at right is shown in Fig. 2. Temperatures were determined using a special preform instrumented with a thermocouple on the inner diameter of the preform. Deposition of SiC occurred initially within the hot (outer diameter) region of the preform. However, because of the low inner temperature, the deposition zone moved very slowly toward the inner diameter. Composites were densified to 80 to 85% of theoretical, however, very long times were required.

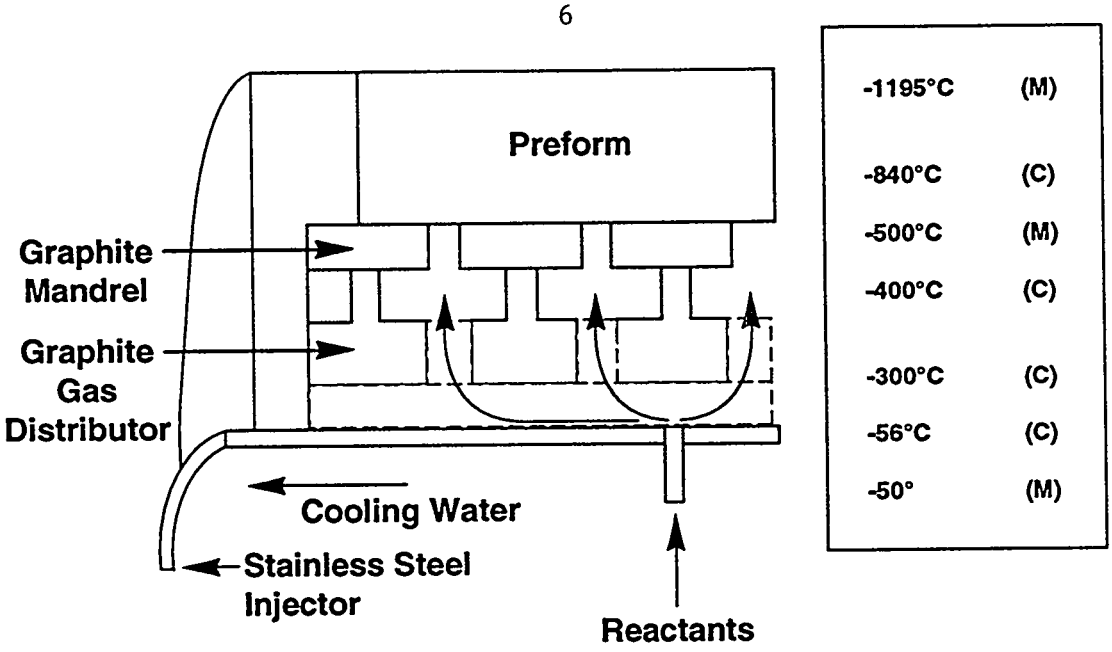

Fig. 2 Magnified view of the equipment used to infiltrate tubular preforms. The temperatures shown at right are either measured (M) or calculated (C).

An optimum temperature gradient has been established for the infiltration of flat plates in previous research. Preforms approximately 1.2 cm thick can be densified in about 24 hours if the hot surface is maintained at 1200°C and the cool surface starts at about 750°C and gradually increases to 950°C. One would anticipate that the inner temperature for a 0.6 cm thick tube should be greater than 750°C. Therefore, modifications were made to the tubular graphite gas distributor to increase the inner temperature. The modifications consisted of machining off the outer surface of the gas distributor and replacing it with insulating Nextel fabric as shown in Figure 3. Such modifications increased the inner temperature from 500 to 630°C. The infiltration times were significantly reduced ($\approx$80 hours) however, additional modifications were still necessary.

A second modification was made to the processing equipment by removing the graphite gas distributor and leaving only an air gap between the graphite mandrel and the stainless steel injector. Infiltration of tubes using this equipment was accelerated considerably. The temperature along the inner diameter of the fibrous preform was increased from 630 to 730°C. Infiltration times were reduced to approximately 40 hours using this apparatus. A further increase in the inner temperature was still required to further reduce the infiltration times. Unfortunately, there was no obvious way to increase the inner temperature with the existing equipment. Cold water entering the stainless steel injector was heated to nearly the boiling point before exiting the injector, therefore, the flow rate of the water coolant could not be reduced. It became clear that a new injector would need to be constructed.

A new stainless steel injector was designed and fabricated that utilized small diameter tubing and reduced the flow of water through the injector. The reduced diameter of the tubing made it impossible to flow the gaseous reactants through the center of the injector. Therefore, a new injector was redesigned and fabricated using concentric tubes. Cooling water flowed through the center tube while the gaseous reactants flowed

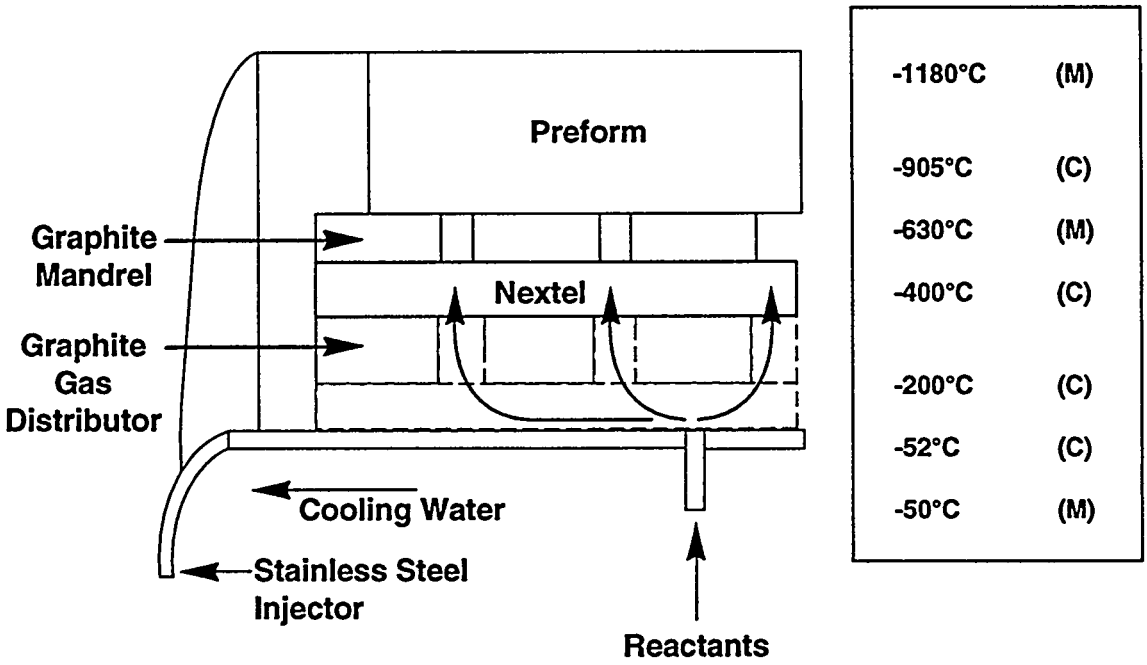

Fig. 3. Modified equipment used to infiltrate tubular preforms after nextel fabric has been introduced to better insulate the preform from the water cooling.

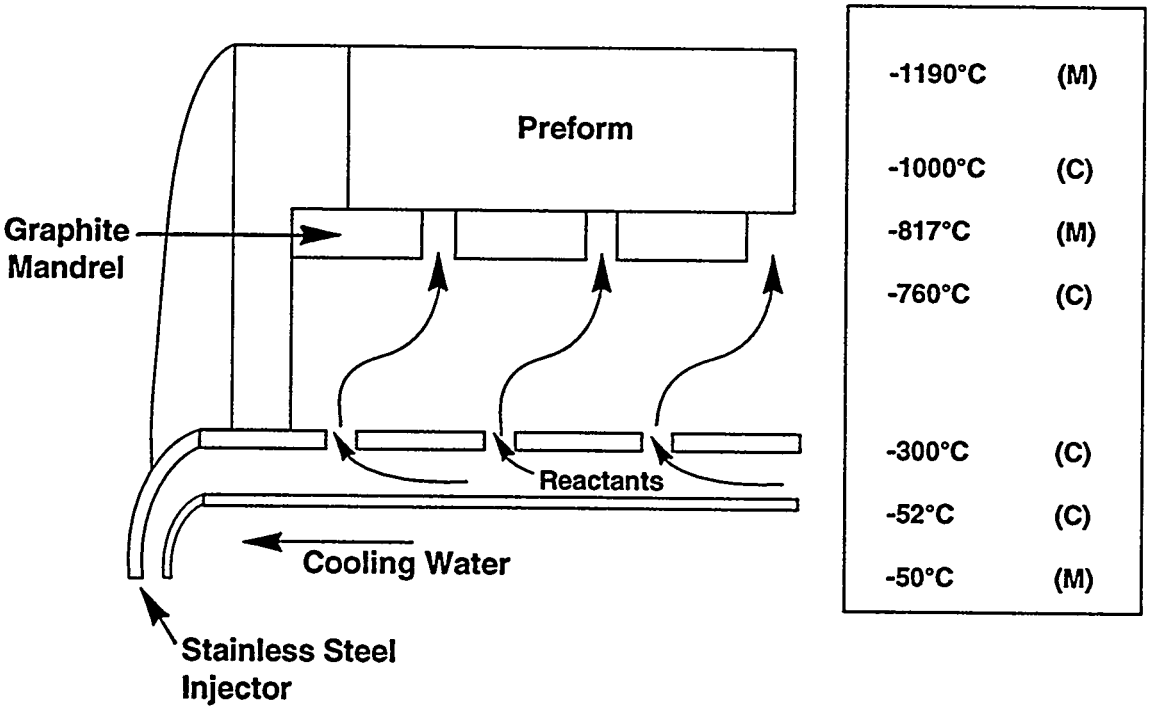

Fig. 4. New stainless steel injector designed to reduce the temperature gradient across the preform and reduce the infiltration times.

between the central tube and the outer tube. Holes were drilled in the outer tube at an appropriate location so that reactants could flow into the fibrous preforms. The new injector produced the temperature gradient illustrated in Fig. 4. The temperature decreased from 1200°C on the outer surface of the tubular preform to 817°C on the cooler inner diameter. Infiltration under these conditions would be expected to progress much more rapidly than the previous configuration with a cool-face temperature of 730°C. The temperature of the outer tube of the stainless injector was 300°C at the start of infiltration, an increase of 250°C over the old injector. Unfortunately, the increased temperature significantly accelerated the rate at which HCl, a byproduct of MTS decomposition, attacked the metallic injector. The injector was essentially destroyed during the initial run.

CONCLUSIONS

Fiber-reinforced SiC-matrix composites are being developed for use in advanced indirectly-fired combustion systems because of the material's oxidation resistance, damage tolerance, and thermal shock resistance. Fiber-reinforced composite tubes that simulate heat exchanger tubes were fabricated by forced CVI but required very long times to densify. Infiltration times for tubes (0.6 cm wall thickness) were reduced from over 150 hours to less than 40 hours by modifying the temperature gradient created by the water-cooled injector and various graphite components. Processing composites using the initial equipment configuration produced a cool-face temperature of about 500°C. Removal of the graphite gas distributor increased the cool-face temperature to about 730°C.

Further modifications to the temperature gradient were made by fabricating a new stainless steel injector. The injector successfully increased the inner temperature to 830°C but also significantly increased the temperature of the metallic injector. The increased temperature (300°C) of the injector accelerated corrosion of the stainless steel by HCl byproducts from the MTS decomposition. Further modifications to the system and temperature gradient will be required to reduce the processing times significantly below 40 hours.

REFERENCES

1. D. P. Stinton, B. E. Foster J. C. McLaughlin, K. Reifsnider and W. Stinchcomb, "Fabrication of Fiber-Reinforced Composites by Chemical Vapor Infiltration, "Proceedings of the Seventh Annual Conference on Fossil Energy Materials, Oak Ridge National Laboratory Report CONF-9305135, ORNL/FMP-92/1, pp 3-11, (1993).

2. S. Yajima, et al., "Synthesis of Continuous SiC Fibers with High Tensile Strength," J. Am. Ceram. Soc., **59**[7-8], 324-27 (1976).

3. S. Yajima, et al., "Anomalous Characterization of the Microcrystalline State of SiC Fibers," Nature, **27**[21], 706-7 (1979).

4. D. P. Stinton, R. A. Lowden, and T. M. Besmann, "Fabrication of Fiber-Reinforced Composites by Chemical Vapor Infiltration, "Proceedings of the Sixth Annual Conference on Fossil Energy Materials, Oak Ridge National Laboratory Report ORNL/FMP-92/1, pp 3-10, (1992).

5. D. P. Stinton, A. J. Caputo, and R. A. Lowden, "Synthesis of Fiber-Reinforced SiC Composites by Chemical Vapor Infiltration," Am. Ceram. Soc. Bull., **65**[2], 347-50 (1986).

6. D. P. Stinton, T. M. Besmann, and R. A. Lowden, "Advanced Ceramics by Chemical Vapor Deposition Techniques," Am. Ceram. Soc. Bull. **67**[2], 350-55 (1988).

7. T. M. Besmann, B. W. Sheldon, R. A. Lowden, and D. P. Stinton, "Vapor-Phase Fabrication and Properties of Continuous-Filament Ceramic Composites," Science, Vol. 253, 1104-9 (1991).

Transport Properties of Ceramic Composites

T.L. Starr

Georgia Tech Research Institute
Georgia Institute of Technology
Atlanta, Georgia 30332

We describe our recently initiated experimental investigation of the transport properties of chemical vapor infiltration (CVI) preforms and densified composites, with particular emphasis on gas permeability and mass diffusivity. The results of this work will be useful both for on-going CVI process development and for evaluation and optimization of composite materials for fossil energy applications.

Permeability values derive from measurements of pressure drop across the composite specimen at a controlled gas flow rate. Previous measurements were limited to composites with a simple cloth-layup architecture. These provided data for CVI model validation and revealed the importance of the large-scale pore structure to gas flow. Ongoing measurements include additional fiber architectures, e.g. 3-D woven and filament wound composites.

Mass diffusivity values derive from measurements of gas composition changes with zero pressure drop (no flow) across the specimen. A gas chromatography-type thermal conductivity detector is used.

Existing thermal conductivity data are reviewed to compare with gas transport results and to identify additional measurement needs.

INTRODUCTION

Transport properties are critical factors in the processing and performance of ceramic matrix composites (CMCs). These properties include gas permeability, mass diffusivity (effective diffusion coefficient) and thermal conductivity, and depend on the density and microstructure of the composite.

Of the various CMC processing methods, CVI is strongly controlled by the transport properties of the preform and partially densified composite. For forced flow CVI, the gas permeability is the critical factor that determines the ultimate density that can be achieved. Mass diffusivity is a controlling property for isothermal CVI where it limits

the densification rate and density uniformity. For thermal gradient CVI the thermal conductivity of the composite controls the steepness of the thermal gradient and how this gradient changes with processing time.

Many applications of CVI composites - fossil energy applications, in particular - depend on their transport properties. Heat exchanger tubes should have high thermal conductivity, and low gas permeability and mass diffusivity. Hot gas filters need high permeability. Hot gas separation processes need uniform mass diffusivity and low permeability.

While much experimental work has focused on measurement of mechanical properties of CMCs, very few experimental measurements of these transport properties exist. Further, understanding of how to modify these properties through preform fiber architecture is limited. Again, experimental measurements are key to development of this understanding.

We have recently initiated experimental investigation of the transport properties of CVI preforms and densified composites, with particular emphasis on gas permeability and mass diffusivity. The results of this work will be useful both for on-going CVI process development and for evaluation and optimization of composite materials for fossil energy applications.

GAS PERMEABILITY

A couple years ago we measured gas permeability of CVI infiltrated composites with a cloth layup architecture[1]. These measurements were made on small (2.5 mm) cube-shaped specimens. Permeability measurements were made with flow parallel and perpendicular to the cloth direction. These results, shown in Figure 1, illustrate several features of composite properties and their measurement. First, there is a great deal of scatter in the measured permeabilities of individual specimens with comparable density. This is due to the small size of the specimens relative to the weave repeat distance of 1.5 mm, and the statistical nature of the spacings between individual tows and between cloth layers.

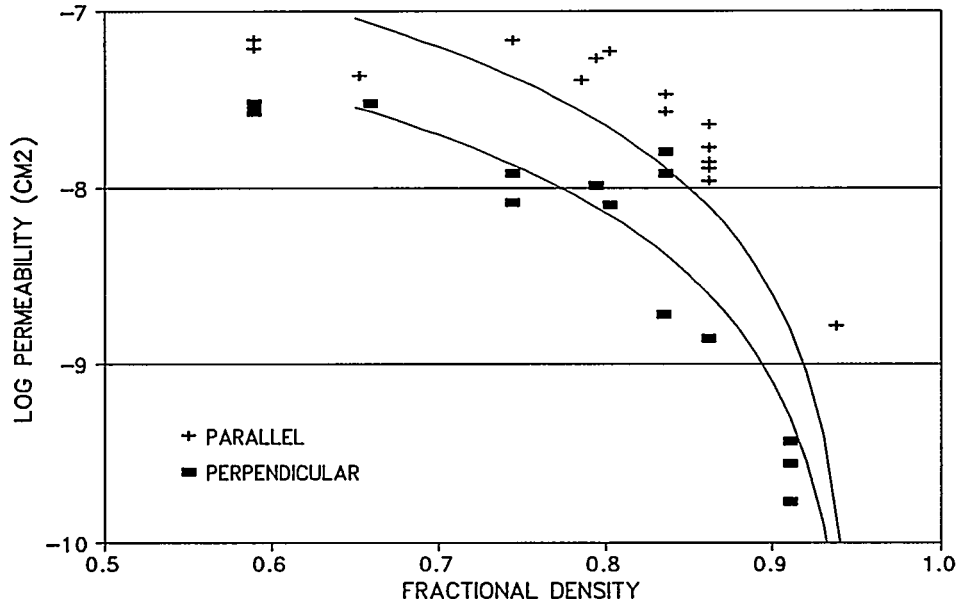

Figure 1. Gas permeability of cloth layup CVI composite. Curve is fit to percolating network model.

For a composite of particular fiber architecture and density, the local value of the transport properties can vary considerably from the average value. Accurate experimental measurement of an average transport property value will require either a larger specimen or measurements on multiple small specimens.

A second feature illustrated in the data is the anisotropy of the transport properties. In this case, permeability is higher for flow parallel to the cloth layers. A similar anisotropy is reported for thermal conductivity[2] of these materials. Experimental measurement of transport properties need to be made and reported for specific orientations relative to the fiber architecture.

Finally, the data above suggests that permeability may exhibit critical behavior. It decreases relatively slowly with increasing density until reaching a critical density where the decrease in permeability is very steep as it approaches zero. For small specimens,

again, the value of this critical density is expected to show considerable variability. For larger structures the average value of this critical density is a measure of the ultimate achievable density for a CVI fabricated composite.

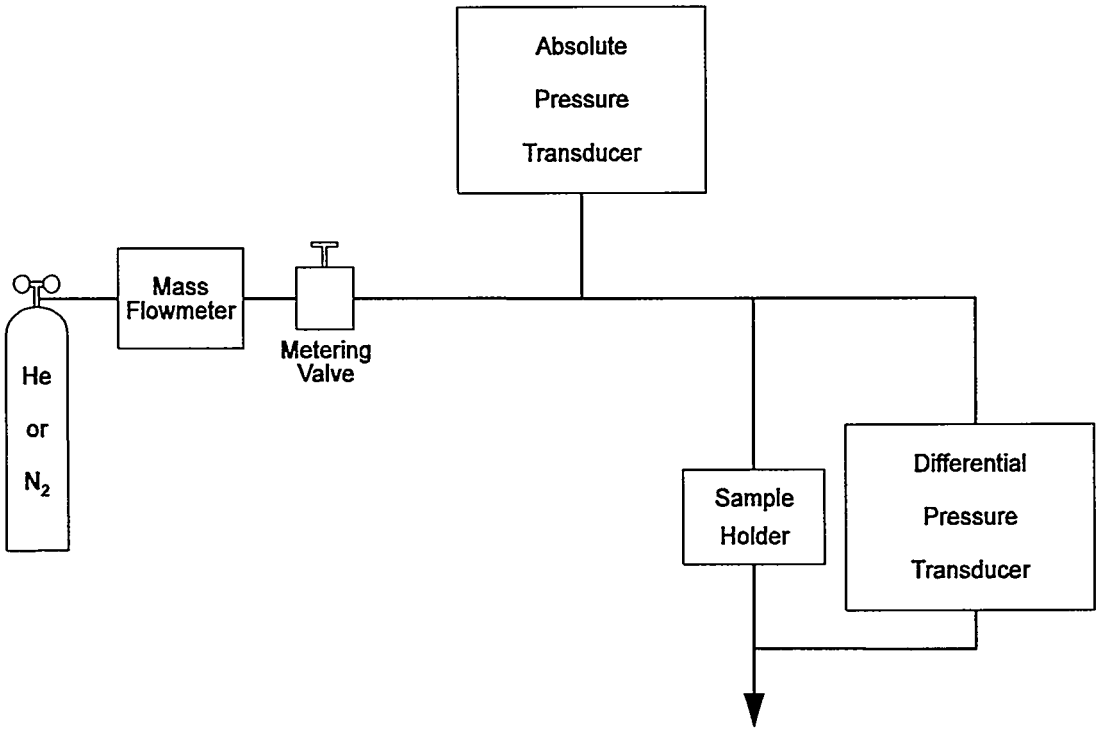

Figure 2. System for measuring gas permeability provides for determining both gas flow rate and pressure difference across a specimen.

Our experimental apparatus for measuring gas permeability is shown schematically in Figure 2. The measurement consists simply of determining both gas flow rate and pressure difference across a specimen. The critical factor in these measurements is extraction and mounting of the test specimen. It must be large enough to encompass a number of unit cells of the composite architecture, but small enough to have uniform density throughout. The specimen mounting method should maintain flow in a well defined direction while minimizing any by-passing.

We are utilizing specimens in the form of right circular cylinders approximately 10 mm in diameter and 5-10 mm in length. We are in the

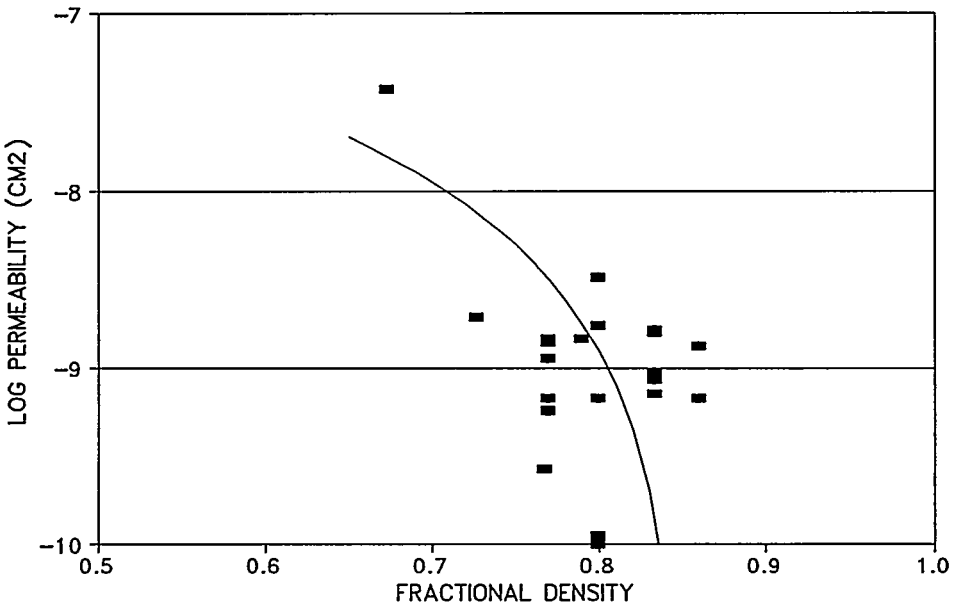

Figure 3. Gas permeability of 3-D weave CVI densified composite.

process of obtaining and machining specimens from CVI densified composites with various fiber architectures including cloth layup, 3-D weave, 3-D braid, spiral weave, and filament wound. Recent results for cloth layup and 3-D weave specimens are shown in Figure 1 and Figure 3.

Given the variability inevitable with these small specimen measurements it is useful to fit the experimental results to a suitable model and use the model parameters to extrapolate to larger specimens and different densities. The pore structure through these composites with woven reinforcement can be considered a network of conducting elements linking two opposing sides of the specimen. As these individual elements close during infiltration the number of parallel conducting paths decreases until, at the "critical" density, the last continuous conducting path is severed. Studies of such "percolating" networks indicates that the conductance decreases as the square of the difference between the density and the critical density[3]. Fits to this model are shown as the curves in Figure 1 and Figure 3. Note that the

critical density for the 3-D weave appears to be significantly lower than that for the cloth layup architecture. The anisotropy of the cloth layup composite derives from the different spacings of the tows in the cloth plane and between cloth layers.

MASS DIFFUSIVITY

The mass diffusivity of a porous material, also known as the effective diffusion coefficient, is related both to the properties of the material and to the nature of the diffusing species. At high pressures (roughly 100 torr and higher) and large pore sizes (roughly 50 μm and larger), the mass diffusivity (D_{eff}) of a porous material is related to the ordinary (Fickian) diffusion coefficient (D_f) for the species,

$$D_{eff} = D_f \frac{(1-f)}{\tau}$$

where f is the volume fraction solid material and τ is a measure of the tortuosity of the pore path through the material. For low pressure and small pores, Knudsen diffusion becomes important and the size of the pores also influences the molecular transport.

While there has been progress in computer modeling of diffusion through CVI preforms and composites[4], we are not aware of any experimental measurements of this property.

We plan to use the system shown in Figure 4 to measure mass diffusivity of preforms and composites. Gas flows are directed across opposing faces of a specimen. One flow is a pure "carrier" gas, e.g. helium, and the other contains a percent of the diffusing species, e.g. 10% methane in helium. With no pressure differential across the specimen the composition of the "carrier" gas stream leaving the specimen holder is a measure of diffusion. This composition will be measured using a gas chromatography-type thermal conductivity detector.

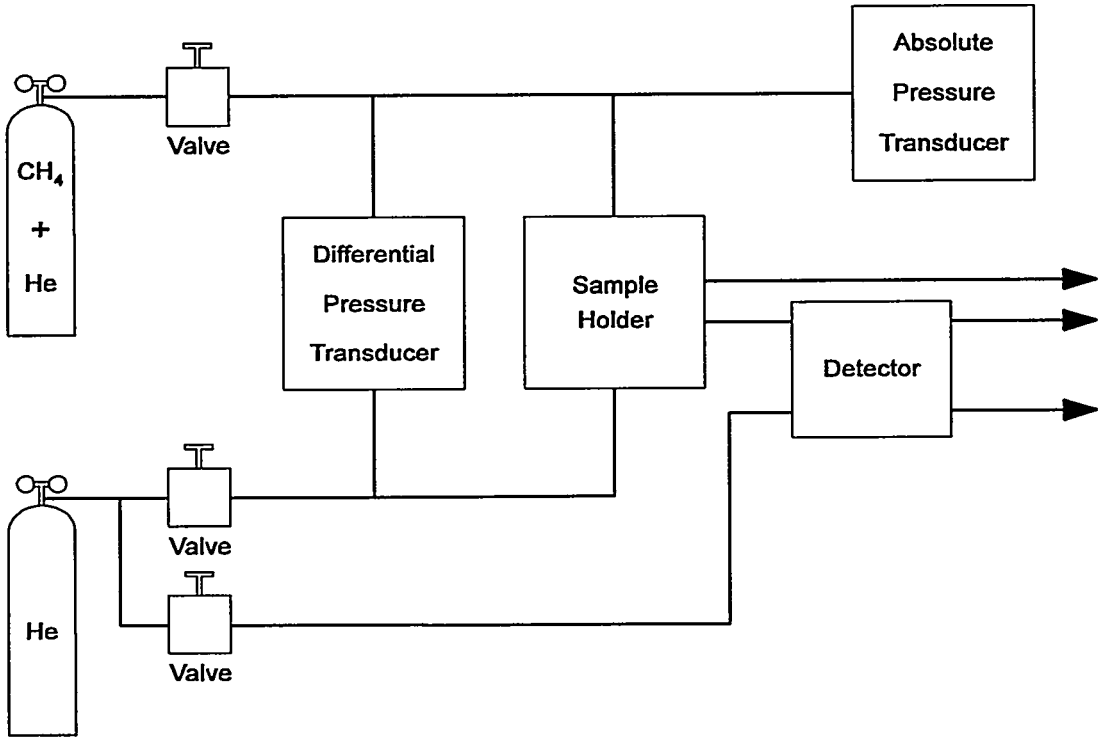

Figure 4. System for measuring mass diffusivity of porous preforms and composites uses a steady flow approach.

Specimen size and orientation effects discussed in the previous section apply to these measurements as well. We will use the same specimens fabricated for gas permeability measurements.

THERMAL CONDUCTIVITY

Like the gas permeability and mass diffusivity, the thermal conductivity of CVI composites depend on the density, microstructure and orientation relative to the fiber architecture. Existing thermal conductivity data are limited, and in most cases, include only "fully" dense materials. Future efforts will include review of existing data and identification of further measurement needs.

SUMMARY

This experimental investigation of the transport properties of CVI preforms and densified composites aims to produce consistent data useful both for on-going CVI process development and for evaluation and optimization of composite materials for fossil energy applications. The ultimate goal is to understand the microstructure-transport property relationship well enough to design fiber architectures for optimum processing behavior.

REFERENCES

1. G.B. Freeman, T.L. Starr and T.C. Elston, "Transport Properties of CVI Preforms and Composites," Mat. Res. Soc. Symp. Proc. 168, 49-54 (1990).

2. H. Tawil, L.D. Bentsen, S. Baskaran and D.P.H. Hasselman, "Thermal diffusivity of chemically vapour deposited silicon carbide reinforced with silicon carbide or carbon fibers," J. Mat. Sci. 20, 3201-3212 (1985).

3. D. Stauffer and A. Aharony, Introduction to Percolation Theory, 2nd. Edition, Taylor & Francis, Washingtion, DC (1992).

4. M.M. Tomadakis and S.V. Sotirchos, "Transport properties of random arrays of freely overlapping cylinders with various orientation distributions," J. Chem. Phys. 98(1) 616-626 (1993).

INVESTIGATION OF PROPERTIES AND PERFORMANCE OF CERAMIC COMPOSITE COMPONENTS

K. L. Reifsnider, W. W. Stinchcomb, L. Olesksuk, S. S. Lee

Materials Response Group
Engineering Science and Mechanics Department
Virginia Polytechnic Institute and State University
Blacksburg, VA 24061-0219 USA

ABSTRACT

The present paper summarizes some recent results of an effort to address the need for reliable and durable structural ceramic composites for high temperature fossil energy environments. The general objectives of the program are to develop and validate a test system and methodology for the mechanical characterization of ceramic composite tubes under multiaxial cyclic and quasi-static thermo-mechanical loading, to use that test system and methodology to test, evaluate, and characterize the properties and performance of ceramic composite tubes in coordination with Oak Ridge National Laboratory (a developer of such tubes), and to develop predictive models for damage tolerance and reliability of ceramic composite components. The present paper reports just two elements of that effort, which bear on the long-term performance of ceramic composites at elevated temperature in ambient air.

TUBULAR SPECIMENS

Tubular specimens with a 2.5 cm. ID, 0.6 cm. wall thickness, and a 20 cm. length were fabricated by a forced vapor infiltration method at Oak Ridge National Laboratory.[1-3] Nicalon fiber was utilized for the fabrication of all preforms.[1-3] Filament winding was used to simulate components such as combustors or headers that require high hoop or radial strengths but relatively modest axial strengths. Three dimensional braiding was used to simulate applications such as burner tubes or heat exchangers that require high axial strengths but only modest hoop strengths. Cloth wrapping was utilized to simulate components that require comparable strengths in both the hoop and axial directions.

Preforms were filament wound onto graphite mandrels at the U.S. Department of Energy K-25 Plant at the Oak Ridge National Laboratory. Fibers were wound 10° off the hoop direction to insure adequate axial strength (OR1, Fig. 1). Adjacent fiber tows were placed in contact with each other to prevent the formation of large pores during the winding of subsequent layers. This winding procedure produced a preform with a fiber loading of ~ 40

vol% and fine porosity distributed throughout the preform. Quadrax Corporation prepared 3D braided preforms on graphite mandrels for this study (OR3, Fig. 1). Because thorough infiltration of braided preforms with low fiber contents (15 - 30 vol%) had proven to be very difficult, special procedures were developed to braid tubular preforms that contained ≈38 vol% Nicalon fibers. Cloth-wrapped preforms were prepared at the Oak Ridge National Laboratory with fiber contents of ≈32 vol% (OR2, Fig. 1).

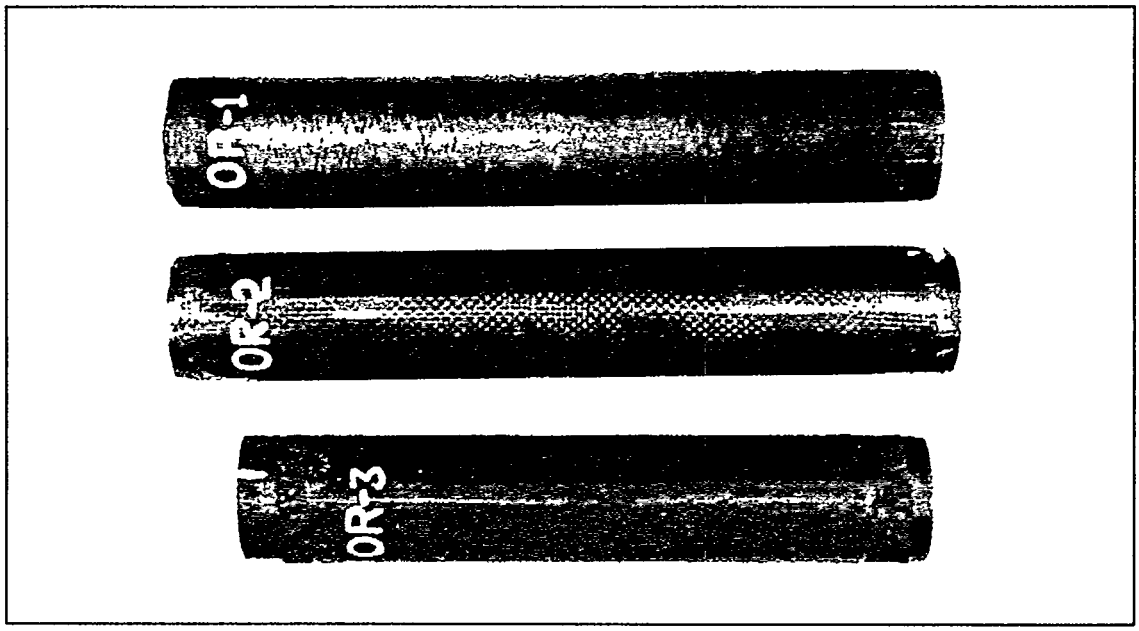

Figure 1 Photograph of braided (OR3), cloth-wrapped (OR2), and filament wound (OR1) Nicalon/SiC tubes tested in the investigation.

FLAT PLATE SPECIMENS

The fiber/matrix interfacial region and its effect on mechanical response were further investigated by conducting tests on a Nicalon/CAS system. The material system used in this investigation, Nicalon/CAS-II, was fabricated (and supplied) by Corning Glass Inc. using a hot-pressing technique. Three different laminates $[0]_8$, $[0/90]_{2s}$, and $[0/90]_{4s}$, manufactured by Corning Glass Inc. were used in this investigation. The $[0]_8$ and $[0/90]_{2s}$ laminates were purchased, and provided by Rolls-Royce Inc. The third type of laminate $[0/90]_{4s}$ was purchased and provided by the Materials Response Group. $[0]_8$ and $[0/90]_{2s}$ specimens were used primarily for flexure and monotonic tension tests to observe some of the basic damage

modes under flexure loading and to characterize heat treatment effects on the tensile strength. $[0/90]_{4s}$ specimens were used primarily for damage characterization of as-received and heat treated specimens under monotonic and cyclic tension loading.

RESULTS

Tubular Specimens

Tensile stress-strain data for tubes subjected to axial loading to approximately 20 MPa have been recorded using a high temperature extensometer to measure axial strains. The specimens were also subjected to torsional loading, and data were taken with strain gages affixed to the specimens. These tests were successful, with no difficulties in specimen slippage or multiaxial load application. The reproducibility of the test data was excellent. The strain gage data were also compared to extensometer readings for axial loading, as a consistency check. The results compared to within about 10 percent, in general. Since the specimens were cloth-wrapped and braided, this is a reasonable comparison. The shear stiffness of the braided tube (127 GPa) was about 30 percent greater than that of the cloth wrapped tube (94 GPa).

Figure 2 shows axial stiffness variations with temperature for the three tubes tested in tension at temperatures up to 800°C. It can be seen that stiffness drops of 15 and 36 percent were observed for specimens OR1 and OR2, respectively. The reason for the magnitude of these variations of stiffness with temperature is not completely determined at this writing. Stiffness changes in Nicalon fibers at temperatures up to 800°C are generally quite small, although significant variations (of the order of magnitude we observed) at temperatures of the order of 1000°C have been reported.[4] Drops in stiffness of the fibers have been shown to be sensitive to the time of exposure and reactive nature of the surrounding atmosphere.[4] Strength reductions for SiC-based fibers at 800°C have also been reported.[5] These reported reductions of the order of 15 percent were smaller than those which we have measured on the filament wound specimens, however. Our strength reduction data are incomplete, however, and more discussion of that topic will be deferred.

Figure 3 shows the results of a repeated test on the cloth wrapped tube, in which the temperature was increased only to 600°C. Notice that the room temperature measurements

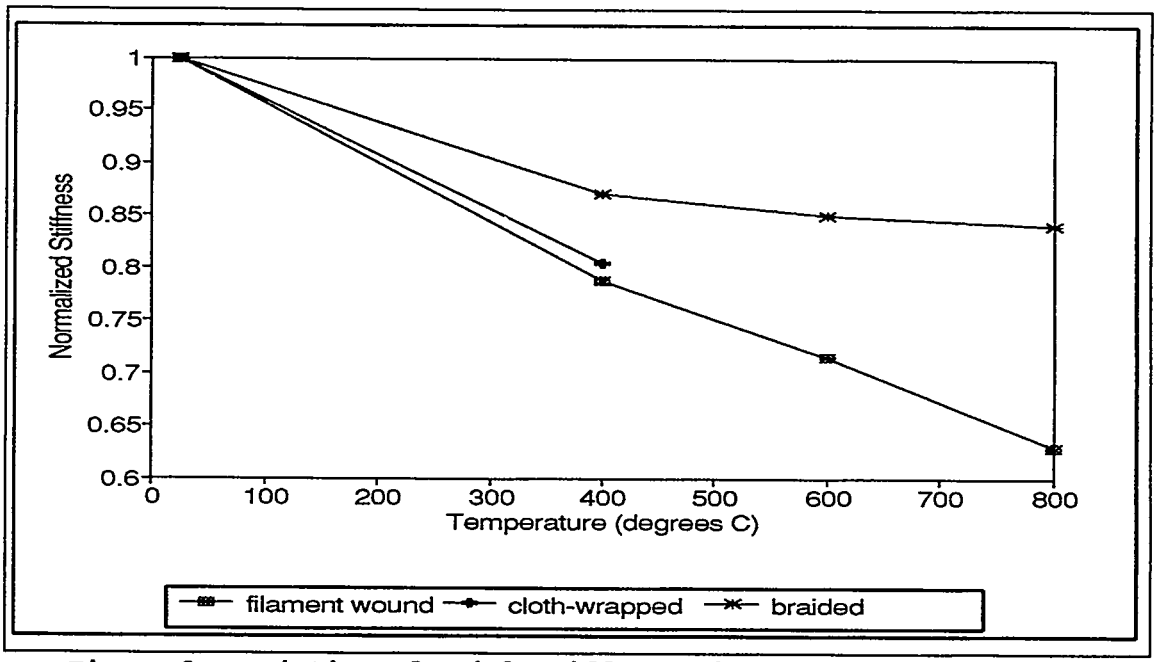

Figure 2 Variation of axial stiffness with temperature for three tubular architectures.

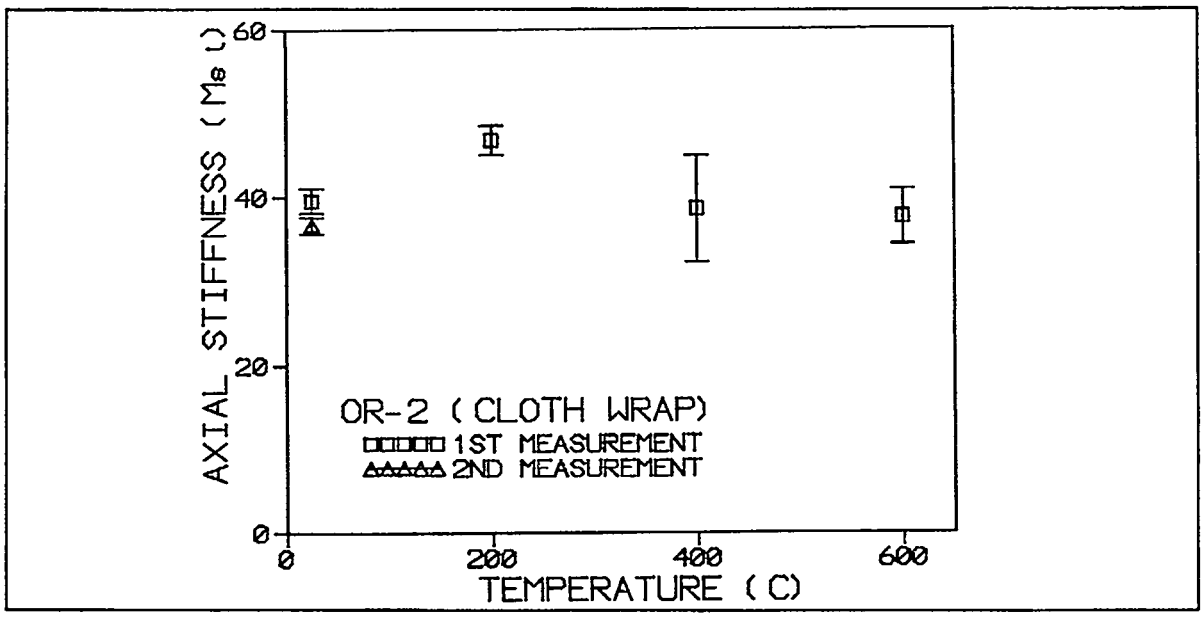

Figure 3 Repeated test of cloth-wrapped specimen up to 600°C.

were repeated after the specimen cooled, showing that the variations in stiffness are not permanent. These stiffness changes are smaller than those obtained during the first test of that tube, shown in Fig. 2. We believe that some of the variation first observed was caused by hot air currents biasing the capacitance extensometer readings. We made a special effort to protect the extensometer from such disturbances during the second test.

It is doubtful that reductions in fiber stiffness totally account for the reductions in composite stiffness observed in our tests. In fact, the literature suggests that when 3-D fiber architectures are used, composite stiffness (and strength) reduction at temperatures up to about 1200°C are of the order of only about 15 percent.[6] It is more likely that the matrix material, and, especially, the carbon interface between the matrix and the fiber is degrading and contributing significantly to stiffness (and, in some cases, strength) loss. In an effort to further identify the nature of some of those effects, sections were made by the/Oak Ridge National Laboratory and subjected to scanning electron microscopy at Virginia Tech.

FLAT PLATE SPECIMENS

An overall longitudinal stiffness reduction curve for an as-received specimen tested at the 65% S_{ult} cycle load level is shown in Fig. 4. This curve displays a rapid reduction of 40% of its original longitudinal stiffness in the first 100 cycles. From 100 cycles to 1000 cycles the reduction rate of longitudinal stiffness decreased and the curve started to level off after 1K cycles. Another decrease of longitudinal stiffness was observed before final failure.

The measured average reduction of longitudinal stiffness during the first 1K cycles in a 65% S_{ult} loaded specimen was as much as 46% of its original longitudinal stiffness. It is acknowledged that fiber debonding would reduce the capability for load transfer between the fiber and matrix. By conducting a discount analysis, we determined that this stiffness change was due to matrix cracking in both the longitudinal and transverse directions.

An important damage feature was noticed on the surface of pulled-out fibers in fatigue-tested specimens. It is shown in Fig. 5 that the fiber surface was severely damaged during the fatigue test due to wear. This type of damage was not observed in the static tensile loaded specimens. Thus, this appears to be a characteristic damage mode in ceramic matrix composites due to cyclic loading under these conditions. It is believed that this wear effect

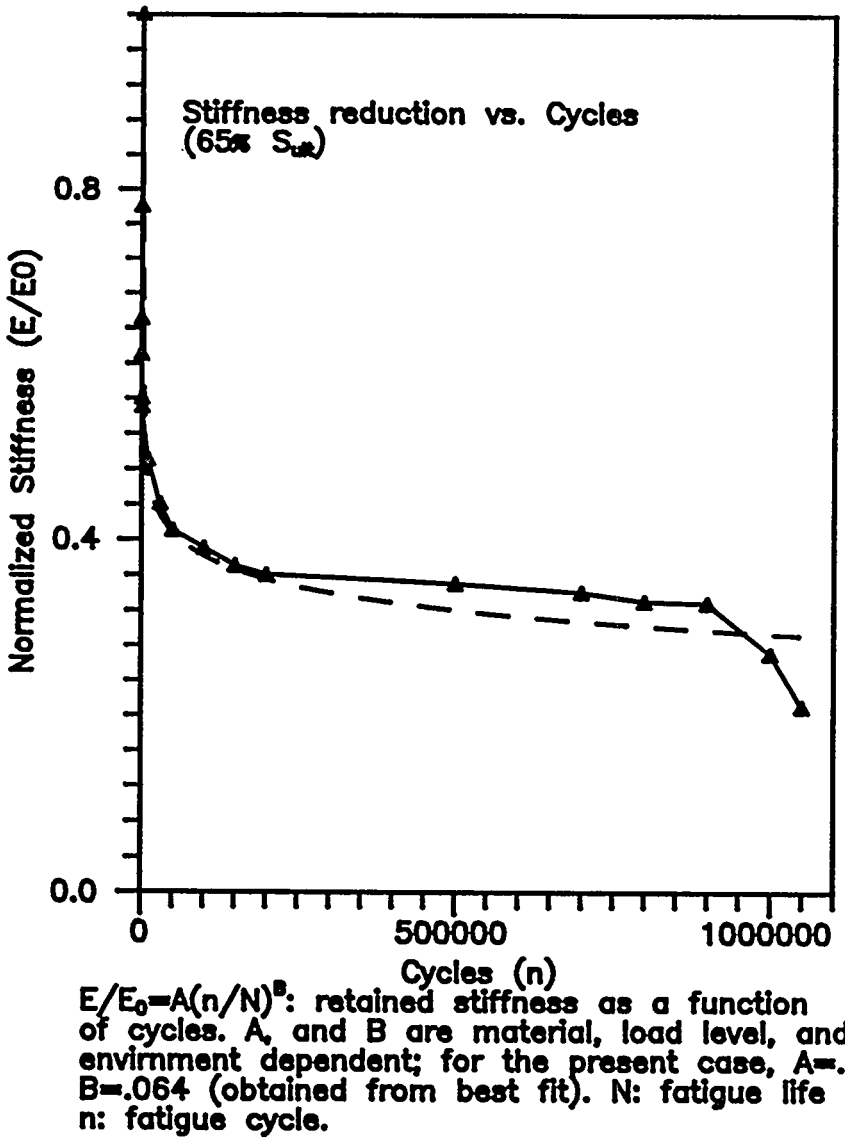

Figure 4 Stiffness reduction versus fatigue cycles for a fatigue tested (65% S_{ult}) as-received specimen.

may be due to the low interfacial bonding strength which allows rubbing between debonded fibers and the matrix under cyclic loading. Figure 5 suggests that such surface damage caused by wearing action was directly related to fiber fracture, i.e., it appears that the fiber surface damage may facilitate fiber fracture. This is believed to be the first report of this phenomenon.[7,8]

The damage shown in Fig. 5 suggests that the carbon coating on the Nicalon fibers has fragmented during the cyclic loading at room temperature. This fragmentation process may create local stress concentrations associated with the local complexity of the geometry

introduced by the fragmentation process, and it may also create small "pits" or "scars" in the fiber during that process. Moreover, the progressive nature of this damage mode may dissipate energy and drive some of the specimen heating observed.

However, this damage mode is greatly influenced by exposure of the material to elevated temperature. Some of our specimens were subjected to 100 hours of exposure to 900, 1000, or 1100° C air. For the last two cases, this exposure was found to reduce or eliminate the carbon fiber coating, and deposit a silicon oxide region in the fiber-matrix interlayer region. This oxide interferes with the fiber-matrix "decoupling" achieved by the carbon coating. In those cases, the fiber damage shown in Fig. 5 was not observed, and corresponding reductions in static strength and life of the materials accompanied that situation. Hence, it appears that the fiber-matrix interlayer fragmentation damage mode, thought to be identified here for the first time, is greatly affected by exposure to elevated temperature, and may become inactive if a "rigid" interlayer such as an oxide forms in that region.

PERFORMANCE SIMULATION - THE MRLIFE CODE

Over the last 12 years, the Materials Response Group has developed a performance simulation code that combines models of ply-level behavior to predict remaining strength and life of composite laminates. The objective of the simulation code is to deal with the evolution of properties and performance, i.e., to bring our models of processes and behavior to a collective consequence, usually to predict durability, damage tolerance, safety of composite components. Figure 6 describes the scope of this objective.

References 9-13 describe that approach. More will be said of the results in subsequent publications.

SUMMARY

Several effects of exposure to high temperature air have been identified. Stiffness reductions observed suggest that degradation of the carbon interlayer between the fiber and the matrix plays a major role in several of these effects. For example, the oxidation of the carbon layer and the formation of silicon oxides in that region can reduce strength and life of ceramic composite material systems. Such oxide formation can also alter damage modes. At room

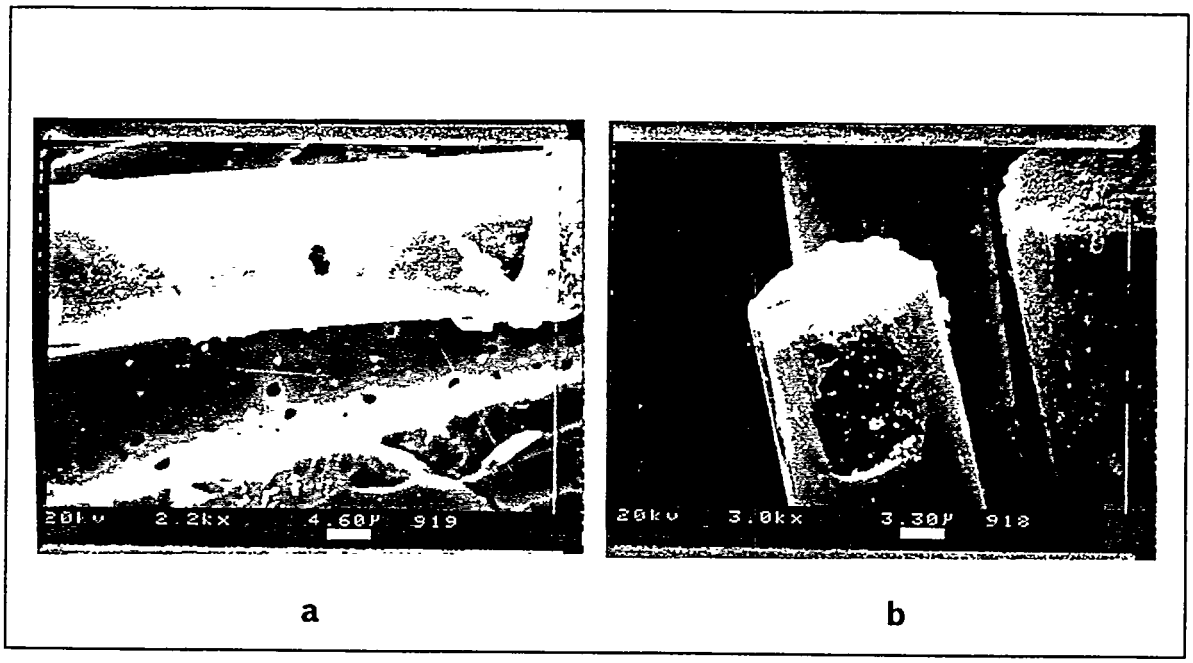

Figure 5 Fiber surface damage (a) caused by fatigue cycling, and relation to a fiber fracture site (b).

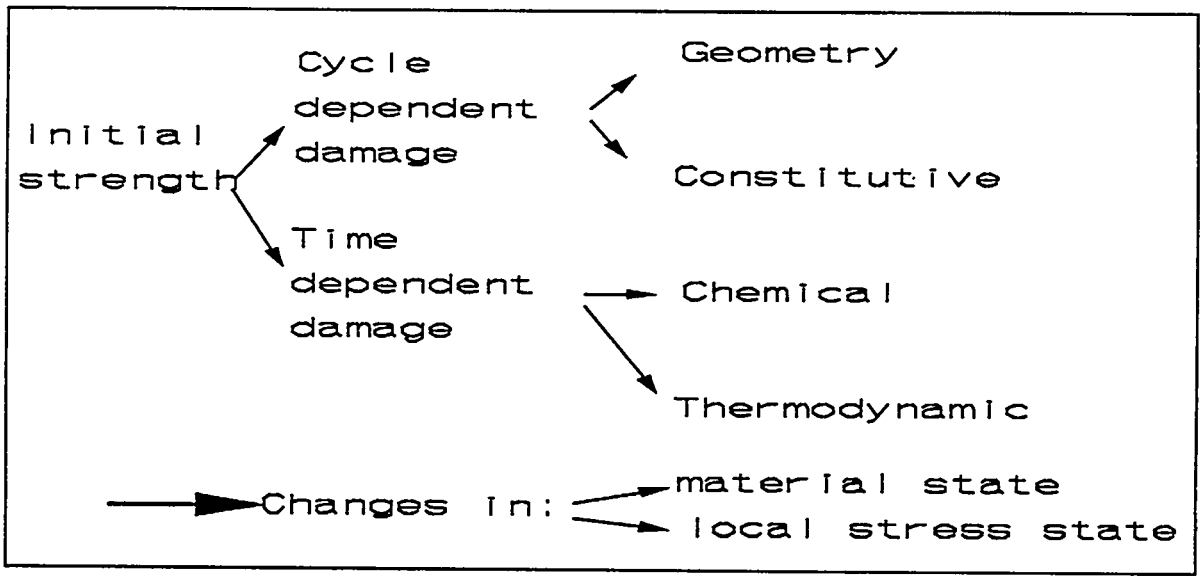

Figure 6 Damage processes in composite material systems.

temperature, we have identified fiber surface damage due to fragmentation of the carbon layer and subsequent rubbing of the fibers and matrix over those fragments, the first known identification of this damage mode. Following soaking at elevated temperatures in air, this damage mode seems to disappear.

An approach to the representation of these, and other cyclic and time dependent effects (and their interaction) has been developed, using a simulation method. The MRLife simulation code series, developed by the authors, forms the basis for the integration of fundamental, mechanistic models of damage development, creep, and creep rupture effects. Preliminary results suggest that this approach will make it possible to predict the remaining strength and life, and, therefore, the damage tolerance of tubular ceramic composite components using this approach. This development addresses perhaps the most pressing need in this field, to deal with methods of establishing and systematically describing the reliability of ceramic composite components, so that such components can be successfully designed and certified.

REFERENCES

1. Stinton, D.P., Besmann, T.M., and Lowden, R.A., "Advanced Ceramics by Chemical Vapor Deposition Techniques," Am. Ceram. Soc. Bull., 67(2), 350-55.

2. Besmann, T.M., Sheldon, B.W., Lowden, R.A., and Stinton, D.P., "Vapor-Phase Fabrication and Properties of Continuous-Filament Ceramic Composites," Science, Vol. 253, 1104-1109 (1991).

3. Caputo, A.J., Lowden, R.A., and Moeller, H.H., Fiber-Reinforced Ceramic Tubular Composites, ORNL Report No. ORNL/TM-10466, Nov. 1988.

4. Rigdon, M.A. & Hong, W.S., "Comparison of High-Temperature Tension Testing Results of Ceramic Fibers," Thermal and Mechanical Behavior of Metal Matrix and Ceramic Matrix Composites, ASTM STP 1080, J.M. Kennedy, H.H. Moeller, and W.S. Johnson, Eds., ASTM, 1990, pp.116-123.

5. Brindley, P.K., Proceedings, Materials Research Society Symposia, Vol. 81, 1987, pp. 419-424.

6. Chulya, A., and Gyekenyesi, "Failure Mechanisms of 3-D Woven SiC/SiC Composites under Tensile and Flexural Loading at Room and Elevated Temperatures," Ceramic Engineering and Science Proc., V. 13, no. 7-8, 1992, pp.420-432.

7. Lee S. S.,"Damage Analysis and Mechanical Response of As-Received and Heat-Treated Nicalon/CAS II Glass Ceramic Matrix Composites," Ph.D. Dissertation, Virginia Polytechnic Institute and State University, May, 1993.

8. Stinchcomb, W.W., Reifsnider, K.L. and Dunyak, T.J., "Investigation of Properties and Performance of Ceramic Composite Components," ORNL/Sub/87-SA946/02, June 1992.

9. Reifsnider, K.L. and Stinchcomb, W.W., "A Critical Element Model of the Residual Strength and Life of Fatigue-loaded Composite Coupons, in Composite Materials:Fatigue and Fracture, ASTM STP 907, H.T. Hahn, Ed., Am. Soc. for Testing & Materials, Philadelphia, PA (1986).

10. Reifsnider, K.L., "Performance Simulation of Polymer-based Composite Systems, in Durability of Polymer-Based Composite Systems for Structural Applications, Free Univ. Brussels, Belgium (in press).

11. Reifsnider, K.L., "Use of Mechanistic Life Prediction Methods for the Design of Damage Tolerant Composite Material Systems," ASTM STP 1157, M.R. Mitchell & O. Buck Eds., American Society for Testing and Materials.

12. Reifsnider, K.L. and Gao, Z., "Micromechanical Concepts for the Estimation of Property Evolution and Remaining Life," Proc. Intl. Conf. on Spacecraft Structures and Mechanical Testing, Noordwijk, the Netherlands, 24-26 April 1991 (ESA SP-321, Oct. 1991) pp.653-657.

13. Christensen, R.M. and Glaser, R.E., UCRL-89646, Lawrence Livermore National Laboratory, 1983.

DEVELOPMENT OF NONDESTRUCTIVE EVALUATION METHODS AND PREDICTION OF EFFECTS OF FLAWS ON THE FRACTURE BEHAVIOR OF STRUCTURAL CERAMICS*

W. A. Ellingson, J. P. Singh, E. A. Sivers, D. L. Holloway,
T. D. Jacobs, S. L. Dieckman, and D. Singh

Energy Technology Division
ARGONNE NATIONAL LABORATORY
Argonne, Illinois 60439

ABSTRACT

Work in this project is directed toward correlation of data obtained from NDE methods with fracture behavior.

In the NDE area, specimens with different cloth lay-up orientations were examined by 3-D X-ray microtomography and image processing to measure and map in-plane fiber orientations. Results show detection sensitivity to better than ± 3°. We also completed initial 3-D FFT image analysis to establish detection of 3-D braid/weave fiber orientation and spacing. Another NDE method, multinuclear (^{13}C, ^{29}Si, and ^{11}B) NMR spectroscopy, is being developed to determine the chemical state of the fiber surface and its potential impact on fiber pullout. We have conducted initial studies to investigate sensitivity to bulk composition of the matrix materials (a,b, amorphous phase, silica, and oxynitride concentration). The first ^{29}Si NMR experiments focused on methods to enhance the signal from the surface by selectively reducing surface relaxation. Additionally, we have determined that there is sufficient sensitivity of ^{11}B NMR for monitoring fiber coatings.

In the fracture behavior area, microstructural and mechanical properties of Nicalon-fiber-reinforced SiC-matrix 2-D laminated composites were studied in specimens with fiber cloth lay-up sequences of 0°/45° and 0°/20°/60°. These were evaluated to (a) estimate the effects of fiber cloth lay-up orientation sequence on mechanical properties and (b) characterize the effects of high-temperature exposure on flaw morphology and fracture behavior. The average first matrix cracking stress and ultimate strength were 86 ± 23 and 153 ± 41 MPa for composites with 0°/45° fiber lay-up sequence and 113 ± 21 and 282 ± 20 MPa for 0°/20°/60° fiber lay-up sequence. The superior mechanical properties of composites with 0°/20°/60° fiber lay-up sequence are believed to be due to differences in composite processing and fiber architecture/design.

Evaluation of effects of a high-temperature environment on fracture behavior showed that strength increased from ≈390 MPa at room temperature to ≈470 MPa at 800°C, but decreased to ≈290 MPa at 1300°C. This strength degradation at high temperature is believed to be related to fiber degradation.

---

* Work supported by the U.S. Department of Energy, Office of Fossil Energy, Advanced Research and Technology Materials Program, under Contract W-31-109-Eng-38.

INTRODUCTION

In order to develop reliable intelligent processing techniques for advanced ceramic matrix composite materials, data must be obtained from nondestructive evaluation (NDE) methods and correlated with process-related fracture behavior. At present, NDE is being conducted on SiC/SiC continuous fiber composites. The composite specimens studied to date are two-dimensional plain-weave specimens made of SiC (Nicalon) multifiber tows with a cloth architecture of 16 x 16 tows per inch and laid up with 100 cloth layers per inch (≈40 vol.% fibers). Work is progressing toward 3-D braid architectures that use SiC (Nicalon) fibers. Of current interest is the nondestructive measurement of density, as well as measurement of fiber orientation. To map density variations and determine fiber orientations, 3-D microfocus X-ray computed tomography (XCT) is being developed with advanced image-processing technology. Solids NMR technology is being developed to study the detailed chemistry of the fiber surface, as well as that of the fiber/matrix interface after infiltration. In this case, we are developing multinuclear solids NMR technology. Fracture behavior effort has concentrated on continuous fiber reinforced ceramic matrix composites (CFCCs). High strength and appropriate architecture of reinforcing fibers and weak fiber/matrix interfaces are requisites for "tough" ceramic composites.[1] The strength and toughness of composites are greatly influenced by the fiber cloth lay-up sequence and the strength of the reinforcing fibers.[2] These reinforcements are susceptible to thermal degradation and mechanical damage introduced during fabrication and in elevated-temperature service environments of composites. In addition, the nature of flaw generation can also be influenced by fiber cloth lay-up sequence. Therefore, it is important to evalute the effects of fiber cloth lay-up sequence and high-temperature environments on flaw generation and resulting mechanical properties of reinforcing fibers and composites.

NDE CHARACTERIZATION OF SiC/SiC CONTINUOUS FIBER COMPOSITES

Fiber Orientation

One parameter of interest for CFCCs with multidirectional lay-ups is the relative angle of the fiber tows between lay-ups. This is important because mechanical properties are known to be affected by misoriented fiber tows. At present, little experimental information is available about the effects of fiber orientation on mechanical properties, but current information suggests that ±5° will have an impact. Figure 1 shows recent experimental results by Gauthier et al.[3] using a five-harness satin-weave SiC fiber infiltrated with SiC by chemical vapor infiltration (CVI) processing. Clearly, a 5° angular variation can cause a 50 MPa change in tensile strength.

We previously reported on the development of XCT together with image processing, to nondestructively measure in-plane fiber orientations.[4] All specimens used in this work were produced with an eight-harness satin weave with 16 tows/in. and infiltrated by Dow Corning's polymer impregnation process. Figure 2 is a block diagram of the procedure used to acquire the 3-D X-ray CT data and image processing used to measure the relative fiber orientation between cloth layers. Figure 3 shows the results obtained on three specimens whose initially unknown fiber orientations were 75°, 45°, and 30°. The measured angles show that the laid-up plies were within ±50°. The results show relative ply angle measured between layers from the top of the specimen to the bottom. It is interesting that in the 30° specimen, between 16.5 and 22 mm from the top, no relative change in ply orientation was detected. It was later confirmed that the plies had been laid without changing angles at the location.

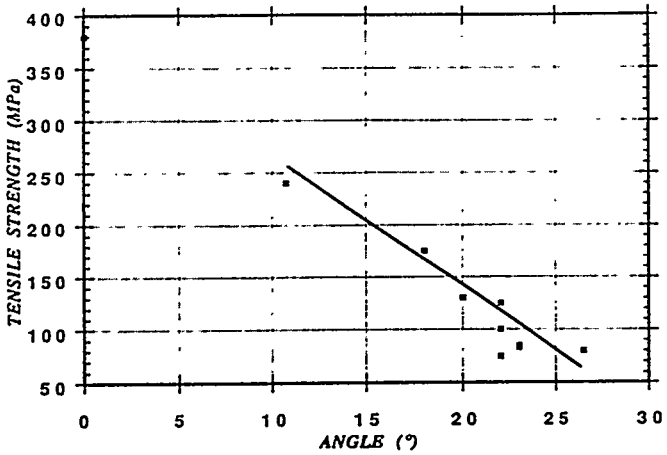

Fig. 1. Influence of fiber misalignment on tensile strength of SiC/SiC with 2-D five-harness satin weave infiltrated by CVI. (After Gauthier et al., Ref. 3).

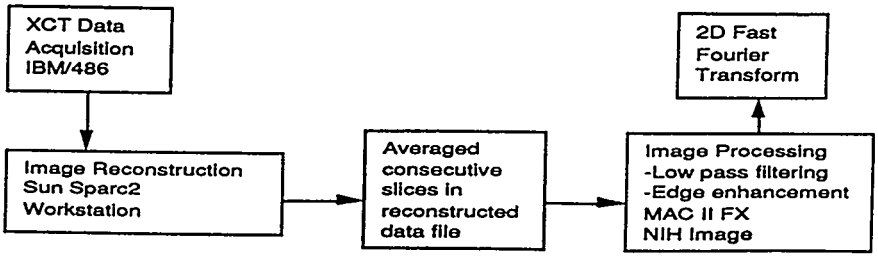

Fig. 2. Block diagram of X-ray data acquisition and subsequent processing for measuring relative between-plane fiber orientation.

EXPERIMENTAL RESULTS

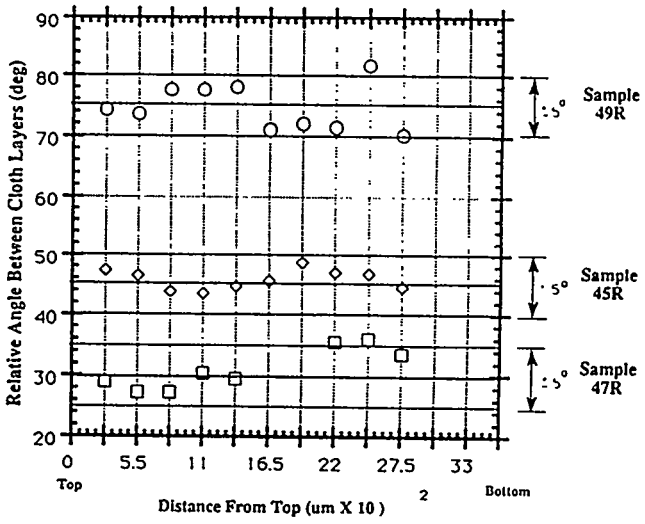

Fig. 3. Nondestructively measured relative fiber orientation between cloth layers in 2-D CVI SiC/SiC, on three specimens.

Density Measurements

It is also important to know the density variations in CFCC materials. We again employed X-ray imaging technology to a set of four specimens made with eight-harness satin weave, but with four different processing times to change the final density. The 50 x 50 x 4 mm specimens had measured geometrical densities of 1.42, 2.02, 2.05, and 2.17 g/cm^3. We used the same X-ray facility as that for the tomographic image data, but in a simple through-transmission configuration. The data were taken with the 1.92 g/cm^3 specimen always in place. Thus, we obtained difference data via the gray scale on the resulting images. This allowed correction for X-ray flux from the X-ray head on any change in the detector system. The resulting data, normalized to the

maximum detected gray scale, plotted versus normalized density (to maximum), are shown in Fig. 4. The results are excellent, as noted.

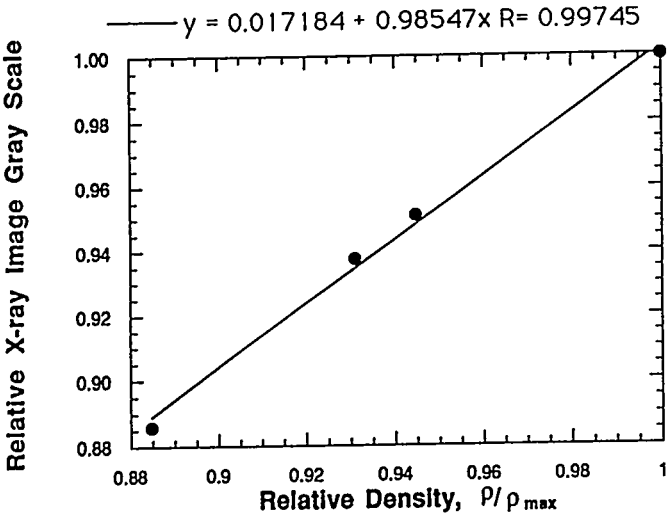

Fig. 4. X-ray through-transmission-measured densities of 2-D laminated SiC/SiC.

Fiber-Matrix Interfaces; Chemical Composition Measurement

Experimental studies continued on the applicability of ^{11}B NMR spectroscopy for the determination of boron-doped carbon and BN coating microstructures on Nicalon fiber in SiC matrixes. Specifically, experiments were initiated on a series of specimens provided by Oak Ridge National Laboratory. The specimens were produced with 40 vol.% Nicalon plain-weave fabric rotated in the typical 0-30° orientation, and with various boron-to-carbon ratios and BN coating thicknesses in the doped and BN-coated fibers, respectively. Initial experiments were performed to determine the overall sensitivity of the nucleus, as well as various experimental parameters such as appropriate spinning speeds and pulse-repetition rates. A series of spectra of the 0.6 μm BN-coated specimen was acquired at 7.1 T by using magic angle spinning (MAS) solid-state NMR techniques spinning between 5 and 12 KHz. These data indicated that spinning speeds in excess of 11 KHz are desirable for these studies (Fig. 5). Additionally, the relaxation-rate studies indicated that the ^{11}B has an extremely efficient quadrupolar-dominated spin-lattice relaxation. Thus, despite the low concentration of ^{11}B in the composite specimens, we determined that the favorable spectroscopic properties (i.e., an isotopic natural abundance of approximately 80.5%, a spin of 3/2 providing efficient spin-lattice relaxation in the solid state, and an overall high

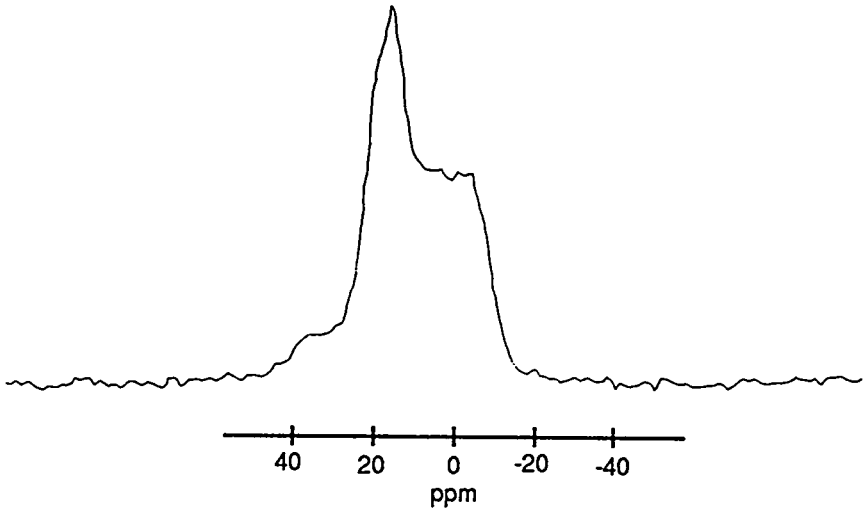

Fig. 5. ^{11}B spectrum of 0.6 μm BN-coated Nicalon fiber acquired at 7.05 T by MAS spinning at 11 kHz. Spectra indicate sufficient sensi-tivity, reasonable peak widths, and sufficient chemical shift dispersion for accurate ^{11}BNMR analysis of both the boron oxides and boron nitrides in the composite specimen.

relative receptivity approximately 13% of that of ^{1}H) of the ^{11}B nucleus provides significant sensitivity to allow accurate qualification of the chemical environment of the boron.

CHARACTERIZATION OF CONTINUOUS SiC FIBER/SiC MATRIX COMPOSITES BY FRACTURE STUDIES

Specimens for Fracture Studies

To evaluate the effects of fiber cloth lay-up sequence on flaw generation and resulting mechanical properties, Nicalon-fiber-reinforced SiC matrix composites with various cloth lay-up sequences and fiber coating thicknesses were obtained from Ceramic Composites, Inc., Annapolis, Maryland. Specifically, during this period, composites with fiber lay-up sequence of 0°/45° and 0°/20°/60°and a carbon coating thickness of 0.4 μm were evaluated. These composites were received in plate form, from which rectangular bars (≈3 x 4 x 40 mm) were machined. The tensile edges of the test bars were beveled to eliminate stress concentrations and thus avoid edge failures. Approximately five specimens were tested per condition.

To study the effects of elevated temperatures on flaw generation and resulting mechanical properties, Nicalon–fiber–reinforced SiC matrix composites fabricated by CVI were obtained from Oak Ridge National Laboratory. As-received composites were approximately 90% dense. Fabrication and room-temperature mechanical properties of the specimens are described elsewhere.[5]

Room-Temperature Mechanical-Property Evaluation and Correlation with Fiber Architecture

Mechanical testing of 0°/45° and 0°/20°/60° SiC/SiC composites was conducted in a four–point–bending mode on a universal testing machine at a loading rate of 1.27 mm/min. The loading and outer support spans were 20 mm and 40 mm, respectively. Both sets of specimens were observed to fail in a graceful manner accompanied by extensive fiber pullout. The first matrix cracking stress was determined from the load at the first deviation from linearity on the load-displacement plot. Ultimate strength was measured from peak load. Work-of-fracture was estimated from the area under the load-displacement plots. For composites with 0°/45° lay-up sequence, the measured values of first matrix cracking, ultimate stress, and work-of-fracture were 86 ± 23 MPa, 153 ± 41 MPa, and 9.8 ± 2.4 kJ/m^2, respectively. For the composites with 0°/20°/60° fiber lay-up sequence, the first matrix cracking stress, ultimate stress, and work-of-fracture were measured to be 117 ± 8 MPa, 283 ± 27 MPa, and 16.04 ± 4.4 J/m^2, respectively. These differences in mechanical properties of the two sets of composites are believed to be partly due to the differences in the fiber architecture in the two sets of composites. Some of the differences may also be due to the differences in processing-related variables in the two sets of composites.

Elevated-Temperature Strength Behavior and Its Correlation with Critical Flaws

To evaluate the effects of high-temperature environments on flaw generation and fracture behavior, the strength of Nicalon–fiber–reinforced SiC composites was evaluated at several temperatures ranging from 800 to 1300°C, followed by microstructural characterization. To this end, composite specimens were first exposed in air for 15 min. at the test temperature. Subsequently, the specimens were tested in vacuum by fracturing in a four–point–bending mode at a crosshead speed of 1 mm/min. The loading and outer support spans were 12.7 mm and 25.4 mm, respectively. As shown in Fig. 6, ultimate strength was found to first increase at 800°C, then decreased rapidly at higher temperatures up to 1300°C. Specifically, strength increased from a room–temperature value of ≈390 MPa to ≈470 MPa at 800°C. Thereafter, it decreased to

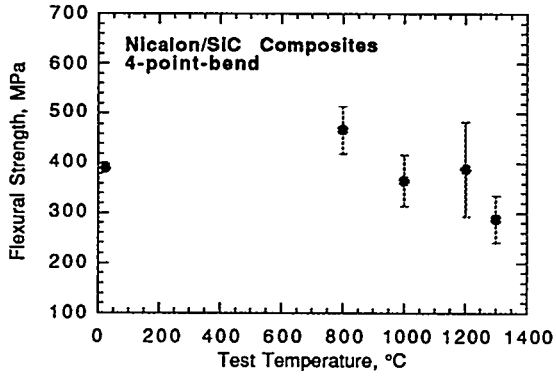

Fig. 6. Variation of ultimate strength as a function of test temperature for Nicalon-fiber-reinforced SiC composites.

≈290 MPa at 1300°C. These strength degradations are believed to be related to fiber degradation, which was evaluated by measuring critical flaw sizes in composites tested at room and elevated temperatures, as discussed below.

Evaluations of Critical Flaw Size

In-situ fiber strength in composites tested at room temperature and 1300°C was evaluated from characteristic fracture features of the fibers. Strength of fractured fibers was determined from the measured values of fracture mirror radii, as shown in Fig. 7, and an empirical relationship proposed by Kirchner and Gruver,[6] as given by

$$\sigma_f \sqrt{r_m} = A_m , \qquad (1)$$

where σ_f is the fiber fracture strength, r_m is the measured fiber mirror radius, and A_m is the mirror constant and is taken to be 3.5 MPa$\sqrt{m}$.

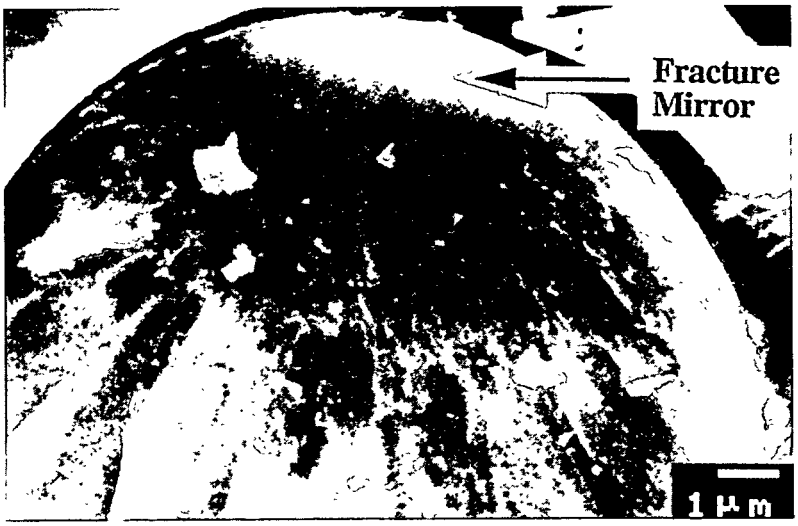

Fig. 7. Micrograph of fractured Nicalon fiber in SiC-matrix composite, showing characteristic fracture features.

The measured values of in-situ fiber strengths were described by the Weibull strength distribution function, as shown by

$$F(\sigma) = 1 - \exp\left[-\frac{L}{L_o}\left(\frac{\sigma}{\sigma_o}\right)^m\right], \tag{2}$$

where $F(\sigma)$ is the cumulative failure probability at an applied stress σ, L_o is the fiber gage length at which Weibull parameters are estimated, L is the standard gage length taken to be 10 mm, σ_o is the scale parameter signifying a characteristic strength of the distribution, and m is the Weibull modulus that characterizes the flaw distribution in the material. Scanning electron microscopy (SEM) of fractured composites (room temperature and 1300°C) were used to determine length distribution of fiber pullout (as shown in Fig. 8), from which the gage length of fractured fibers was determined. Fiber gage length was taken to be approximately equal to fiber pullout lengths and was 320 μm in room-temperature tests and 200 μm in high-temperature tests, respectively. Using these value of fiber gage lengths, we estimated the values of σ_o to be 1.20 GPa and 0.84 GPa for room- and high-temperature-tested composites, respectively.

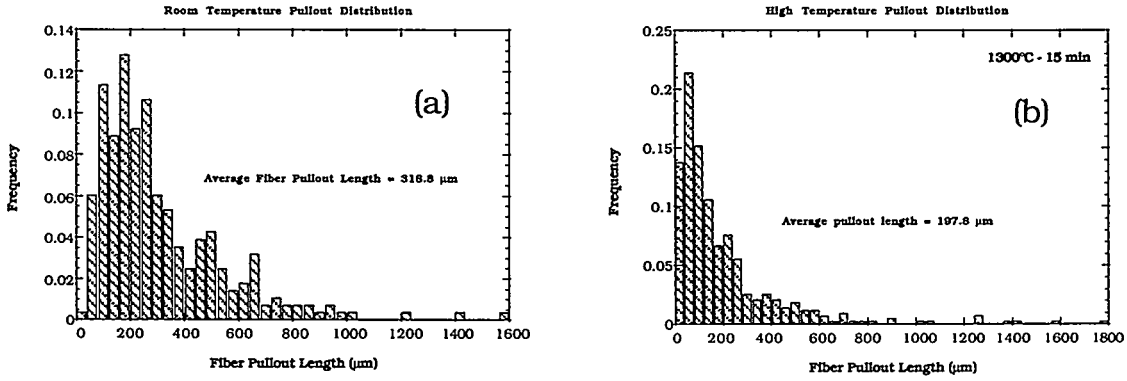

Fig. 8. Length distribution of Nicalon fiber pullout in Nicalon/SiC-matrix composite tested at (a) room temperature and (b) 1300°C.

Figure 9 shows the fiber strength distributions of Nicalon fibers in composites tested at room temperature and 1300°C, together with those of as-fabricated fibers. The as-fabricated strength distribution was obtained from bundle tests conducted on fiber tows.[7] Although the Weibull modulus in the three cases did not change (7.1 for the as-fabricated fibers, 6.0 for the fibers in composites tested at room temperature, and 5.2 for fibers tested at 1300°C), fiber strength after incorporation in the composite was approximately 50% lower than that of the as-fabricated fibers. This reduction in fiber strength may have been caused either by the increased severity of preexisting flaws or by the introduction of new flaws during processing (by thermal and mechanical damage). There is a further 30% decrease in fiber strength in composites tested at 1300°C.

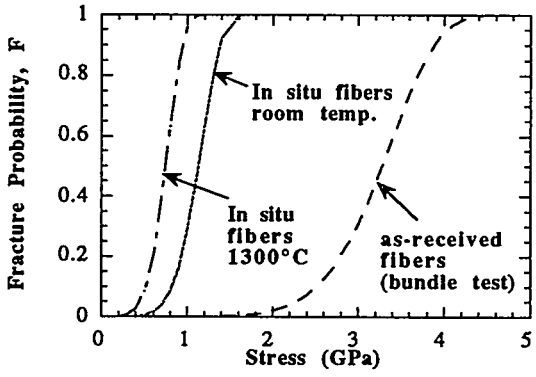

Fig. 9. Weibull strength distribution of Nicalon fibers in as-fabricated state (bundle test), after processing (mirror size evaluation), and after high-temperature testing.

Strength degradation of Nicalon fibers due to high temperatures is well documented in the literature. Tensile strength loss of more than 30 and 70% has been reported for ceramic-grade Nicalon fibers by exposure at 1000 and 1200°C, respectively, for 12 h in a wet-air atmosphere.[8] This is attributed to microstructural and stoichiometric changes in the fibers at elevated temperatures. Similar changes, although not as severe, are expected for the carbon-coated Nicalon fibers investigated in this study. High processing temperatures (≈1200°C) and long exposure times (>24 h) in the fabrication of the composites make it difficult to prevent fiber degradation. Okamura et al.[9] have shown that formation of an SiO_2 film can also contribute to reduction of fiber tensile strength and Young's modulus.

REFERENCES

1. A. G. Evans and D. B. Marshall, "The Mechanical Behavior of Ceramic Matrix Composites," Overview No. 85, Acta Metall., **37** [10] 2567–2583 (1989).

2. T. Mah, M. G. Mendiratta, A. P. Katz, R. Ruh, and K. S. Mazdiyasni, "Room Temperature Mechanical Behavior of Fiber-Reinforced Ceramic Matrix Composites," J. Am. Ceram. Soc., **68** [1] C-27 – C-30 (1985).

3. G. Gauthier, G. Bessenay, Y. Honnovat, "Influence of Fiber Alignment on Tensile Strength of SiC/SiC (CVI, 2D 5 Harness Satin Weave)," in 4th Intl. Symp. on Ceramic Materials and Components for Engines, Goteborg, Sweden, pp 970–984, 1991.

4. W. A. Ellingson, J. P. Singh, D. L. Holloway, S. L. Dieckman, D. Singh, E. A. Sivers, S. H. Sheen, and M. J. Wheeler, "Development of Nondestructive Evaluations Methods and Prediction of Effects of Flaws on the Fracture Behavior of Structural Ceramics," Proc. 6th Annual Conf. on Fossil Energy Materials, Fossil Energy AR&TD Materials Program, ORNL/FMP-92/1, pp. 119-130 (1992).

5. D. P. Stinton, A. J. Caputo, and R. A. Lowden, "Synthesis of Fiber-Reinforced SiC Composites by Chemical Vapor Infiltration," Am. Ceram. Bull., **65** [2] 347–350 (1986).

6. H. P. Kirchner and R. M. Gruver, "Fracture Mirror in Alumina Ceramics," Phil. Mag. **27** 1433–1446 (1973).

7. D. Singh and J. P. Singh, "Effect of Processing on Strength of Nicalon Fibers in Nicalon Fiber-SiC Matrix Composites," Ceram. Eng. Sci. Proc., Vol. 13, [7-8] 257-266 (1992).

8. T. J. Clark, R. M. Arons, and J. B. Stamatoff, "Thermal Degradation of Nicalon SiC Fibers," Ceram. Eng. Sci. and Proc., **6** [7–8] 576–588 (1985).

9. K. Okamura, M. Sato, T. Matsuzawa, and Y. Hasgawa, "Effect of Oxygen on Tensile Strength of SiC Fibers," Polymer Preprints, **25** [1] 6–7 (1984).

ENGINEERING-SCALE DEVELOPMENT OF THE VAPOR-LIQUID-SOLID (VLS) PROCESS FOR THE PRODUCTION OF SILICON CARBIDE FIBRILS

W. E. Hollar, Jr. and T. P. DeAngelis

The Carborundum Company
Technology Division
P.O. Box 832
Niagara Falls, NY 14302

and

C. T. Hua, F. K. Ko and F. Scardino

Advanced Product Development
2500 Pearl Buck Road
Bristol, PA 19007

ABSTRACT

As composite reinforcements, VLS SiC fibrils have attractive mechanical properties including high strength, high modulus, and excellent creep resistance. To make use of their excellent mechanical properties in a composite, a significant volume fraction (> 10%) of aligned, long fibrils (> 5 mm) needs to be consolidated in the ceramic matrix. The fibrils must be processed into an assembly that will allow for composite fabrication while maintaining fibril alignment and length. We are investigating several approaches to achieve this goal, including spun yarn, wet casting, and tape forming.

A modified yarn spinning process has been tested. This concept consisted of fibril disentangling and alignment followed by a yarn forming step. The primary difficulty with this approach occurred during disentangling, where fibril fracture occurred. Two alternative processes are under development to avoid this problem. These are slurry and tape-assisted forming of aligned fibrils. These techniques have been demonstrated using fibrils as well as model ceramic fibers. The future direction for process development will be discussed.

INTRODUCTION

VLS SiC fibrils are high aspect ratio, fine diameter single crystal SiC fibers. As ceramic reinforcements they have unmatched tensile strength, modulus, and creep resistance.[1] These properties suggest that fibrils could be a premium reinforcement for ceramic matrix composites (CMC). Despite their potential, the fibril manufacturing process has never advanced beyond the laboratory scale. As a result, production costs are extremely high and material inventories are low, preventing any serious evaluation of the fibrils in composite applications.

Carborundum completed a Phase I program in early 1993.[1] The goal of Phase I was to determine the feasibility of scaling up the process to an engineering scale system capable of producing

100 - 500 lb/year of fibrils. This goal was accomplished through evaluation of controlling scaleup parameters in a 12" tall reactor. This work resulted in an improved understanding of the requirements for reactor scaleup, and culminated in the development of a computer model capable of simulating reactor performance as a function of process conditions and reactor geometry. The Phase I results demonstrated the feasibility of reactor scaleup. The remainder of Phase I focused on evaluating process specifications which determine the production cost of SiC fibrils. This effort included evaluation of the post-processing requirements and the demonstration of a process gas recycle system. The tradeoffs between production rate and the product characteristics were evaluated. These results provided crucial data for process economic evaluation.

The potential market for SiC fibrils can only be properly evaluated by determining their performance in a composite. There have been initial indications that SiC fibrils can produce exceptional composite properties. For example, inclusion of 4.3% SiC fibrils in an aluminum metal matrix composite produced a 64% increase in tensile strength.[2] This was accomplished by using aligned, long SiC fibrils, which resulted in a strong property enhancement. The use of long, aligned SiC fibrils in a CMC with a proper debond coating has not yet been demonstrated.

Ceramic matrix composites containing moderate amounts of long, aligned SiC fibrils have the potential to behave like a continuous fiber reinforced composite. Because of their high strength, a relatively low loading of fibrils would produce composite behavior. Successful demonstration of this predicted behavior could make SiC fibrils an attractive candidate for many CMC applications. To achieve this result, a process for aligning long (> 5 mm) fibrils in a preform and consolidating them into a fully dense composite must be demonstrated. Thus, a process for fabricating linear, aligned assemblies of fibrils is a crucial step in making fibrils a serious CMC reinforcement candidate. This requirement resulted in Phase II of the program.

The Phase II program has three objectives: 1) determine whether linear, aligned assemblies of fibrils can be formed using a scalable process; 2) produce demonstration samples for composite fabrication experiments; and 3) complete the process economic analysis.

EXPERIMENTAL APPROACH

The unique properties of SiC fibrils make forming them into yarns or other aligned assemblies very challenging. Fibrous ceramic materials are difficult to form into textile assemblies compared to typical fibers such as wool, cotton, and manmade fibers because ceramic fibers tend to be stiffer, shorter, smoother, and thinner. All of these properties make disentangling, alignment, and incorporation into a

yarn more difficult. SiC fibrils are especially challenging, due to their relatively short length and high stiffness.

All processes for forming yarns or other linear assemblies involve similar processing steps. Figure 1 shows the process concept for SiC fibrils. The fibrils are typically collected in the form of tangled mats. For conversion to a yarn, this mat must be opened and aligned. The loose, aligned assembly is then attenuated into a desired density. Finally, a technique like spinning is used to integrate the aligned assembly into a structure with acceptable mechanical properties.

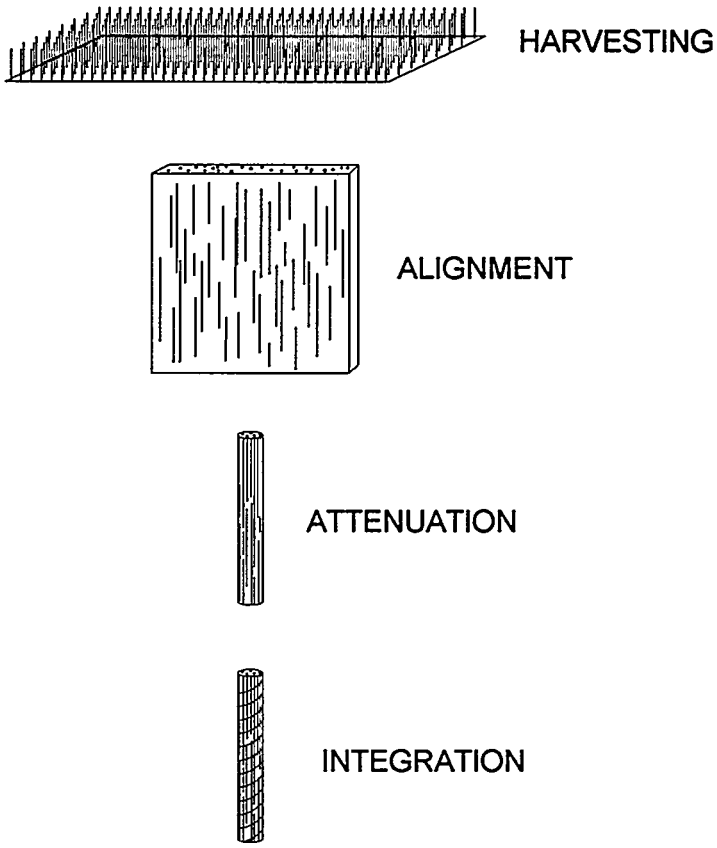

Fig. 1. General Process Concept for the Conversion of SiC Fibrils to a Yarn

Yarn forming processes can be divided into two categories: traditional and nontraditional. The forming of cotton-based yarns is a traditional process. It consists of carding to open and align the tangled fiber mat followed by attenuation into a sliver. The sliver is essentially an aligned assembly with minimal physical coherence. The final step is spinning, which applies twist to the fibers to entangle them. This entanglement gives the yarn its mechanical strength which allows handling and processing by weaving, braiding, or other processes.

Previous efforts to form ceramic fibers into yarns were reviewed. Nontraditional processes have been developed mainly for ceramic fibers to deal with their unique properties. There are a number of variants described in the literature. Some examples include modified spinning processes, inclusion of carrier fibers to promote formability, and the addition of adhesives or binders to improve mechanical properties. These techniques are designed to overcome difficulties or limitations that result from the unique properties of ceramic fibers.

There have been previous attempts at forming yarns and textiles from SiC whiskers and fibrils. The most recent work was done as a cooperative effort between Los Alamos National Laboratory (LANL), Texas Tech University, and the Woven Structures Division of HITCO.[3] They initially tested a traditional spinning process which produced poor results. They eventually settled on a slurry processing route; this concept is being evaluated further under the present program.

The literature results on spinning ceramic fibers in general and SiC fibrils in particular led to the following conclusions. First, any process based on traditional yarn spinning processes would require substantial modification to successfully spin ceramic fiber. Second, the unique properties of the SiC fibrils might render traditional processes unfeasible and require creative, nontraditional approaches to yarn forming. Therefore, this program focused on simultaneous evaluation of a modified traditional process and two nontraditional processes for forming linear, aligned assemblies of fibrils.

EXPERIMENTAL RESULTS

Screening experiments on one traditional and two nontraditional processes were completed. The traditional process evaluated was air vortex spinning. This process provides a relatively gentle means of yarn spinning by air flow entanglement. Experimental efforts focused on the carding and spinning steps.

The two nontraditional approaches were: 1) a wet-laid concept similar to that used by LANL, and 2) an adhesive tape approach. These are described in more detail below.

Preliminary screening experiments used several different fibers. The traditional process used chopped Nicalon® fiber as a model for SiC fibrils. Cotton fibers were used as a carrier fiber for the traditional processing experiments. The nontraditional techniques were tested with both chopped Nicalon® fibers and SiC fibrils. The experimental apparatus and procedures are described in more detail below.

Traditional Process

The experiments on the traditional process focused on the two critical steps: carding and spinning. Process variations designed to help overcome the stiffness of SiC fiber were employed. The carding and spinning steps are the critical steps in the yarn spinning approach. Figure 1 shows the relationships of these steps; carding is the alignment process and spinning is the integration process.

The carding process was evaluated by hand carding Nicalon® fibers and cotton. The purpose of carding is to align the fibers and disentangle or "open up" the structure. The success of the carding process depends on proper configuration of the card clothing. The card clothing consists of materials ranging from metal to cloth with a variable number of points per unit area. The combination of the card material and point density determines the effectiveness of the carding process. Hand carding was chosen since it made rapid screening of different card clothing possible.

The results of the hand carding experiments were not promising. Five carding materials were used including both metal and cloth materials with low and high point densities. Each was tested with pure Nicalon® fibers, pure cotton, and mixtures of the two fibers. The pure Nicalon® fibers could not be carded. There was substantial breakage and poor alignment. Inclusion of the cotton as a carrier fiber did not improve the situation; the cotton and SiC fibers tended to segregate with minimal effective alignment of the Nicalon® fibers.

The primary result from this work was that the development of clothing for the successful carding of SiC fibrils was not feasible. Also, the carding process caused substantial breakage of the Nicalon® fibers. As a result, it was decided to abandon this approach.

A lab scale spinning apparatus using an air vortex spinning concept was constructed. The design of the unit is shown in Figure 2. A lab scale spinning system including controls was set up and tested using cotton fiber. Cotton yarn was successfully spun using the apparatus.

The feasibility of the fibril spinning process was evaluated using a mixture of cotton and Nicalon® fibers. The results were poor. Unlike the spinning of cotton, the spinning process was frequently interrupted by a blockage of Nicalon® fibers. The uniformity of the yarn was poor, consisting mostly of cotton with occasional patches of ceramic fiber. Finally, the process proved to be extremely damaging to the fibers; most of the SiC ended up in a filter used to catch debris from the process. The broken materials had been shortened to 1 - 2 mm, making them useless for further spinning.

Overall, the traditional process was unsuccessful in forming discrete SiC fibers into aligned assemblies. Even though substantial modifications were made to deal with the fiber stiffness (a gentle spinning process, modified card clothing, and addition of a carrier fiber), the traditional process did not produce acceptable results. Without an effective carding step, downstream process steps like spinning

are impossible. Both spinning and carding proved to be extremely damaging to the fibers. This damage resulted in substantial shortening and low process yields. For these reasons it was decided to stop work on the traditional process and focus on the nontraditional processes.

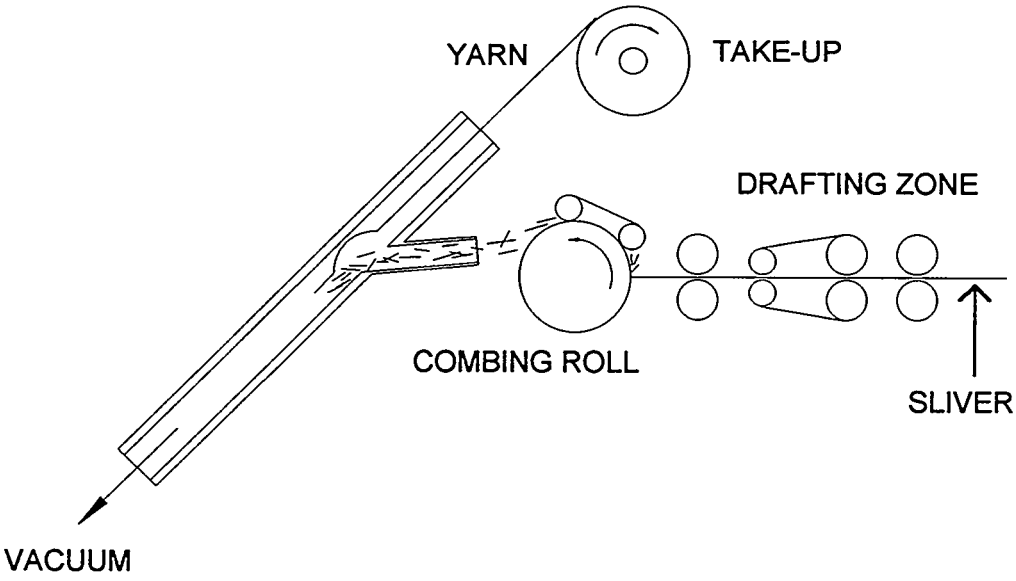

Fig. 2. Lab Scale Air Vortex Spinning Apparatus

Nontraditional Processes

The traditional processing experiments provided several important clues regarding process requirements to form aligned assemblies of SiC fibrils. The main conclusion was that substantial damage occurred to the fibers during handling. To be successful, the forming process needs to be gentle and all handling steps should be minimized. Furthermore, an alternative to carding as the alignment process is necessary. Finally, the assembly needs to be consolidated using techniques other than twisting; it was not effective and caused substantial fiber damage.

Two nontraditional techniques were evaluated--the wet-laid and adhesive tape techniques. Both address the major issues associated with the traditional process. Both use less aggressive techniques to align the fibrils. Both techniques used polymeric materials (carriers) to provide the mechanical strength necessary for fabrication of the assemblies into preforms.

The tape process concept is shown in Figure 3. As-grown fibrils on their growth substrate are aligned by mechanical action or fluid flow. The aligned fibrils are then harvested by collection with adhesive tape. The tape serves to maintain the fibril alignment and protect the fibrils from further

damage. The tape can be cut to desired dimensions and processed into different forms by braiding and weaving. The tape would be burned out after fabrication of the composite preform when it is no longer needed to provide strength.

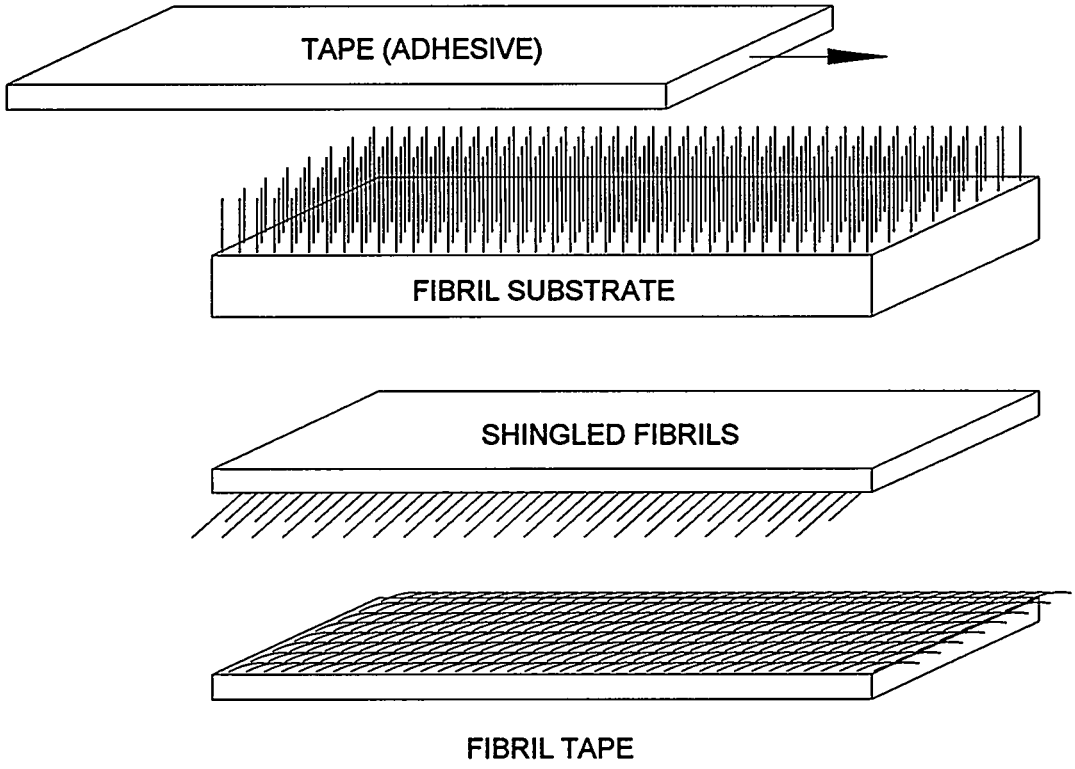

Fig. 3. Adhesive Tape Fabrication Steps

The alignment of fibrils on the growth substrate is the process step required to make the tape concept successful. A high degree of alignment is critical to maximize the impact of the fibrils in the composite. Several different techniques were tested. These techniques could be broken down by their alignment mechanism. Mechanical techniques used brushes to align the fibrils. Different types of brush designs (materials of construction, bristle size/design/density) were tested. Fluid flow techniques use the drag force exerted by a flowing fluid to cause alignment. Both air and liquid media were tested. Mechanical brushing appeared to give the best results.

Fibril coated tapes were fabricated using as-grown SiC fibrils. Fibril loading of 10 weight % resulted; the degree of alignment was variable. These results seemed to indicate feasibility of the concept; however, improvements in the technique are necessary. There are several areas for improvement in the concept. Further improvements in the alignment will be evaluated through

modifications of the fibril length and density, along with continued development of the mechanical alignment process.

The wet-laid process is an adaptation of a technique originally developed by LANL, Texas Tech, and HITCO. The fibrils are dispersed in a liquid and are poured into an evacuated trough. The flow of the slurry in the channel tends to align the fibrils. The resulting product is similar to thick yarn.

An evacuated channel was used to demonstrate the proof of concept of the wet-laid process. This device allowed casting of several inch strands of aligned fibrils. These strands tend to have some mechanical strength due to residual liquid. Both Nicalon® model fibers and SiC fibrils were evaluated in wet-laid experiments. The assemblies produced by this process had a high degree of alignment. This technique will require the addition of a continuous carrier fiber to maintain the alignment of the fibrils and to provide mechanical strength. A 12" section of "yarn" was hand-fabricated by wrapping a polymer monofilament around the outside of the several wet-laid strands made from Nicalon® fiber. This wrapping step produced a sample that could be handled without falling apart. The wet-laid technique has potential as a method of forming linear, aligned assemblies.

To summarize, both nontraditional techniques produced promising results. Both techniques at least partially aligned the fibrils, and both appeared to be less damaging to the fibrils during processing. Both techniques will require further development to confirm their feasibility and resolve technical challenges. The required efforts are described in the next section.

DISCUSSION OF RESULTS

Each nontraditional technique has both advantages and disadvantages; these have been summarized in Table 1. The adhesive tape technique has the highest likelihood of preserving the as-grown length of the fibrils. However, the tape characteristics are strongly dependent on the characteristics of the as-grown fibrils including growth density and uniformity as a function of position on the growth substrate. This approach also depends on developing a technique for aligning the as-grown fibrils. A subtask of the fibril production effort will be devoted to modifying the characteristics of the as-grown product. The goal will be to achieve fibril characteristics which improve the alignment and uniformity of the tapes. We will also evaluate the ability to remove catalyst balls from the fibrils on the tapes and the impact of tape removal on the final properties of the aligned assemblies.

The wet-laid approach has the advantage of using beneficiated fibrils. It will not depend on modification of the growth process; it can use conventional beneficiated fibril product. Most important, the technique produced well-aligned assemblies in the preliminary samples, which indicates that product alignment should not be an issue. On the downside, the fibril dispersion step will shorten the product.

Also, the product will require either a binder and/or wrapping of a yarn or monofilament to provide mechanical strength. These disadvantages need to be addressed through further development experiments.

Table 1. Advantages and Disadvantages of Nontraditional Forming Processes

Process	Adhesive Tape	Wet-Laid
Advantages	Reduced handling of fibrils	High degree of alignment
	Minimizes damage	Utilizes beneficiated fibrils
	Tape provides strength	Utilizes all fibril lengths
	Utilizes all fibril lengths	
	High degree of bending	
Disadvantages	Burnout of tape required	Fibril damage during dispersion
	Low fibril/tape ratio	Requires development of carrier for strength
	Residual catalyst	Burnout of carrier material required
	Impact on synthesis process	
	Alignment and uniformity	

Both nontraditional approaches have the potential to achieve linear assemblies with high fibril yield. This will be an important economic consideration since the cost will be directly proportional to yield at this stage of the process. The expected features of the product of each nontraditional process are summarized in Table 2. Both approaches have the potential to form well-aligned, linear assemblies of SiC fibrils with acceptable mechanical strength for subsequent fabrication into composite preforms. Both techniques appear to have excellent potential for further scaleup and automation for manufacturing.

Table 2. Likely Qualities of SiC Fibril Linear Assemblies Produced by the Proposed Nontraditional Approaches

Quality	Adhesive Tape	Wet-Laid (Cross Wrap)	Wet-Laid (Binder)
Orientation	High	High	High
Density	Medium	High	Medium
Strength	Medium	High	Low
Uniformity	Medium	High	High
Fineness	Medium	Low	Medium
Damage	Medium	Medium	Medium
Processability	Medium	High	Low

Further work has been planned for both nontraditional techniques focusing on process and product improvements. The primary goal will be to overcome the technical challenges associated with

each concept and identify any critical technical issues associated with each technique. Also, we will begin the evaluation of physical and mechanical properties of the aligned assemblies. These results will be used to guide further product improvements.

CONCLUSIONS AND PLAN

A modified traditional yarn forming process was unsuccessful in forming yarns from a SiC model fiber. The high stiffness of SiC fibers prevented successful carding and spinning. Further work on the approach has been abandoned.

Two nontraditional approaches did show promise in producing aligned assemblies of SiC fibrils. The initial tape samples had variable degrees of alignment and variable fibril loading uniformity. The wet-laid approach formed assemblies with a high degree of alignment. This wet-laid product will require the addition of a binder or a continuous fiber wrapping to provide the necessary mechanical strength.

We will now focus on further development of both nontraditional processes. The tape will require improvements in the fibril alignment and loading uniformity. The wet-laid approach needs to incorporate a carrier material without losing the high degree of alignment observed in preliminary experiments.

The plan for the remainder of the year includes:

1. Continue development of both nontraditional approaches.
2. Evaluate the aligned assembly properties.
3. Evaluate the impact of the nontraditional processes on the growth process.
4. Deliver preforms for CVI consolidation.
5. Complete the process economic analysis.

REFERENCES

1. W. E. Hollar, Jr. and W. H. Mills, "Engineering Scale Development of the Vapor-Liquid-Solid (VLS) Process for the Production of Silicon Carbide Fibrils," Phase I Final Report to DOE/ORNL, 1993.

2. R. D. Maier and T. W. Krucek, "VLS Silicon Carbide Whisker Reinforced Metal Matrix Composite by the Squeeze Casting Process," U.S. Patent Number 5,207,263, 1993.

3. F. D. Gac, W. J. Parkinson, J. J Petrovic, and P. D. Shalek, "Whisker Reinforced Structural Ceramics," Semiannual Progress Report to DOE/ORNL, 1987.

HYDROGEN PRODUCTION USING INORGANIC MEMBRANES

D. E. Fain and G. E. Roettger

Oak Ridge K-25 Site*
P. O. Box 2003
Oak Ridge, TN 37831-7271

ABSTRACT

The plan for developing ceramic membranes to separate hydrogen from gasified coal has been to fabricate membranes with gradually decreasing pore size, to study the transport mechanisms, and to determine the pore size needed to achieve large separation factors at high permeance. The transport properties and separation factors of the membranes are being measured with various gases at increasing temperatures. A mathematical model was developed using known transport mechanisms. The transport data is being used to continually evaluate and improve the model. Experimentally, it has been observed that the separation factor, measured at room temperature, decreases as the pore radius decreases from about 30 to 5 angstroms. Without the guidance of the mathematical model, we would have concluded long ago that the probability of fabricating a ceramic membrane with a high separation factor was extremely low and terminated the project. However, the model indicated that at sufficiently low pore size, the separation factor would reach a minimum and start increasing rapidly toward an infinite separation factor. The progress has been slower than was expected because of difficulties in accurately characterizing the membrane pore size. A new method using the mathematical model to interpret data from a high temperature flow test system has been developed to estimate the pore size. Progress is now continuing toward decreasing the pore size. A large number of membranes have been evaluated over the range of pore radii from 30 Å to about 2.5 Å. Transport measurements have been made and separation factors evaluated for 15 of those membranes over a temperature range of 22 to 275°C and a pressure range of 85 to 185 cm hg. The smallest pore size membrane appears to have a mean pore radius of about 2.5 Å and a high temperature extrapolated separation factor for helium and carbon tetrafluoride of 330. In addition, a variable volume adsorption measurement system has been upgraded to permit adsorption measurements at temperatures up to 275°C. Adsorption data is needed to extend the mathematical model to higher temperatures.

---

*The Oak Ridge K-25 Site is managed by Martin Marietta Energy Systems, Inc. for the U.S. Department of Energy under contract No. DE-AC05-84OR21400.

INTRODUCTION

The major purpose of this project is to develop a ceramic membrane that will efficiently separate hydrogen from gasified coal at temperatures of 1000°F (538°C) or higher. Very high separation factors are needed for commercially useful membranes. Such high separation factors should be achievable with a ceramic membrane that has pores sufficiently small to separate gas molecules on the basis of molecular size. Therefore an important secondary purpose of this project is to develop an understanding of transport mechanisms in ceramic membranes so that maximum separation factors can be achieved by design. The scientific approach to achieve this understanding is focused on fabricating well characterized membranes with progressively smaller pores, measuring the transport and adsorption properties of a well chosen range of gases, and studying the various transport mechanisms within the context of a mathematical model that can be used to design maximum separation factors at any temperature. A key objective for FY 1994 is to achieve a separation factor of 50 or higher at temperatures greater than 1000°F.

A high precision high temperature (room temperature to 275°C) gas flow test system is being used with good success to determine the functional dependence (pressure and temperature) of the transport of helium, carbon dioxide, and carbon tetrafluoride as test gases. Safety precautions are being established for using hydrogen as an additional test gas. A variable volume apparatus has been constructed to measure adsorption isotherms over the same range of temperatures. The transport mechanisms are then interpreted in the context of a mathematical model. In addition, a method is being investigated to extrapolate the separation factors to very high temperature where only diffusive flow will be present. A relatively simple model can then be used to calculate a pore size from the extrapolated separation factor. This method is expected to be useful only for membranes with mean pore radii less than 10 A.

A hard sphere model was developed earlier for the pure diffusion of gas molecules of different sizes in a circular capillary. It is assumed that this condition will be approximated at very high temperatures. With the assumption of several different transport mechanisms, and using gas flow and adsorption data measured at room temperature, the model was extended to predict separation factors at room temperature. The calculated separation factors from the model are shown in Fig. 1. A current objective is to expand the model to other temperatures. This objective should be achievable using available gas transport data from the high temperature flow test in conjunction with independently determined gas adsorption data over the same range of temperatures.

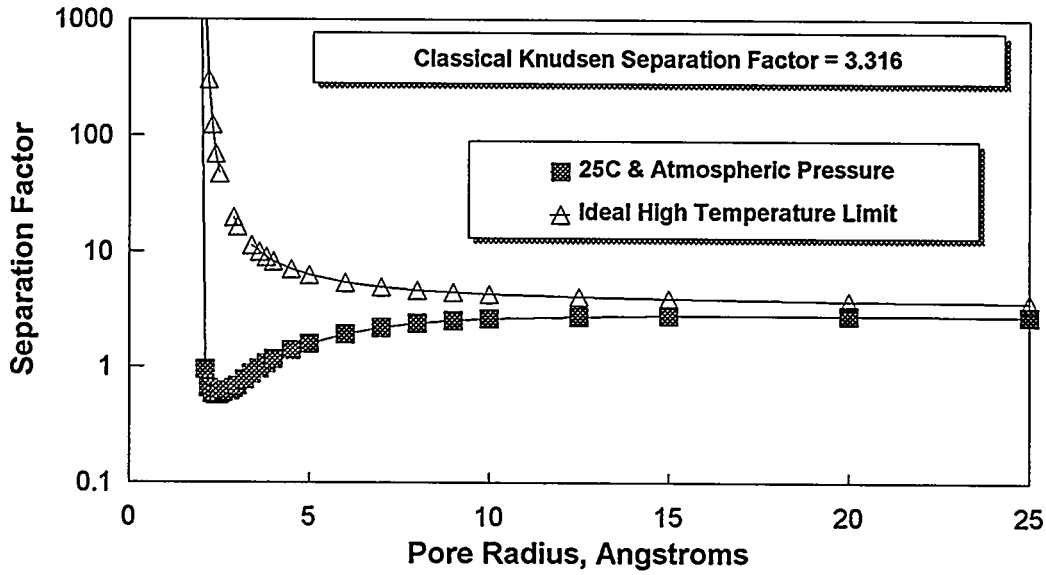

Fig. 1. Transport model calculations for He-CO_2 separation factors at room temperature and at the ideal high temperature limit.

DISCUSSION OF CURRENT ACTIVITIES

The membrane fabrication techniques that are currently being developed are showing good progress in producing ceramic membranes having small pore sizes. Experimental alumina membranes have been produced and tested that have mean pore radii ranging from 30 to 5 Å and that have high temperature separation factors as high as 13 for the helium/carbon tetrafluoride gas pair. Recently a membrane was produced that we believe has a mean pore radius of about 2.5 A and that has a separation factor at room temperature of 22, a separation factor at 250°C of 75, and a high temperature extrapolated separation factor of about 330.

The ceramic membranes are being tested in our high temperature flow test system using helium, carbon dioxide, and carbon tetrafluoride as test gases. High precision flow measurements are made with each of the test gases at several temperatures between 20°C and 275°C and over a pressure range of approximately 85 to 185 cm Hg. Examples of the flow data obtained with helium on alumina membranes having mean pore radii of approximately 5 Å and 30 Å are shown in Figs. 2 and 3, respectively. The flow data are plotted as a permeance (sccm/sq cm/cm Hg) versus average pressure (average of the forepressure and backpressure). A linear (least squares)

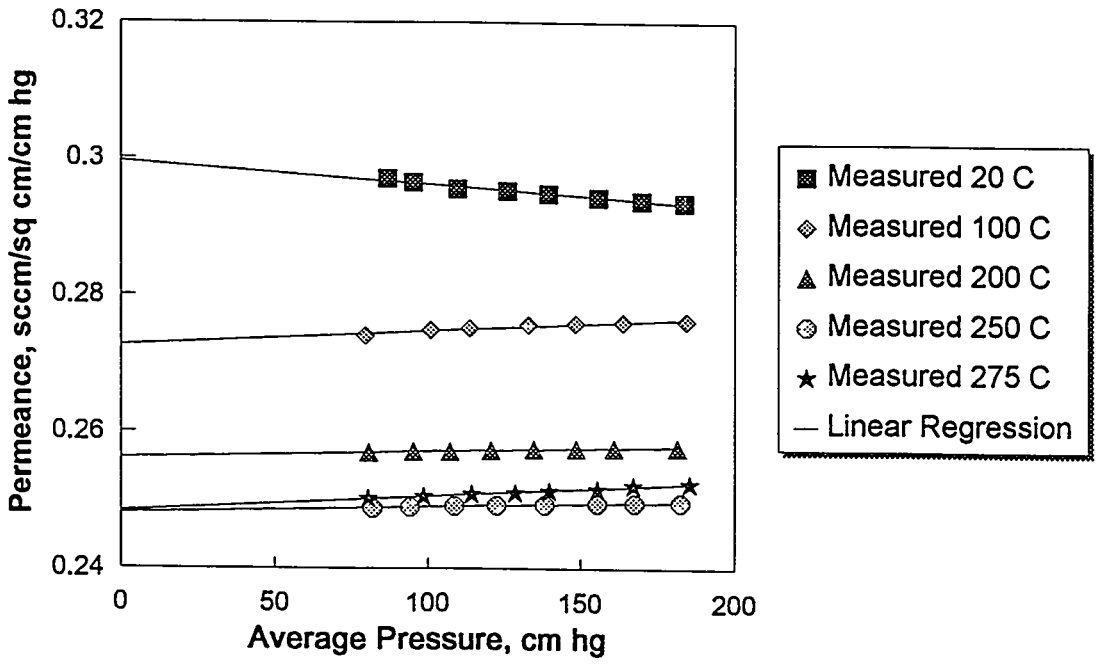

Fig. 2. Helium flow data measured at several temperatures through alumina membrane having 5 Å mean pore radius.

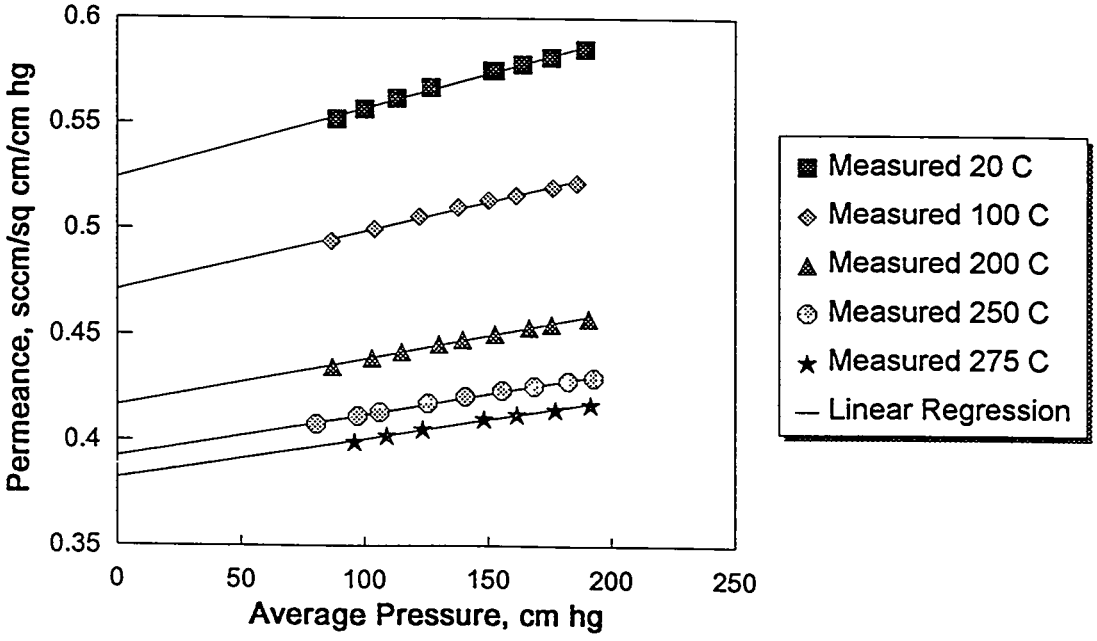

Fig. 3. Helium flow data measured at several temperatures through alumina membrane having 30 Å mean pore radius.

fit is included in the plots for data taken at each temperature. Similar data are available for carbon dioxide and carbon tetrafluoride. A somewhat better way of observing the flow data is shown in Figs. 4 through 7 which show transport probabilities for helium and carbon tetrafluoride for membranes having mean pore radii of 5 Å and 30 Å. The transport probability can be calculated by dividing the measured flow in molecules per unit time per unit area by the difference in the incident rate in molecules per unit time per unit area on the two sides of the membrane. For free molecule or Knudsen flow, the transport probability extrapolated to zero pressure should be a function only of the physical properties of the membrane and independent of type of gas molecule and temperature. Therefore, a graph of transport probability vs pressure summation (sum of highside and lowside pressure) emphasizes any deviations in the extrapolated zero pressure transport probability from free molecule or Knudsen flow. A convenient means of condensing the data is to plot the zero pressure transport probabilities for the various gases versus temperature as shown in Figs. 8 and 9. The ideal separation factor for a gas pair at a given temperature is calculated from the ratio of the extrapolated zero pressure permeances for that gas pair at the given temperature. The ideal separation factor is also given by the square root of the molecular weight ratio times the ratio of the zero pressure transport probabilities at the given temperature.

Separation factors for the gas pairs may, thus, be determined from the flow data measured at room temperature, 100°C, 200°C, 250°C, and 275°C. Several methods have been used in an attempt to extrapolate the separation factors to very high temperature. It appears that an Arrhenius-type plot (ln separation factor plotted against the reciprocal of the absolute temperature, 1/T) provides the best fit of any method attempted so far. While there is currently no theoretical explanation for using such a plot, it does appear to be an excellent means of extrapolating the separation factor to very high temperature. The helium/carbon tetrafluoride separation factors determined for a recent alumina membrane and plotted in this manner are shown in Fig. 10. The pore size of this membrane was too small to measure with our Dynamic Pore Size Test.

Extrapolation of the least squares fit (Fig. 10) to a zero value of I/T provides an estimate of the separation factor at the high temperature limit where adsorption and surface flow effects would be eliminated. The high temperature separation factor of 12.99 can be interpreted using the hard sphere model to provide an estimate of the mean pore size of the membrane. Those calculations indicate that a membrane mean pore radius of 4.98 Å is required to provide a high temperature separation factor of 12.99 for the helium/carbon tetrafluoride gas pair.

The effects of membrane pore size on the separation factor/temperature data are shown in Fig. 11, which contrasts data measured on two alumina membranes having mean pore radii of 30 Å and 8.9 Å (as determined by the Dynamic Pore Size Test). For the 30 Å membrane at room

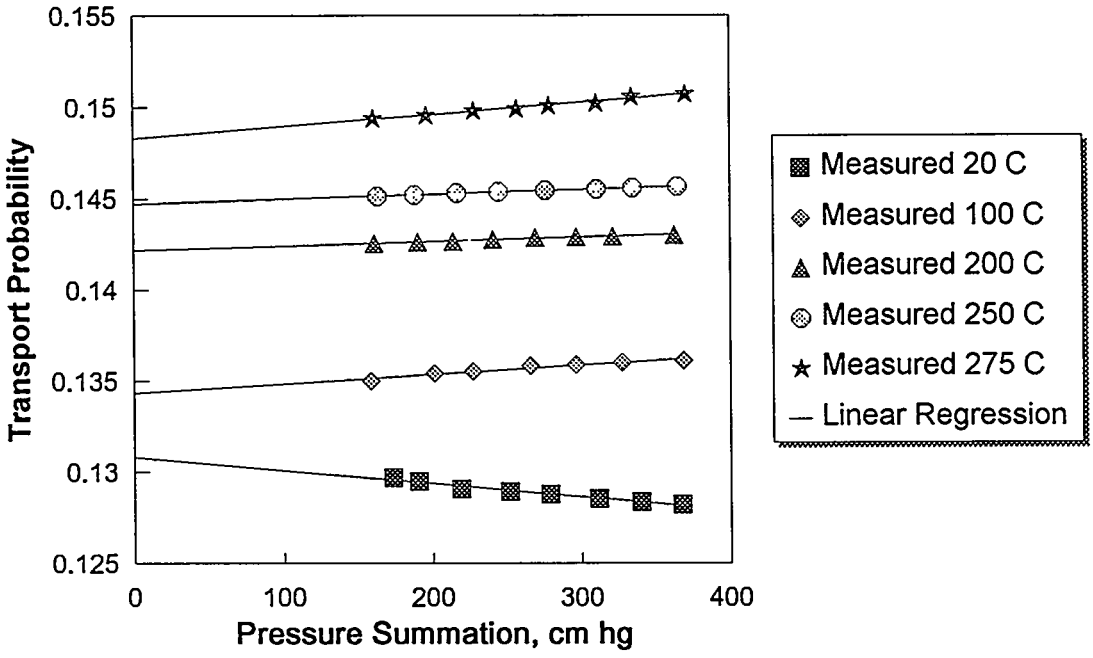

Fig. 4. Transport probability for He flow data measured at several temperatures through alumina membrane having 5 Å mean pore radius.

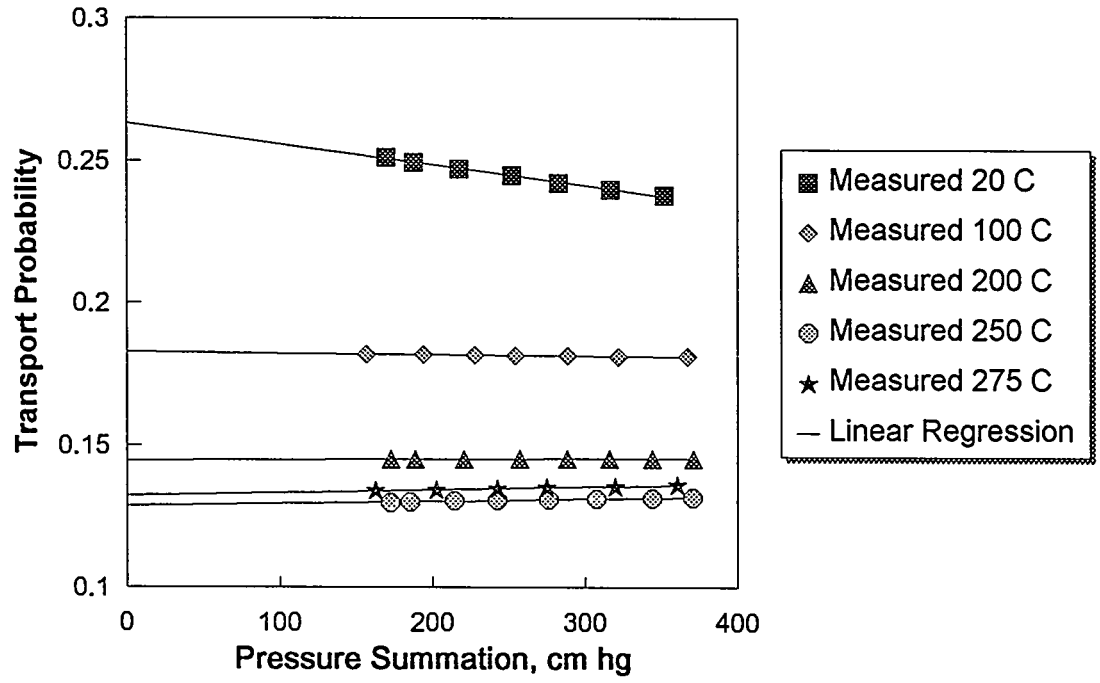

Fig. 5. Transport probability for carbon tetrafluoride flow data measured at several temperatures through alumina membrane having 5 Å mean pore radius.

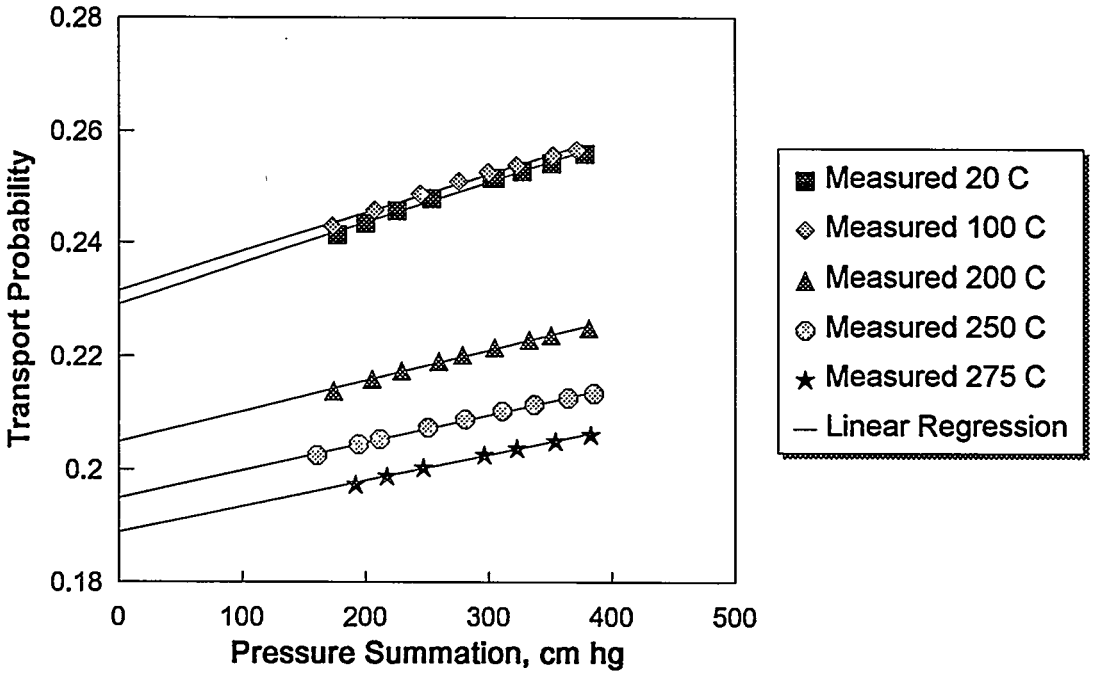

Fig. 6. Transport probability for helium flow data measured at several temperatures through alumina membrane having 30 Å mean pore radius.

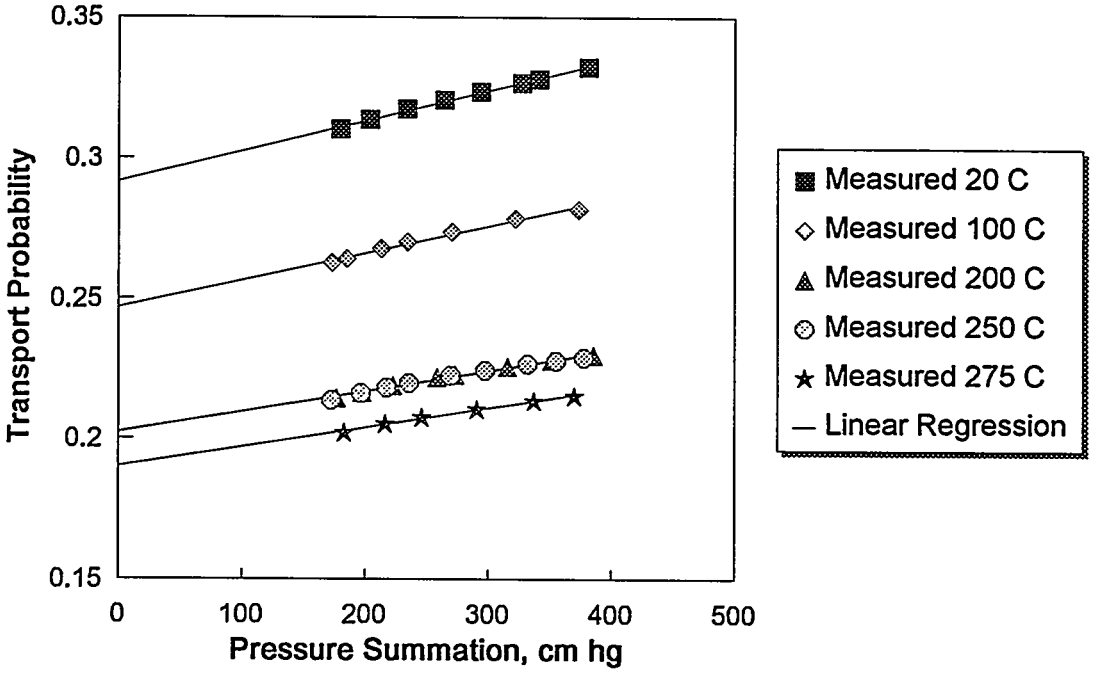

Fig. 7. Transport probability for carbon tetrafluoride flow data measured at several temperatures through alumina membrane having 30 Å mean pore radius.

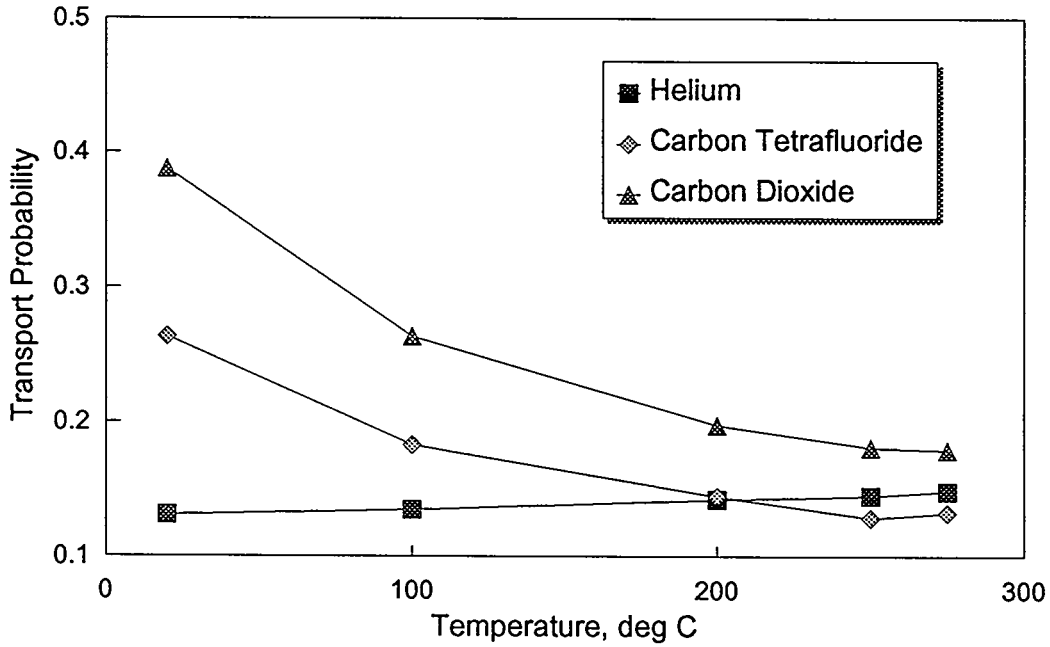

Fig. 8. Zero pressure transport probability measured at various temperatures on alumina membrane having 5 Å mean pore radius.

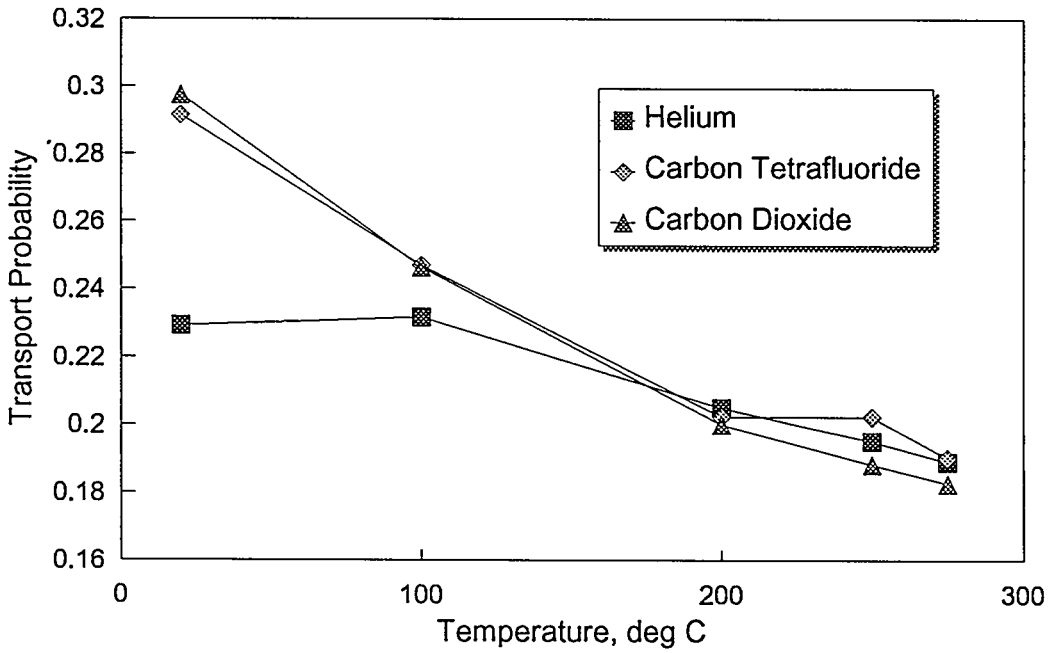

Fig. 9. Zero pressure transport probability measured at various temperatures on alumina membrane having 30 Å mean pore radius.

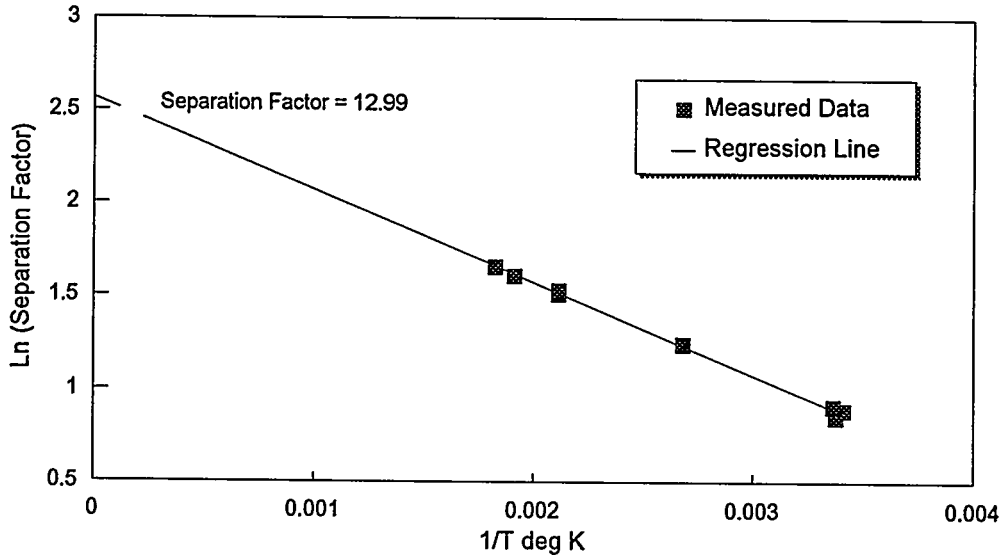

Fig. 10. He/CF_4 separation factors measured on alumina membrane having mean pore radius of 5 Å.

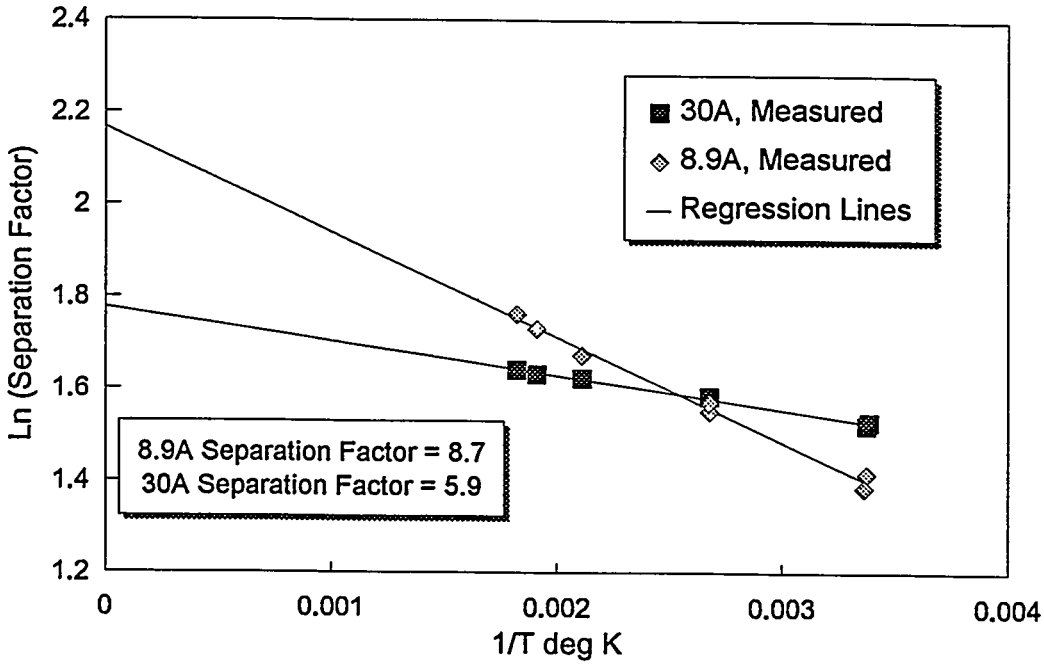

Fig. 11. He/CF_4 separation factors measured on alumina membranes having mean pore radii of 30 Å and 8.9Å.

temperature, the data show a separation factor of 4.60 (approximately the Knudsen value), and the separation factors increase only slightly at higher temperatures. Separation factors determined at room temperature for the 8.9 Å membrane are considerably lower than for the 30 Å membrane due to increased surface flow of the heavier gas in the small pores. The separation factors of the 8.9 Å membrane increase with temperature at a relatively high rate as adsorption and surface flow are reduced and the benefits of smaller pore size are realized.

A total of 15 alumina membranes have been tested in the high temperature flow test system. The mean pore radii of these membranes ranged from 30 Å to about 2.5 Å. The separation factors determined for these membranes at room temperature and at the high temperature limit are plotted against the membrane mean pore size in Fig. 12. These empirical values show good agreement with the trends predicted by the transport model and shown earlier in Fig. 1.

The flow tests that have been performed on 15 membranes to date have provided a large database of gas transport data at several temperatures up to 275°C. These data, used in conjunction with independently determined gas adsorption data, will permit the temperature dependencies of gas transport mechanisms to be determined and incorporated into the gas transport model. A variable volume adsorption measurement system has been upgraded to permit gas adsorption to be measured on membrane materials at temperatures up to 275°C. The variable volume consists of a cylinder and a piston. The pressure and temperature of the gas in the cylinder are measured by a calibrated pressure transducer and thermocouple as the volume of the cylinder is changed. A fixed amount of gas is introduced into the cylinder. A sample holder of predefined volume is connected to the variable volume. The holder is enclosed in a heated chamber that provides temperatures up to 275°C. Using the volume, pressure, and temperature determinations, the mass of gas present in the gas phase can be accurately determined over a range of pressures. The difference between the initial mass of gas introduced and the amount in the gas phase is the amount adsorbed.

The variable volume adsorption measurement system is being used to measure the adsorption of gases on alumina membrane material over a range of pressures and at various temperatures up to 275°C. The test gases being used include helium, carbon dioxide, and carbon tetrafluoride, i.e., the same gases used to evaluate membranes in the high temperature flow test system. These adsorption data will be used with the existing analytical expression (and others if needed) for the various transport mechanisms to regression fit the permeability data as shown in Figs. 2 through 7. With these regression equations, separation factors at different temperatures can be calculated (as in Fig. 1).

REFERENCES

(None)

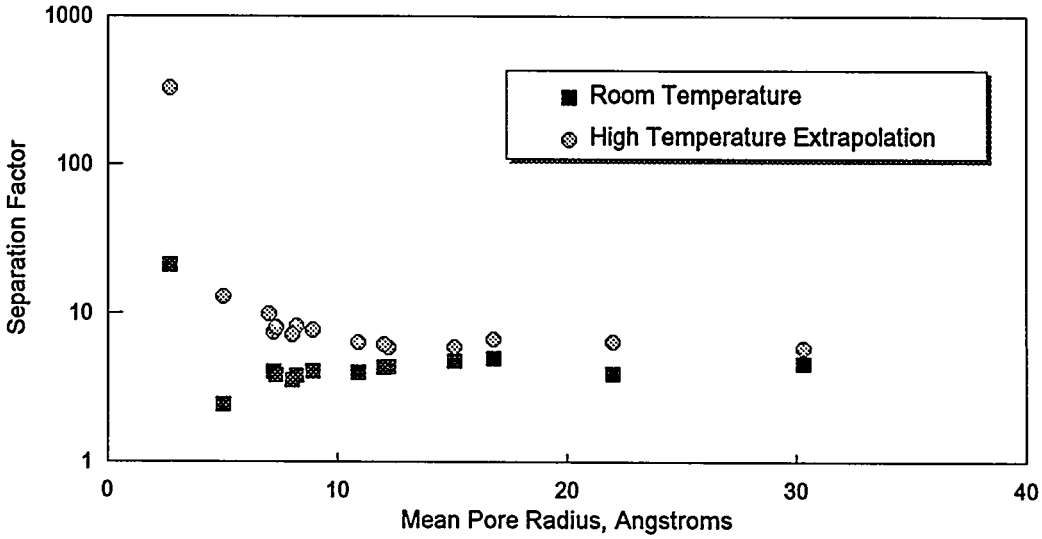

Fig. 12. Summary of He/CF_4 separation factors at room temperature and at the high temperature limit determined from flow data.

CARBON FIBER COMPOSITE MOLECULAR SIEVES

T. D. Burchell

Oak Ridge National Laboratory
P.O. Box 2008
Oak Ridge TN 37831-6088

ABSTRACT

The separation of gases is widely effected via the Pressure Swing Adsorption process. Here we report the synthesis and characterization of a novel adsorbent carbon materials called Carbon Fiber Composite Molecular Sieve. The unique combination of properties exhibited by this material makes it ideal for application in Pressure Swing Adsorption Systems, where its utilization will result in significant gains in process economics.

INTRODUCTION

A novel adsorbent carbon composite material has been developed comprising carbon fibers and a binder. The materials, called Carbon Fiber Composite Molecular Sieve (CFCMS), was developed through a joint research program between Oak Ridge National Laboratory and the University of Kentucky, Center for Applied Energy Research. The composite is strong and porous, allowing fluids to easily flow through the material. At the same time, when activated, the carbon fibers provide a high micropore surface area (> 1900 m^2/g) capable of rapid adsorption and desorption. The activated fiber micropore distribution is very narrow, with mean micropore sizes < 10Å, allowing molecular sieving on the basis of molecular size and shape. A potentially large application for our carbon fiber composite molecular sieve (CFCMS) material is gas separation using the Pressure Swing Adsorption (PSA) process.

Separation by adsorption is based on the selective accumulation of one or more components of a gas mixture on the surface of a microporous solid. When a gaseous mixture is exposed to an absorbent for sufficient time, an equilibrium is established between the adsorbed phase and the gas phase. The gas phase becomes richer in the less selectively adsorbed component. The attractive forces responsible for adsorption are of the van der Waals type. Desorption can be achieved either by increasing the temperature of the system or by reducing the adsorbate pressure. The desorption step also regenerates the adsorbent surface for reuse during the subsequent adsorption step. Thus, the adsorptive separation process consists of a cyclic sequence of adsorption and desorption steps. When desorption is achieved by decreasing the pressure, the process is called pressure swing adsorption. One of the components of a gas mixture is selectively adsorbed at higher partial pressure and desorbed subsequently by lowering the partial pressure. The change in partial pressure of the component gas can be caused either by decreasing the total pressure, changing the composition of the gaseous mixture, or by a combination of both.

Here we report the synthesis and characterization of CFCMS material, particularly with respect to structure, physical properties, and the effect of burn-off on crush strength. The activation, pore structure and adsorptive behavior of CFCMS is reported elsewhere.[1]

EXPERIMENTAL

CFCMS materials were subjected to microstructural examination using an 1S1 SS40 scanning electron microscope. Fiber length distributions were obtained by repetitive measurements on SEM photomicrographs. Macropore size data were obtained using a Micromeritics Autopore II mercury intrusion apparatus. Intrusion measurements were performed over the pressure range vacuum (~10μm Hg) to 90,000 psia. Equilibration times of 10 and 60 seconds were used for the low and high pressure measurements, respectively. Samples of CFCMS were compression tested using an Instron electromechanical test machine with a crosshead speed of 0.5 mm/min. CFCMS samples were steam activated for various times to achieve burn-offs in excess of 40%.

RESULTS AND DISCUSSION

CFCMS Synthesis

The CFCMS material was fabricated at ORNL using a process initially developed by the DOE for the production of thermal insulators for NASA space missions.[2] Petroleum pitch derived carbon fibers were mixed in a water slurry with powdered phenolic resin. The slurry is transferred to a molding tank and the water drawn through a porous mold under vacuum. The resulting green artifact is dried, cured in air at 60°C, and stripped from the mold. The composite is cured at ~150°C in air prior to carbonization under an inert gas. The CFCMS synthesis route is illustrated in Figure 1. A schematic diagram of the molding arrangement is shown in Figure 2. The fabrication process allows the manufacture of slab or tubular forms. Moreover, we believe that it will be possible to mold contoured plates, and tubes, to near net shape via this synthesis route. Once carbonized, CFCMS is readily machined to more complex geometries. The carbonized bulk density of our CFCMS material is typically 0.3-0.4 g/cm^3.

Characterization

Figure 3 (x200 magnification) shows the structure of our CFCMS material. The chopped fibers are bonded at their contact points. The carbon fibers are approximately 10-20 μm diameter, whereas the macro-voids between the fibers are typically >30 μm in size. The resultant open structure allows free flow of fluids through the material and ready access to the carbon fiber surface. Figure 4 shows a histogram of the lengths of the carbon fiber used for the production of our standard product. The distribution mode is ~400 μm and the fiber lengths are widely distributed and range from 100 to 1000 μm. These data are shown in Figure 5 as a probability plot, and indicate the data to be reasonably represented by a normal distribution with a mean of approximately 450 μm. Mercury porosymetry data taken on the CFCMS material in the unactivated condition are shown in Figure 6. These data indicate the macropore size range to be approximately 10-100 μm. These macropores are the voids between the fibers, and the mercury porosymetry data for macropore sizes are in agreement with the visual observations made from SEM images (Fig. 3).

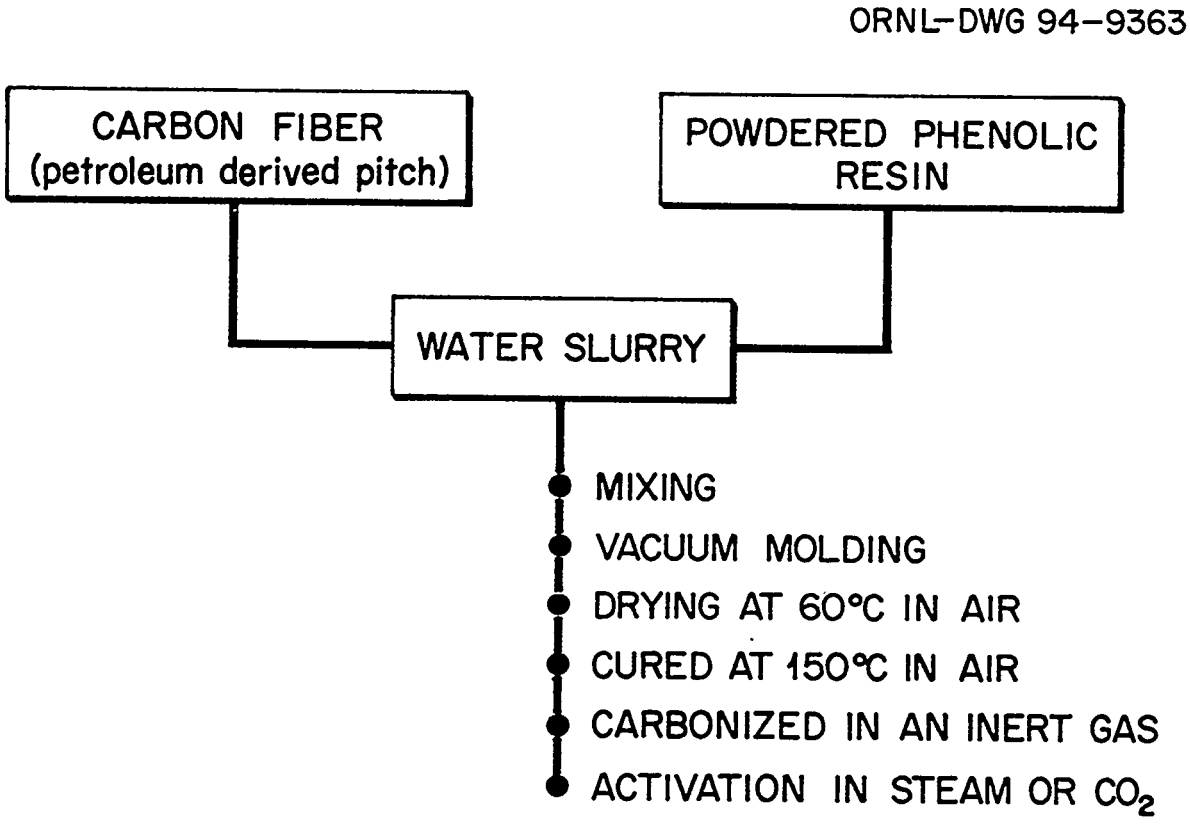

Fig. 1. The synthesis route for CFCMS.

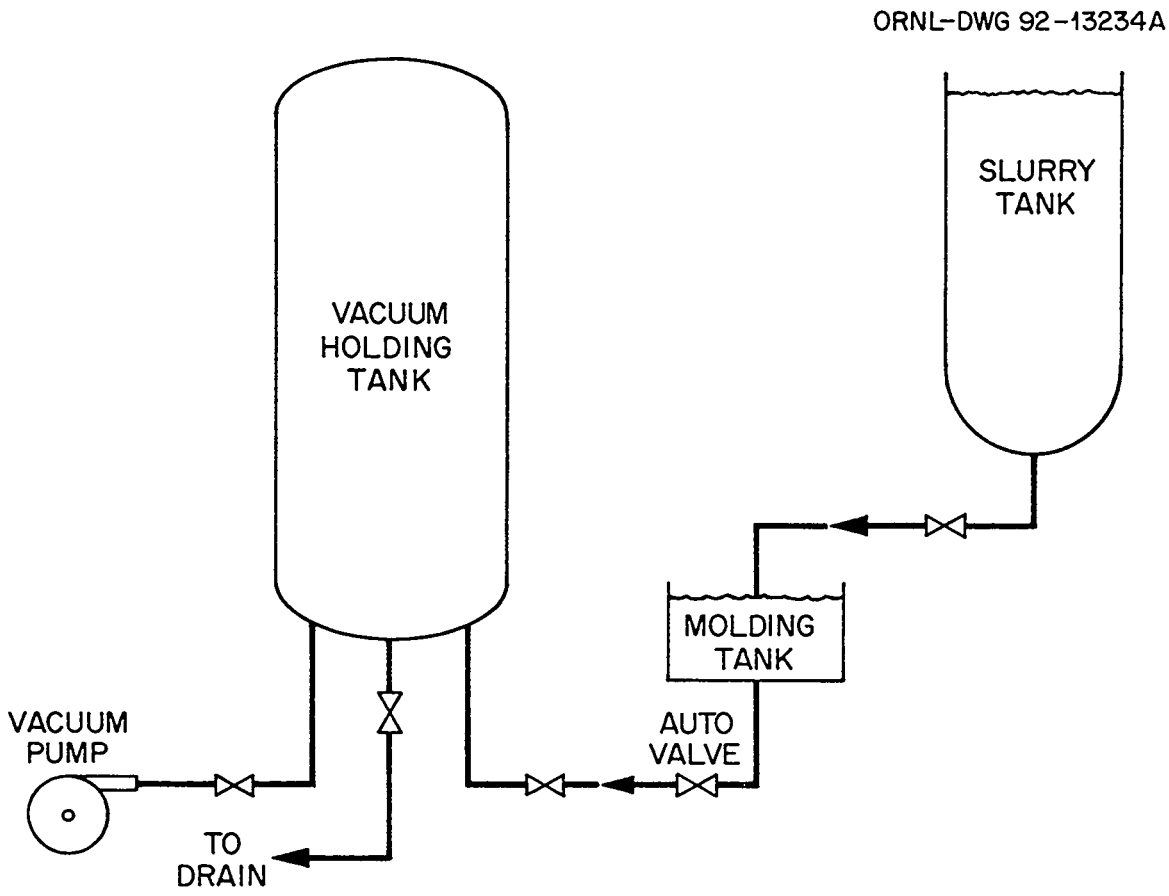

Fig. 2. Schematic illustration of the CFCMS molding apparatus.

Fig. 3. SEM micrograph of carbon fiber composite molecular sieve (magnification x 200).

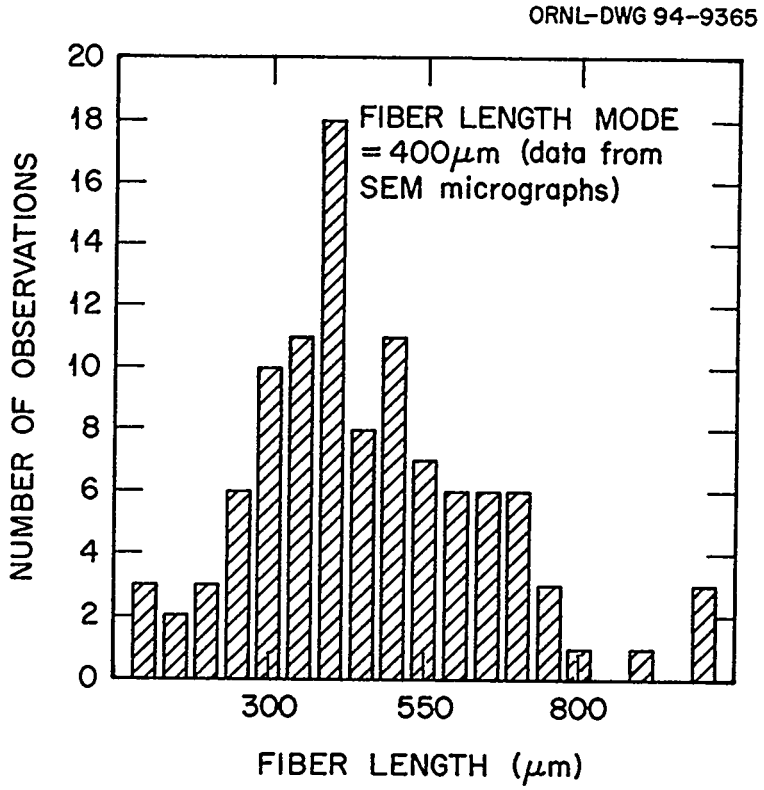

Fig. 4. CFCMS carbon fiber length histogram

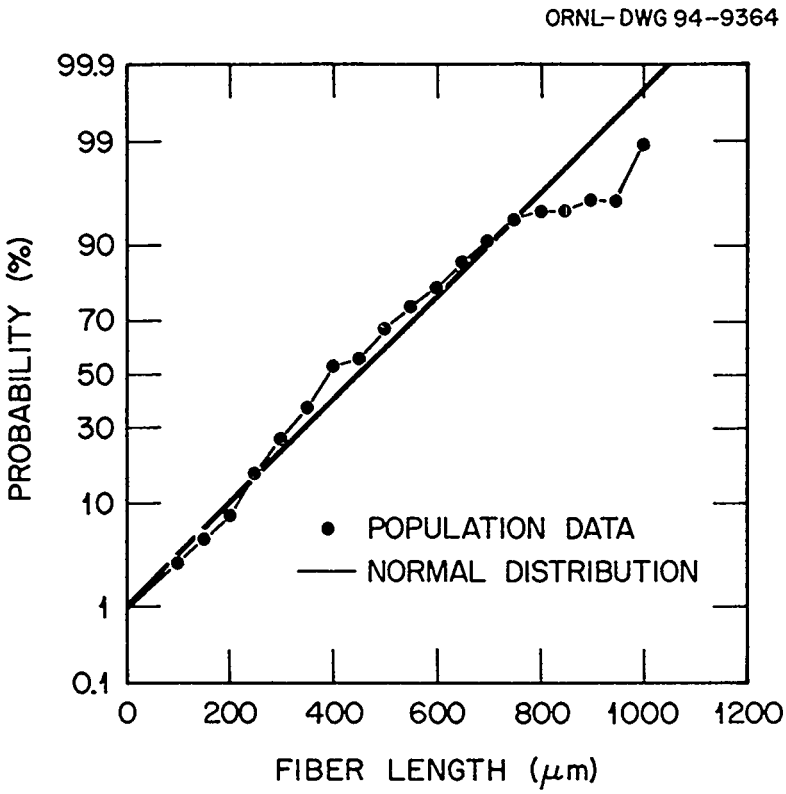

Fig. 5. Probability plot showing fiber length distribution is approximately normal.

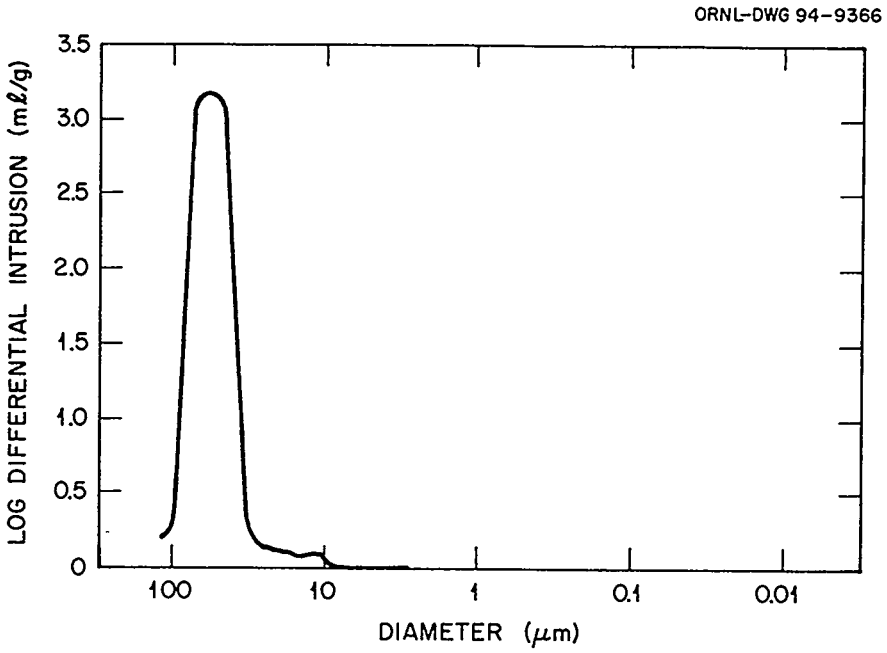

Fig. 6. CFCMS macropore size distribution obtained from mercury intrusion data.

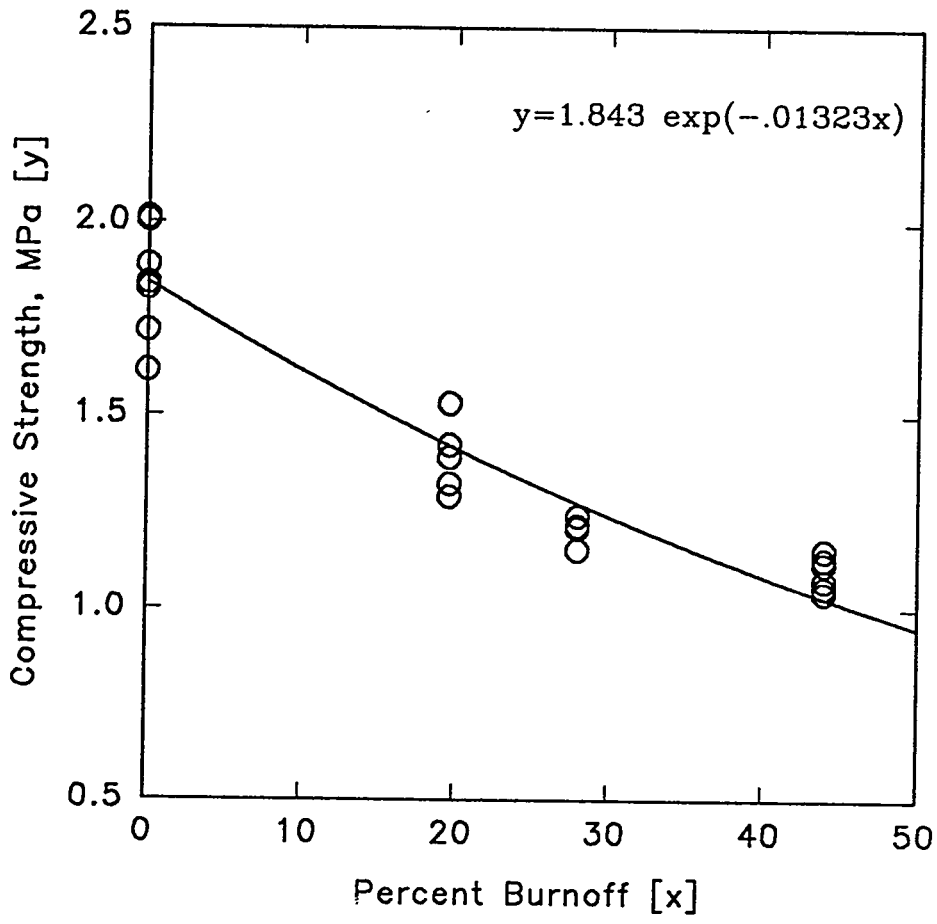

Fig. 7. The effect of burn-off on CFCMS crush strength.

The effect of burn-off on crush strength is shown in Figure 7. The strength is degraded by less than 50% at burn-offs up to 40%. Moreover, the reduction of strength is almost linear with burn-off, rather than the strong exponential dependance more typically exhibited by thermally oxidized carbons.

Conventional activated carbons and carbon molecular sieves (CMS) are granular. During operation in a PSA system, granular materials can settle resulting in the formation of channels which allow the fluid stream to by-pass the adsorbent. The height of a PSA vessel is limited by the relatively low crush strength of granular carbons. CFCMS is unique in that it is monolithic and can be manufactured in large sizes, potentially eliminating the attrition, dusting, and settling problems associated with granular carbons. Moreover, current restrictions on PSA bed size and orientation will be removed because CFCMS is a strong monolith. PSA system efficiency will be improved by the superior gas absorption kinetics[1] of CFCMS materials compared to conventional CMS material.

CONCLUSIONS

A novel porous monolithic carbon fiber composite material, known as CFCMS, has been developed and shows considerable potential for use in PSA gas separation systems. The material can be fabricated in large sizes yet retains the advantageous gas adsorption and separation properties of its precursor carbon fibers. The CFCMS material structure contains large voids (>30 μm) between the 10-20 μm diameter fibers which allows for free flow of fluids through the material. A crush strength of >1 MPa is retained after activation to 40 wt% burn-off.

ACKNOWLEDGEMENTS

The author would like to acknowledge the contributions of his coworkers in this project, Charlie Weaver, Bill Chilcoat, Loren Fuller and Mike Rogers. Research sponsored by the U.S. Department of Energy, Office of Fossil Energy, Advanced Research and Technology Development Materials Program [DOE/FE AA 15 10 10 0, Work Breakdown Structure Element ORNL-1(E)] under contract DE-AC05-84OR21400 with Martin Marietta Energy Systems, Inc.

REFERENCES

1. Frank Derbyshire, "Activation and Micropore Structure Determination of Carbon Fiber Composite Molecular Sieves" In. *Proc. Fossil Energy Materials Conference*, Oak Ridge, Tennessee, May 10-12, 1994.

2. George C. Wei and JM Robbins, "Carbon-Bonded Carbon Fiber Insulation for Radioisotope Space Power Systems," *Ceramic Bulletin, Vol. 64, No. 5*, p. 691, 1985.

ADVANCED MATERIALS, ELECTROCHEMICAL STUDIES, AND ELECTROCHEMICAL CATALYSIS STUDIES FOR SOLID OXIDE FUEL CELLS

T. R. Armstrong, J. L. Bates, L. R. Pederson, P. J. Raney,
J. W. Stevenson, and W. J. Weber

Pacific Northwest Laboratory[1]
P. O. Box 999
Richland, WA 99352

ABSTRACT

Lattice expansion, phase stability, and oxygen permeation behavior of interconnect materials, particularly the lanthanum calcium chromites and the lanthanum strontium chromites, have been examined over a wide range of temperatures and oxygen partial pressures. In an operating solid oxide fuel cell, the interconnect must be stable in both oxidizing and reducing environments. Under reducing conditions, below approximately 10^{-10} atm. oxygen partial pressures, oxygen vacancies can be created depending on the temperature and the extent of strontium or calcium substitution for lanthanum. Reduction caused a substantial increase in the unit cell volume and isothermal linear expansion behavior. For $La_{0.70}Ca_{0.30}CrO_3$,the isothermal linear expansion change at 1000°C was 0.3 percent in Ar-4% H_2-3% H_2O referenced to air. Reduction followed by re-oxidation of the chromites was accompanied by a segregation of a calcium-rich phase to the grain boundary surfaces and microcracking, with a significant loss in mechanical strength as well as electrical conductivity. Oxygen permeation rates through sintered lanthanum were below 0.05 sccm/cm^2 for 3 mm-thick disks. This small oxygen flux may serve to maintain the interconnect at oxygen partial pressures above those where deleterious reactions can occur.

INTRODUCTION

The interconnect in a solid oxide fuel cell must be simultaneously stable in both oxidizing and reducing environments. The reducing or fuel side may experience oxygen partial pressures from 10^{-18} to 10^{-6} atmospheres, while the oxidizing side may have oxygen partial pressure from 10^{-6} to 4 atm. Such extreme conditions limit the possible candidate materials to either lanthanum or yttrium chromites. In the past decade much work has centered on deriving air-sinterable chromites and understanding their physical properties; little work, however, has focused on the stability of the chromites in dual (reducing/oxidizing) environments.[1-3]

Anderson[4,5] has shown that oxygen vacancies form in p-type materials, such as the doped lanthanum or yttrium chromites, below 10^{-10} atmospheres at 1000°C and is accompanied by a corresponding decrease in the electrical conductivity. Schafer and Schmidberger[1] have reported that linear expansion of doped chromites increases with both decreasing oxygen partial pressure

---

[1]Operated by Battelle Memorial Institute for the US Department of Energy under Contract DE-ACC06-76RLO 1830

and increasing dopant concentration (Ca or Sr). Miliken et al.[3] observed immediate and drastic decreases in the mechanical strength of the interconnect upon exposure to a reducing environment. Sakai[2] found that both Ca or Sr modified lanthanum chromite showed phase segregation upon prolonged exposure to dual (oxidizing/reducing) environments.

STABILITY OF CHROMITE INTERCONNECTS

The use of different materials (e.g., combinations of manganite, chromite, stabilized zirconia, and nickel) in state-of-the-art high-temperature SOFCs results in several materials-related fabrication and performance problems. One of the most critical technical concerns is the physical, chemical, and electrical stability of the interconnect (typically a doped lanthanum chromite) in the dual SOFC environment (i.e., simultaneous exposure to oxidizing and reducing atmospheres at elevated temperature). During operation in this environment, the interconnect must maintain adequate electrical conductivity while remaining gas tight. In addition, interactions with other SOFC components and changes in physical dimensions must be minimized. The dependence of the physical properties of sintered lanthanum chromites upon ambient oxygen partial pressure and temperature (using electrical conductivity, dilatometry, thermogravimetric analysis, and oxygen permeation measurements) were studied. $La_{1-x}A_xCrO_3$ and $Y_{1-x}Ca_xCrO_3$, where A is Ca or Sr and x was varied from 0.1 to 0.4 were evaluated in this study. The oxygen partial pressure was varied using a CO_2 buffered Ar -4%H_2 gas system, enabling expansion measurements to be made over a partial pressure range from 10^{-5} to 10^{-18} atmosphere at 800, 900, and 1000°C.

Figure 1 shows a plot of the isothermal linear expansion at 800, 900, and 1000°C for $La_{0.7}Ca_{0.3}CrO_3$ (denoted LCC-30) as a function of oxygen partial pressure. This sample shows no effect of reducing environment from ambient pressure to 10^{-9} atmosphere at 1000°C. At lower oxygen partial pressures the sample steadily expands, reaching a maximum expansion of ≈0.3% at 10^{-18} atmospheres. Figure 1 also clearly shows that the onset of expansion moves towards lower oxygen partial pressures with decreasing temperature, indicating an increase in activation energy necessary for the expansion to occur. Figure 2 is a plot of the isothermal linear expansion of $La_{0.7}Ca_{0.3}CrO_3$ as a function of temperature and time in Ar-4%H_2. The slopes of the expansion versus time plots indicate that the activation energy (kinetics) for expansion increases with increasing temperature. The slope change from 0.0006 %/min at 700°C to 0.013 %/min at 900°C.

Figure 3 shows the isothermal linear expansion of both Ca and Sr doped lanthanum chromites as a function of the dopant concentration at 1000°C in Ar-4% H_2. A linear increase in linear expansion was observed with increased Ca concentration. Results from Sr doped chromites indicate that dopant size has little effect on the linear expansion. Figure 3 also shows the increase

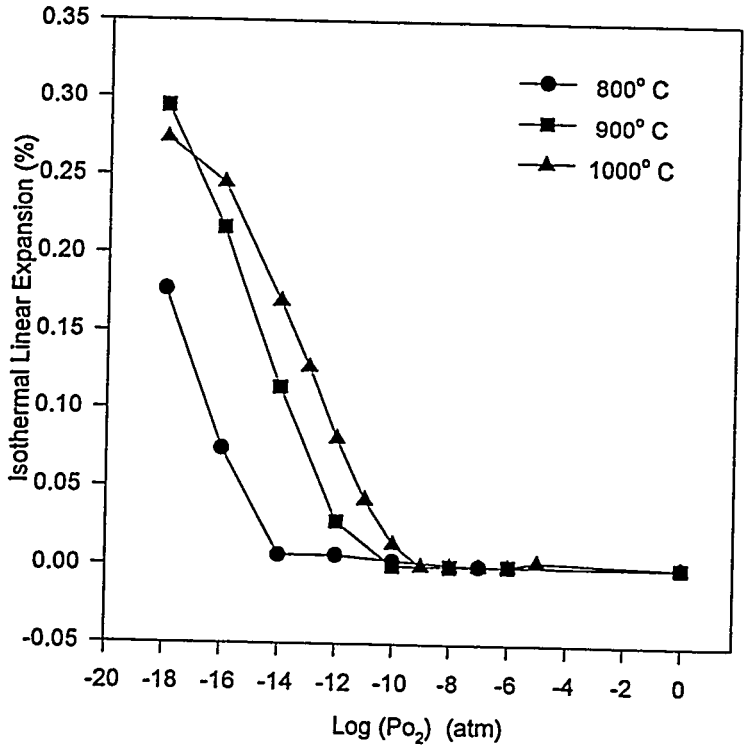

Figure 1. Isothermal linear expansion for LCC-30 as a function of oxygen partial pressure.

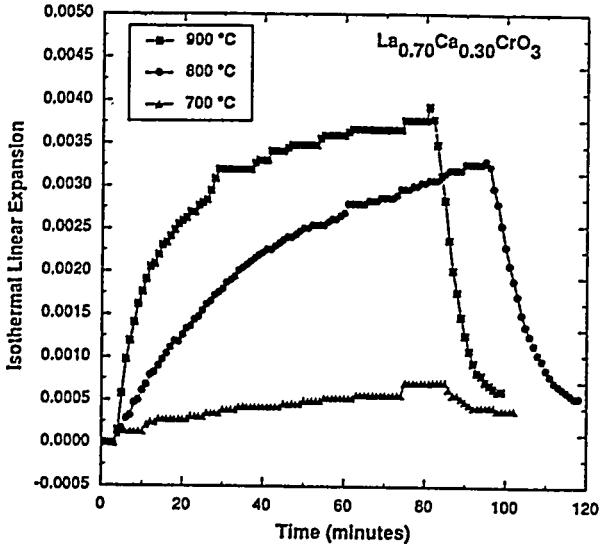

Figure 2. Isothermal linear expansion for LCC-30 as a function of time after introduction of 4% hydrogen in argon.

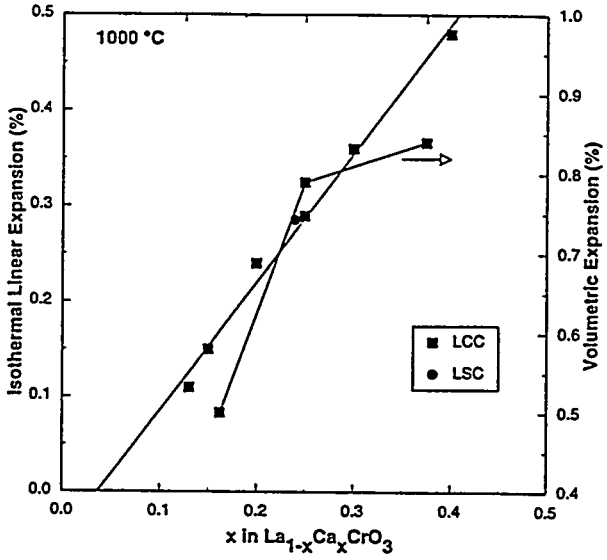

Figure 3. Isothermal linear expansion for LCC and LSC interconnect materials as a function of dopant concentration at 1000°C in Ar-4% H_2.

in unit cell volume upon reduction at 1000°C. The figure shows that the unit cell volume change is directly proportional to the concentration of dopant. The observed increase in linear expansion of the sample corresponds directly to the increase in the unit cell size.

The expansion observed in these samples can be directly related to the formation of oxygen vacancies as reported by Anderson.[4,5] Removal of oxygen from the perovskite lattice results in a decrease in the shielding of the anions by the cations. This reduction in the shielding causes the positively charged cations to repel each other, resulting in a net volumetric increase in the unit cell and linear expansion of the sample.

It is well known that A-site enriched chromites undergo liquid phase sintering due to the formation of transient liquids at elevated temperatures. These liquids are a result of calcium chromate exsoluting from the perovskite lattice at ≈700 to 1000°C and then melting at 1050°C. At 1200°C, the calcium chromite appears to redissolve into the perovskite lattice. After sintering, these chromites contain liquid-phase remnants. Evidence of liquid formation has not been reported in A-site depleted samples, although these have been found to contain isolated Cr-rich deposits. It has not been reported in the literature whether this phenomena of chromate exsolution is reversible when the samples are thermally cycled or how the remnant liquid phase in the microstructure reacts when exposed to reducing environments.

The microstructure of $La_{1-x}Ca_xCrO_3$ samples was examined after exposure to reducing environments, oxidizing environments (control), and/or sequential exposure to reducing and oxidizing conditions. Control samples examined after sintering or after heating in air at 1000°C showed no discernable phase segregation or impurity phases at the grain boundaries. Similarly, samples exposed to severe reducing conditions (10^{-18} atm at 1000°C) showed no phase segregation. However, $La_{1-x}Ca_xCrO_3$, particularly where x was 0.3 or greater, (Figure 4) showed a change in the fracture mechanism after exposure to a reducing environment. Prior to reduction, $La_{0.7}Ca_{0.3}CrO_3$ showed intergranular fracture, as shown in Figure 4. After reduction, however, the fracture mechanism changed to intragranular fracture. This indicates that grains became weakened as a result of the large lattice expansion that these samples experienced.

Samples undergoing sequential exposure to reducing and oxidizing environments showed other microstructural features. Figure 5 shows micrographs of $La_{0.7}Ca_{0.3}CrO_3$ after being reduced at 10^{-18} atm at 1000°C and then being re-oxidized. The control sample, prior to reduction and re-oxidation, showed no discernable impurity or secondary phases present at the grain boundaries (Figure 5). However, after sequential exposure to a reducing and oxidizing environment, a Ca- and Cr-rich secondary phase was apparent in the microstructure. This phase is most likely calcium chromate and an amorphous phase similar in composition. As shown in Figure 4, the fracture mechanism changed following reduction. After re-oxidation, however, the fracture mechanism was intragranular. Intragranular fracture occurred in the sequentially exposed

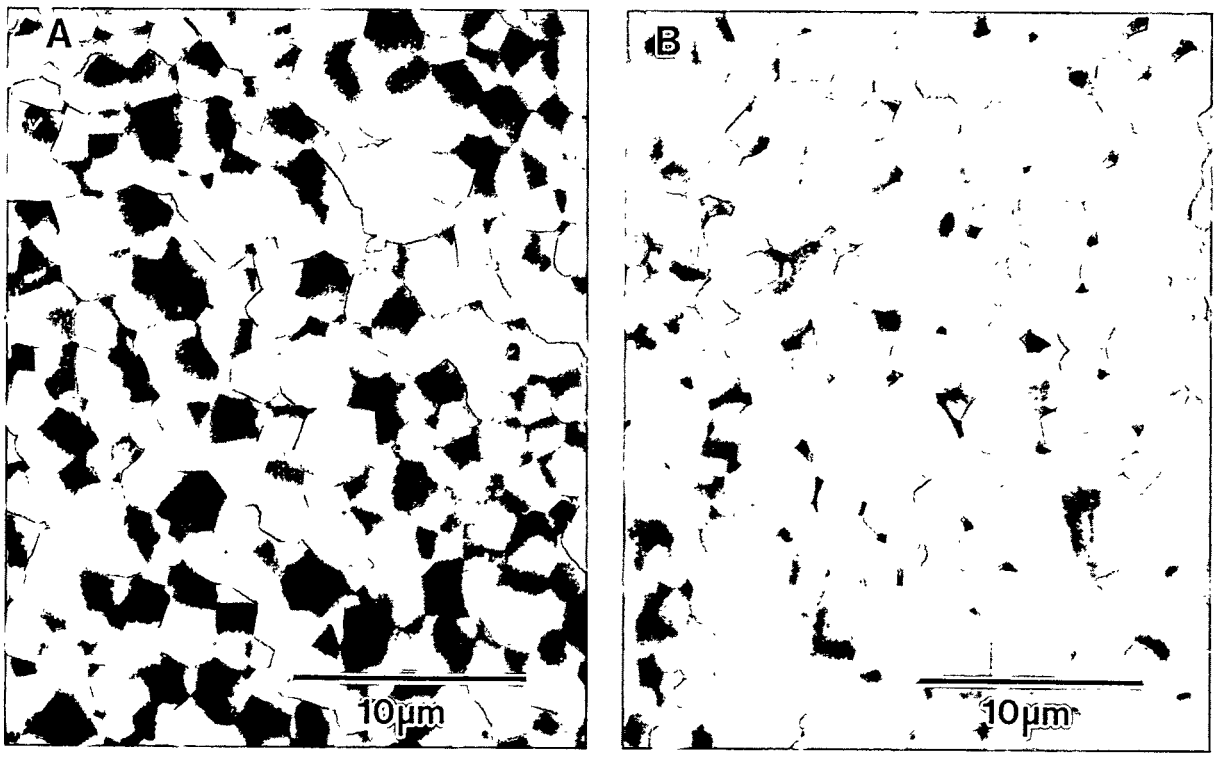

Figure 4. Microstructure of LCC-30 fracture surface prior to reduction (control) A) and following reduction B). No obvious intergranular phase formation was apparent, note change in fracture mechanism.

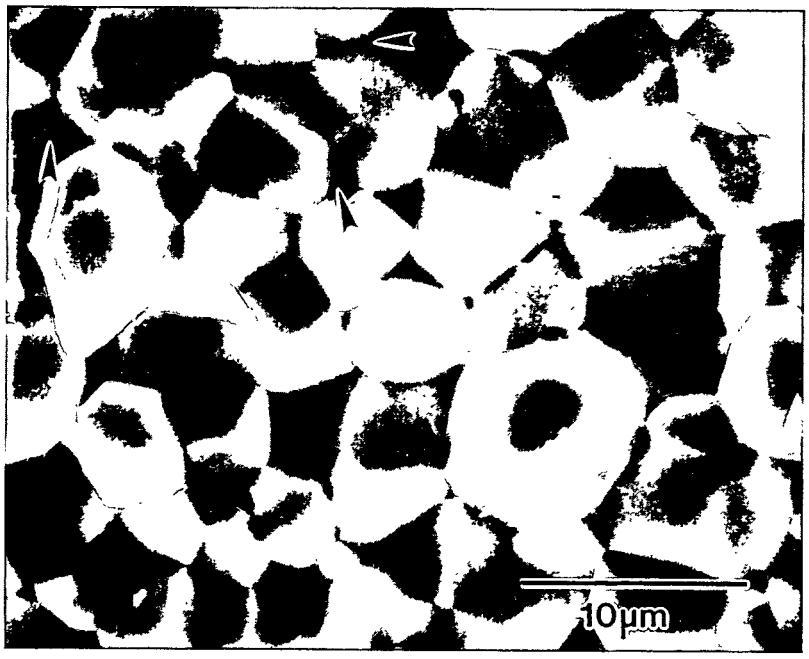

Figure 5. Micrograph of LCC-30 fracture surface following reduction and re-oxidation. Intergranular segregation of a calcium-rich phase was observed.

samples due to the presence of a weak interfacial phase, either calcium chromate or an amorphous phase.

The presence of calcium chromate can be supported by thermogravimetric analysis (TGA) of the $La_{1-x}Ca_xCrO_3$ samples during the oxidation-reduction process. Because oxygen is being removed from the lattice it can be directly monitored by weight loss or gain measurement. Figure 6 shows a typical TGA plot of $La_{0.7}Ca_{0.3}CrO_3$ during reduction and reoxidation. The weight loss due to oxygen removal from the lattice corresponds directly with the samples linear expansion. Further, upon reoxidation there is an net gain in mass of oxygen. This may be direct evidence of the formation of calcium chromate in the microstructure, since the formation of this phase is accompanied by a net grain in oxygen. Repeated reduction and re-oxidation led to much enhanced rates of weight loss and gain, indicating a permanent change in microstructure.

The chromite interconnect in an SOFC should be gas-tight since, in multi-stack planar designs, it directly connects the fuel electrode of one cell with the air electrode of another. If the interconnect were not gas-tight, part of the fuel would be consumed without producing any electricity. Partial reduction of the interconnect at the fuel electrode can create oxygen vacancies and support ionic transport of oxygen from the air to the fuel side. Estimations of the likely oxygen flux in these materials vary considerably - by more than two orders of magnitude.[6,7]

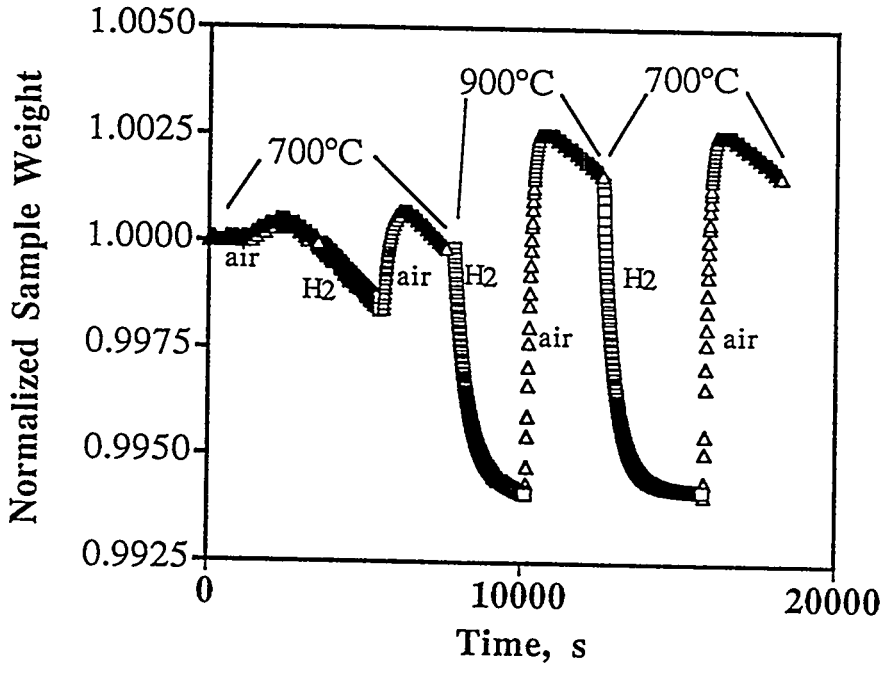

Figure 6. TGA results for LCC-30 in air and in 4% hydrogen in argon.

Oxygen fluxes through sintered LCC pellets were determined using mass spectrometry. Flowing air or oxygen was present on one side, while 4% hydrogen/argon was introduced on the other. The seals were shown to be helium leak-tight. Rates of permeation were calculated both from the quantity of water that was produced on the hydrogen side and from the quantity of hydrogen that was consumed. Oxygen permeation fluxes as a function of temperature are given in Figure 7, while leakage currents as a function of the oxygen partial pressure are given in Figure 8. Permeation rates are in reasonably good agreement with the findings of Yokokawa et al.[6], but considerably smaller than those given by Yasuda and Hikita.[7] It is noted that a small oxygen permeation may be desirable, because the effective oxygen partial pressure within the interconnect may be maintained in a regime where lattice expansion in a reducing atmosphere can be avoided.

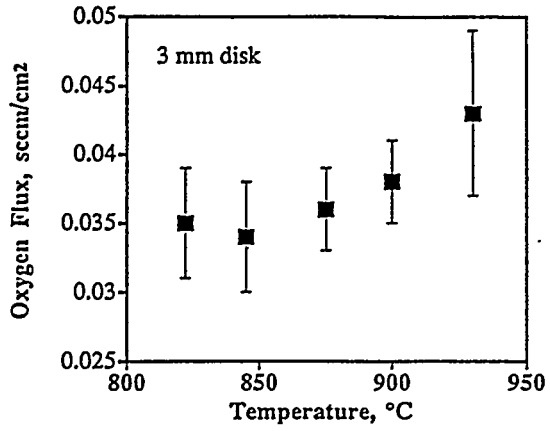

Figure 7. Oxygen permeation through an LCC-30 disk as a function of temperature. Rates were measured by mass spectrometry for air versus 4% hydrogen in argon.

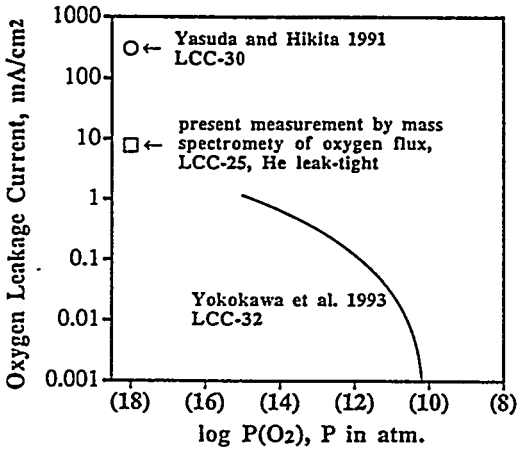

Figure 8. Oxygen leakage currents through LCC interconnect material, including the data of Yokokawa et al.[6] and Yasuda and Hikita.[7]

REFERENCES

1. W. Schafer and R. Schmidberger, in High Tech Ceramics, Ed. by P. Vincenzini, Elsevier Science Publishers, pp.1737-1742 (1987).

2. N. Sakai, T. Kawada, H. Yokokawa, and M. Dokiya, in Science and Technology of Zirconia V, pp.764-775 (1994).

3 C. Milliken, S. Elangovan, and A. Khandkar, in Proceedings of the 3rd International Symposium on Solid Oxide Fuel Cells, Eds. S. C. Singhal and H. Iwahara , The Electrochemical Society, Pennington, NJ, p.335 (1993).

4. H. U. Anderson, in Proceedings of the 14th Riso International Symposium on Materials Science, Roskilde, Denmark, September 6-10, pp.1-18 (1993).

5. H. U. Anderson, J. H. Kuo and D. M. Sparlin, in Proceedings of the 1st International Symposium on Solid Oxide Fuel Cells, Ed. by S. Singhal, The Electrochemical Society, Pennington, NJ, pp.111-128 (1989).

6. Y. Yasuda and T. Hikita, in Proceedings of the 2nd International Symposium on Solid Oxide Fuel Cells, Eds. F. Gross, P. Zegers, S. C. Singhal, and O. Yamamoto, The Electrochemical Society, Pennington, NJ, pp. 645-652 (1991)

7. H. Yokokawa, T. Horita, N. Sakai, T. Kawada, M. Dokiya, and B. A. van Hassel, in Proceedings of the 3rd International Symposium on Solid Oxide Fuel Cells, Eds. S. C. Singhal and H. Iwahara, The Electrochemical Society, Pennington, NJ, pp. 364-373 (1993).

TESTING OF FULL SIZE FIBER REINFORCED HOT-GAS FILTERS FABRICATED BY CHEMICAL VAPOR DEPOSITION

R. G. Smith, J. H. Eaton, B. L. Weaver, J. L. Kahnke

3M Company
Bldg 203-1-01, 3M Center
St. Paul, MN 55144-1000

The goal of the work described here has been to develop a hot gas candle filter which is light weight, has a thin wall, resists mechanical and thermal shock, and is resistive to alkali attack. A ceramic fiber reinforced, ceramic matrix composite approach has been followed to fabricate this new candle filter. Filter testing results and mechanical property testing results on as fabricated and tested filters will be presented.

Based on the first test results of two ceramic composite candle filters at the Westinghouse Science and Technology Center in March of 1993 improvements were made in the filter's construction and fabrication processing. Twelve improved full size, 60 mm diameter by 1575 mm length, filters were fabricated. In this extension to the contract six of the ceramic composite candle filters were tested at the Westinghouse Science and Technology Center in December of 1993. All six filters met or exceeded performance requirements set for them.

The filters were tested for 172 hours at 820 C and a 689 kPa operating pressure in a simulated PFBC environment using natural gas heating and the Old and Red Grimethorpe ashes. In addition, 14 thermal shock tests were completed over a twelve hour period. Thirty four samples were taken on the clean side of the test vessel with an average ash concentration of 2.6 ppm versus the 2000 ppm ash feed rate. All samples were below the 10 ppm upper limit requirement. A uniform base pressure of 7.5 kPa was established at 3.5 cm/sec face velocity and the filters cleaned with 2070 kPa air pulses into the chamber after the filter pressure increased to 7.5 kPa above the base pressure.

INTRODUCTION

The objective of this contract was to develop and fabricate an initial set of ceramic fiber reinforced, ceramic matrix composite, hot gas candle filters for testing in a simulated pressurized fluidized bed combustion (PFBC) environment. The development of the ceramic composite filter was based on the technology developed and patented at Oak Ridge National Laboratory[1]. The specific objective of the extension to the original development contract being reported here was to test a second set of ceramic composite, hot gas candle filters in a simulated PFBC environment at Westinghouse Science and Technology Center.

The initial use for these ceramic composite, hot gas candle filters is to remove hot particulate material from PFBC and integrated gasification combined cycle (IGCC) power plant processes[2]. In these environments the filters are subjected to temperatures of 850 C and higher in operating pressures of about 1013 kPa (10 atmospheres) while filtering fine ash particulate. The filters are repeatedly cleaned and therefore thermal shocked by a "back flush" with a room temperature air pulse. The atmosphere can be either reducing or oxidizing depending upon the process. In addition, the PFBC and IGCC processes can have environmental conditions in the system which are corrosive to some of the ceramic materials used in various manufacturer's filters.

The use of ceramic fiber reinforced, ceramic matrix composite, hot gas candle filters brings a number of benefits to the filtering system. These include:

- light weight.
- a balance of toughness and strength.
- good thermal mechanical properties at high temperature.
- excellent thermal shock resistance.
- thin filter walls with higher permeability.
- capability to retro fit into existing filter holders.

From May 1992 to June 1993 R&D on the ceramic composite technology was completed and four full scale filters were fabricated[3,4]. Two of the ceramic fiber reinforced hot gas candle filters were tested for 100 hours in a simulated PFBC test at Westinghouse Science and Technology Center. The Westinghouse test showed that a workable filter surface on a strong substrate had been developed. The test also pointed out several weak points in the filter construction. The first of the two main points which

required further work was the chemical vapor infiltration (CVI), bonding of the filter surface to the intermediate layer and substrate, which had been suspect during the filter fabrication. The second point was reinforcing the seal flange to permit forming a tighter seal. Both ceramic composite filters survived the thermal transients as would be expected of a composite filter construction versus the thermal and mechanical problems monolithic materials can suffer.

With these promising results a second, longer simulated PFBC test was proposed and approved to test six improved ceramic composite, hot gas candle filters. 3M improved the fabrication process and the construction of each of the filter's layers and then fabricated twelve additional filters. Six of these were tested in December, 1993[5]. An as fabricated and a tested 3M Ceramic Composite Filter, type 203, are shown in Figure 1.

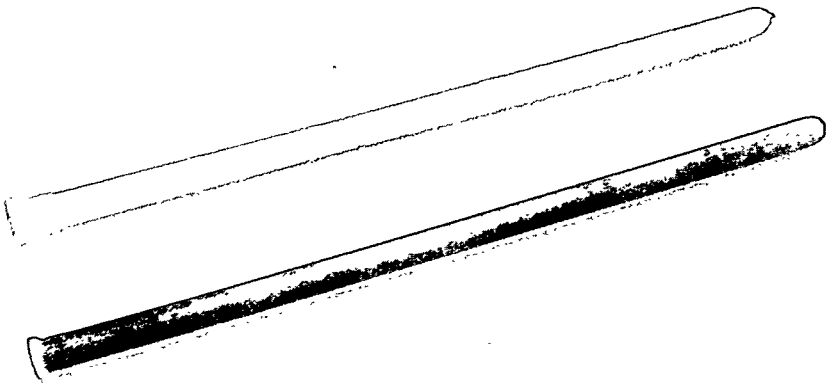

Figure 1. 3M Ceramic Composite Filter, type 203.

WESTINGHOUSE FILTER TEST CONDITIONS

The six hot gas candle filters were tested at the Westinghouse Science and Technology Center's high temperature, high pressure test facility to measure filter cleanability and operating characteristics at PFBC conditions. The filters were mounted in a standard monolithic candle filter holder. Prior to mounting the filters the pressure drop of each was measured at room temperature as a function of

equivalent face velocity by flowing air into the top of the filter through a seal. After mounting the filters and closing the test system the filter pressure drop was determined at various face velocities at both room temperature and at operating temperature.

The test was setup for 175 hours at a filter temperature of 815 - 830C (1500 to 1525 F) with a system operating pressure of 690 to 860 kPa (100 to 125 psig) using the Old and Red Grimethorpe ashes from the Grimethorpe PFBC. The inlet gas flow had an ash concentration of 2000 ppm. The air flow rate was 499 kgm/hr (1100 lb/hr) with a filter face velocity of 3.55 cm/sec (7 ft/min). Cleaning pulses were triggered when the differential pressure from ash cake buildup reached 7.5 to 9.5 kPa (1.1 to 1.4 psi). The cleaning pulses were 0.4 second duration pulses from a pressure tank at 2068 kPa (300 psig). The test was run on a 12 hour day schedule for the first three days and then run 24 hours per day until finished. Air samples were taken from the clean side of the chamber through high efficiency filter paper at various times throughout the filter test to calculate clean side ash concentration.

During the change over from the Old Grimethorpe ash to the Red Grimethorpe ash 14 turbine trip simulations were run to subject the filters to the thermal shocks typical of a system trip or fast shutdown. These involved shutting off the gas burner and decreasing the air flow to zero in steps to cause rapid cooling of the filters. The air flow and gas burner were then restarted to rapidly bring the temperature back to operating conditions.

FILTER TEST RESULTS

The individual ceramic composite filter pressure drops as a function of face velocity, 0.199 kPa (0.03 psi), were about half a typical monolithic ceramic filter element[6]. The pressure drop measurements in the test system were 1.9 kPa (0.28 psi) at a face velocity of 3.3 cm/sec (6.55 ft/min) at room temperature and 2.5 kPa (0.37 psi) at a face velocity of 3.5 cm/sec (6.93 ft/min) at 815 C (1500 F). The system measurements are higher than the individual filters because they represent the total test system of filters, holders, plenum and pulse system.

According to Westinghouse personnel, typical Delta-P values for ceramic candle filters are 0.99 to 3.5 kPa (0.14 to 0.51 psi) for new filters and 1.99 to 6.96 kPa (0.29 to 1 psi) for used filters at 843 C (1550 F) and a face velocity of 3.55 cm/sec (7 ft/min).

The filters were pulse cleaned approximately every two and a third hours while using the Old Grimethorpe ash for a total of 49 pulses. The filters were pulse cleaned every one and a third hours using the Red Grimethorpe ash for a total of 30 pulses.

Thirty four clean side ash concentration samples were taken during the test with sampling times ranging from 30 minutes to 5 hours for a total of about 100 hours of sampling. The average value was 2.5 ppm with one early sample at 6.49 ppm and the remainder below 4 ppm. The clean side ash concentration is shown in Figure 2. The clean side sampling did not indicate any seal leakage occurring. The maximum ash concentration allowed on the system clean side in order to protect the turbines is 10 ppm.

Using filter face velocity, a measure of the gas flow through the filters, Westinghouse calculated a relative filter permeability, which is a ratio of the filter's permeability at a point in the test to its initial permeability. The relative permeability is plotted versus the cleaning cycles in Figure 3. The graph shows an equilibrium being achieved at about 50 cleaning cycles. This would indicate the filters were well conditioned and working in a relatively constant ash buildup and pulse clean cycle. This consistent ash buildup and pulse cleaning cycling continues after the thermal transient tests also. When the test chamber was opened the six filters had a uniform, approximately 1.5 mm thick ash coating on the filter surfaces as would be expected of a functioning set of hot gas filters.

During the thermal transients run at the end of the Old Grimethorpe ash filtering cycles the chamber inlet temperature dropped from the operating temperature of 815 C (1500 F) to the range of 315 to 426 C (600 to 800 F). These drops occurred in about 4 to 5 minute periods which gave an average rate of 98 C/min (177 F/min). No thermocouples were available in a position to record the filters exact temperature change. All six filters survived the thermal transients intact as would be expected of a ceramic composite filter construction versus the thermal and mechanical problems monolithic materials can suffer in these conditions.

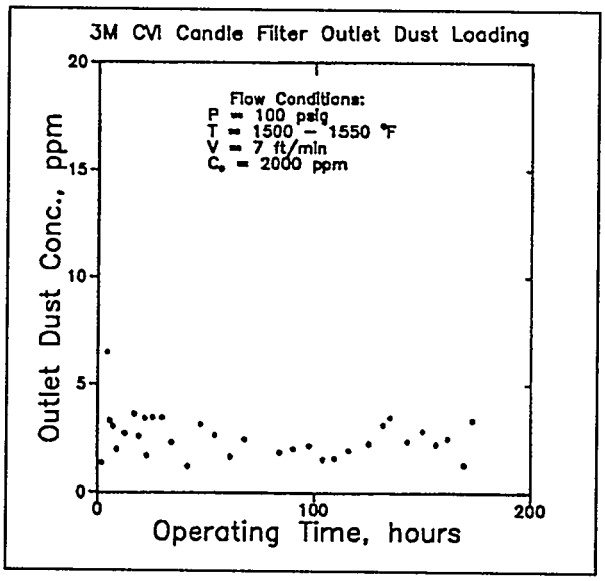

Figure 2. PFBC filter test outlet ash concentration.

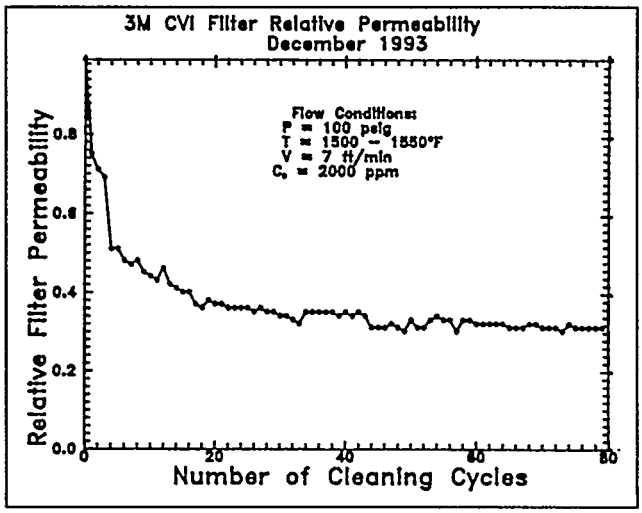

Figure 3. PFBC filter test relative permeability.

PHYSICAL PROPERTY TESTING

The 3M Ceramic Composite Filters were tested to determine their mechanical properties. These composite properties differ significantly from traditional ceramics in that ceramic composites have a graceful failure mode. This means that even with lower ultimate strengths, the ceramic composites may well have higher durability in use because of their ability to carry a load even after cracking begins.

Mechanical properties of the ceramic composite candle filters were determined in three different ways. Two of these tests are well known, "traditional" physical tests: o-ring diametral compression and cylindrical tube longitudinal tension.[7] The third consisted of a real world object based test: flange deflection or bend testing. This test was intended to simulate ash bridging between filters in a PFBC power plant.

O-Ring Diametral Compression Test

The goal was to compare mechanical properties of o-rings from as fabricated filter tube samples and from the filters tested at WSTC. One inch wide o-ring sections were compressed between two 5" diameter plates while a Sintech model 10/D materials testing workstation recorded the load vs. displacement data. All samples were tested at a constant crosshead speed of 2.0 mm/min. Figure 4 shows two sets of curves: the top set are from as fabricated filters while the bottom set are the filters that were tested for

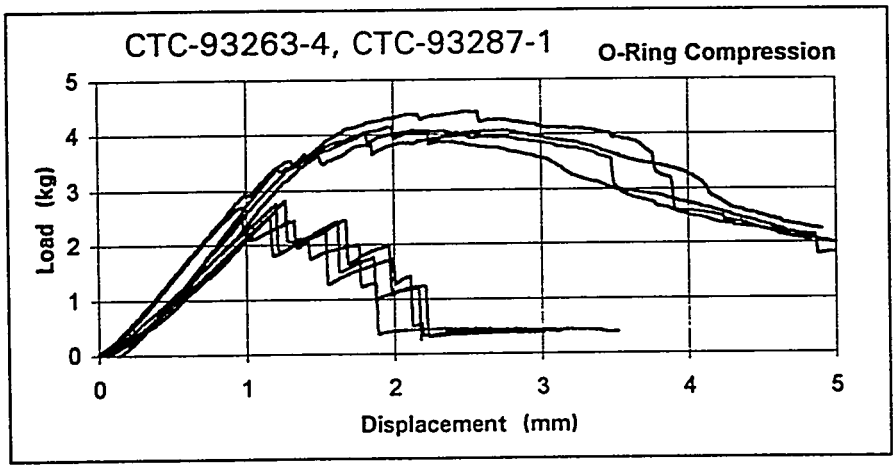

Figure 4. O-Ring compression of as fabricated and filter tested samples.

172 hours at WSTC. As the graph shows, the tested filters retained ~70% of their initial peak load strength while maintaining the same stiffness.

Tube Longitudinal Tension Test

As fabricated filter tube sections, 5" long, were tensile tested. Pipefittings were epoxied into both ends of the filter tube section as a means of mounting the sample. Loading plugs were then threaded into the pipe fittings and attached to the test machine using u-joints to allow for positioning. The Sintech 10/D workstation again recorded the load vs. displacement data. All samples were tested at a constant crosshead speed of 1.0 mm/min. Figure 5 shows typical load displacement curves for as fabricated filters.

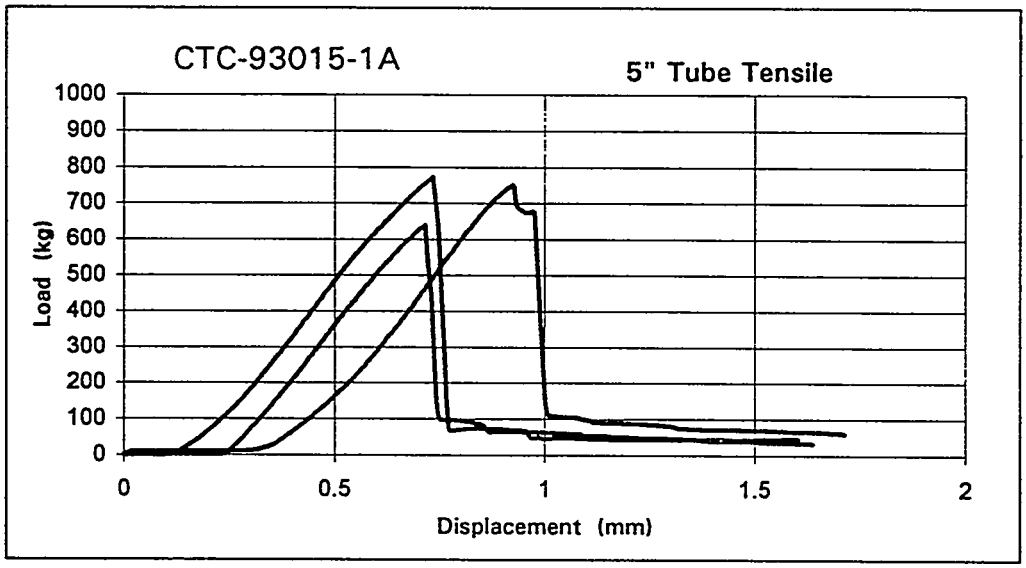

Figure 5. Longitudinal tensile test of as fabricated filter tubes.

Flange Displacement Testing

The purpose of this test was to simulate test the real world filter deflections that occur in a filter system due to problems like ash bridging. Candle filters were cut off 8" from the top of the flange. A pipefitting was epoxied into the end opposite the flange, and a flat loading fixture was threaded into the pipe fitting. The Sintech 10/D workstation again records the load vs. displacement data. All samples

were tested at a constant crosshead speed of 2.0 mm/min. Figure 6 shows a typical load displacement curve for an as fabricated candle filter. It should be noted that at ~8mm the filter comes into contact with the male mounting collar which starts to cut into the filter. At the end of this test no damage was observed at the flange, and the cut in the side wall of the filter did not cause complete failure. Note that a 35mm deflection of an 8" long filter section corresponds to a deflection of 263mm (10.4") at the tip of a full size 60" long filter.

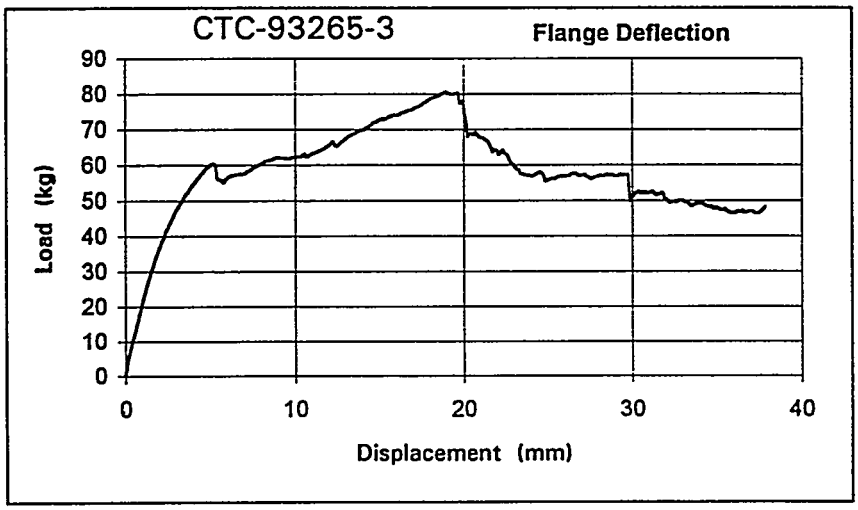

Figure 6. Deflection of as fabricated filter flange in filter tubesheet mounting.

CONCLUSIONS

Ceramic composite hot gas candle filters have been fabricated and tested in a simulated PFBC environment at Westinghouse Science and Technology Center. The WSTC test showed that a workable filter surface on a strong substrate that can withstand system thermal shocks has been developed. Completion of these 172 hours of simulated PFBC testing and thermal transients plus maintaining less than 4 ppm clean side ash concentration provide a basis for moving to the next step of testing in a real PFBC system. This real PFBC environment would provide a test of long term exposure and corrosion effects.

As shown above, the 3M Ceramic Composite filter does show fiber reinforced ceramic composite behavior, most notably in the o-ring compression and the flange bend tests. What is significant from all three tests is that even after mechanical "failure" each test sample remains intact and holds its initial

shape. This suggests that the SiC matrix fails but the fibers remain continuous. This ability to continue to carry a load and resistance to catastrophic failure after physical damage is a key feature of a ceramic composite product. In a working environment these composite properties could provide the time for a controlled shutdown.

ACKNOWLEDGMENTS

This research was sponsored by the U. S. Department of Energy, Office of Fossil Energy, Martin Marietta Energy Systems, Inc., Oak Ridge National Laboratory, and 3M Company. The assistance of D. J. Pysher, M. G. Simpson, C. T. Coffin, G. M. Tsugawa, E. M. Fischer, all of 3M; D. P. Stinton of Oak Ridge National Laboratory, and T. E. Lippert, E. E. Smeltzer, G. N. Schneider, W. R. Kuba, and A. W. Fellers, all of Westinghouse is gratefully acknowledged.

REFERENCES

1. D. P. Stinton, R. A. Lowden, and Ramsey Chang, Fabrication of Fiber-Reinforced Hot-Gas Filters by CVD Techniques, Ceramic Engineering & Science Proceedings, vol 9, no. 9-10, p. 1233-1244, 1988.

2. T. E. Lippert, M. A. Alvin, D. M. Bachovchin, G. B. Haldipur, R. A. Newby, and E. E. Smelzer, Development and Commercialization of Hot Gas Filtration Systems, In Proceedings of 1991 International Conference on Fluidized Bed Combustion, Montreal, Canada, 1073-1080, April 21-24, 1991. ASME, NY, NY.

3. R. G. Smith, Fabrication of Commercial-Scale Fiber-Reinforced Hot Gas Filters by Chemical Vapor Deposition, Semiannual Progress Report on subcontract No. 93X-SB482C with Martin Marietta Energy Systems, Inc., Oct. 1992.

4. L. R. White, Fabrication of Commercial-Scale Fiber-Reinforced Hot Gas Filters by Chemical Vapor Deposition, Final Progress Report on subcontract No. 93X-SB482C with Martin Marietta Energy Systems, Inc., Jan. 1992.

5. R. G. Smith and J. H. Eaton, Fabrication of Commercial-Scale Fiber-Reinforced Hot Gas Filters by Chemical Vapor Deposition, Final Technical Report on subcontract No. 93X-SB482C with Martin Marietta Energy Systems, Inc., April, 1994.

6. E. E. Smeltzer, 3M CVI Hot Gas Candle Filter Test Program, Test under General Order No. MP-12775-CE for 3M Company, Jan. 27, 1994.

7. Prediction of the Strength of Ceramic Tubular Components: Part 1 - Analysis, O. M. Jadaan, D. L. Shelleman, J. C. Conway, Jr., J. J. Mecholsky, Jr., and R. E. Tressler, Journal of Testing and Evaluation, Vol 19, No. 3, May 1991, p 181 - 191.

ADVANCED ELECTROLYTES AND SYNTHESIS OF ADVANCED CATALYSTS AND MEMBRANE MATERIALS

T. R. Armstrong, J. L. Bates, G. W. Coffey, J. J. Kingsley, L. R. Pederson, J. W. Stevenson, W. J. Weber, and G. E. Youngblood

Pacific Northwest Laboratory[1]
P.O. Box 999
Richland, WA 99352

ABSTRACT

Mixed conductors in the lanthanum strontium cobalt chromium iron oxide system and protonic conductors in the strontium ytterbium cerate system are being evaluated for possible use in gas separation and purification, as electrolytes and electrodes in solid oxide fuel cells, and as sensors. Recent activities include materials synthesis, sintering behavior studies and microstructural characterization, development of methods to prepare novel shapes, electrical property characterization, and permeation testing.

Single-phase LaSrCoCrFe oxides, being investigated for use as dense oxygen separation membranes, have been prepared by combustion methods. Sintering conditions were developed to obtain full density. The addition of up to 10 mole percent chromium, intended to improve the stability in a reducing environment, also significantly enhanced densification via liquid phase sintering. Compositions having a high A-site strontium content (80% or greater) were susceptible to internal cracking during cooling, due to large changes in oxygen stoichiometry. These are highly (mixed) conductive materials, with activation energies for conduction in the 0.08 to 0.17 eV range and conductivities to more than 500 S/cm. Passive oxygen fluxes varied with temperature, composition, and the oxygen concentration gradient. At 1000°C, high purity oxygen fluxes in excess of 1 sccm/cm^2 surface area of the membrane were observed.

Protonic conductivity in the strontium ytterbium cerates was shown to have a large grain boundary component. Protonic conductivity in these materials requires the presence of water, which reacts with oxygen vacancies to yield hydroxyl groups that support proton conduction. Transference numbers were determined for protons, oxygen ions, and electrons as a function of temperature. Protonic conduction dominated in hydrated cerates up to 450°C. At higher temperatures, oxygen ion and electronic conductivity became progressively more important. Hydrogen could be pumped across the cerate membrane by applying a dc voltage. At 800°C, pure hydrogen fluxes greater than 1 sccm/cm^2 could be driven across the membrane.

INTRODUCTION

Because of attractive potential applications, mixed conductors in the lanthanum strontium cobalt chromium iron oxide system and protonic conductors in the strontium ytterbium cerate system are being studied. Mixed conductors, materials that conduct both ions and electrons, are

---

[1] Operated by Battelle Memorial Institute for the U. S. Department of Energy under Contract DE-AC06-76RLO 1830.

potentially useful as semipermeable membranes in gas separation, as electrodes in solid oxide fuel cells, and as membrane reactors. Protonic conductors can be used as electrolytes in solid oxide fuel cells, as hydrogen sensors, in gas purification systems, and in steam electrolyzers.

Perovskites in the $La_{1-x}Sr_xCo_{1-y}Fe_yO_{3-z}$ are mixed-conducting oxides that exhibit high p-type electronic conductivity.[1-3] Even though the contribution of oxygen ion conductivity to the total conductivity is often quite small (less than one percent), the magnitude of oxygen ion conduction can be quite large. At 800°C, oxygen conductivities of $La_{1-x}Sr_xCo_{0.8}Fe_{0.2}O_{3-z}$ perovskites have been found to be as much as 100 times larger than obtained for yttria-stabilized zirconia.[1-2] Ionic conductivity is favored by extensive substitution of Sr^{2+} for La^{3+} in these materials, which leads to oxygen vacancy formation.

The use of these mixed conductors in practical applications requires compositions and structures that provide maximum mass transport rates as well as good mechanical and chemical stability. Highly substituted perovskites in this system, which often give the highest conductivities, also may become unstable and decompose.[3] Instability has been found to be a significant problem for $SrCo_{0.8}Fe_{0.2}O_x$ perovskites when used as a membrane reactor for the partial oxidation of natural gas.[4] These ceramics tended to fracture as a result of an approximately 2 percent increase in the lattice volume for the inner wall exposed to a reducing environment relative to the outer wall that was exposed to air. Such volume changes are less of a concern when such materials are used for oxygen separation applications.

Although proton conduction in inorganic solids was first reported more than two decades ago,[5] only the ABO_3-type perovskites have been shown to be sufficiently stable under conditions of high temperature and both oxidizing and reducing environments needed for practical applications such as solid electrolytes in solid oxide fuel cells.[6,7] Sites for proton conduction are believed to be created when water reacts with oxygen vacancies. Oxygen ion and electronic conduction also occur, becoming progressively more important at elevated temperatures.[6-8]

(LaSr)(CoCrFe) OXIDE OXYGEN SEPARATION MEMBRANES

To date, this study has focused on four compositions in the $La_{1-x}Sr_xCo_{1-y}Fe_yO_{3-z}$ system: $La_{0.6}Sr_{0.4}Co_{0.2}Fe_{0.8}O_3$, $La_{0.6}Sr_{0.4}Co_{0.1}Cr_{0.1}Fe_{0.8}O_3$, $La_{0.2}Sr_{0.8}Co_{0.2}Fe_{0.8}O_3$, and $La_{0.2}Sr_{0.8}Co_{0.1}Cr_{0.1}Fe_{0.8}O_3$. These compositions are designated 6428, 64118, 2828, and 28118, respectively. A modified version of the glycine-nitrate combustion process[9] was used to synthesize the required powders. Following calcination in air at 850° C for 12 hours, phase-pure perovskite powders were obtained. Relative sintered densities greater than 90% were obtained for all four compositions using sintering temperatures in the range 1200-1250° C. Under identical sintering conditions, compositions containing Cr (i.e., 64118, 28118) exhibited higher sintered

densities than the corresponding compositions without Cr (i.e., 6428, 2828). This enhancement in densification may result from the formation of a liquid phase, possibly $SrCrO_4$, during the sintering process. A similar explanation has been proposed to explain the sintering behavior of Sr doped lanthanum chromite.[10]

Grain sizes for sintered specimens tended to increase with increasing Sr content and to decrease with the addition of Cr. The average grain sizes for specimens sintered in air at 1200° C for 2 hours were 2.3, 0.9, 1.0, and 0.3 μm for 2828, 6428, 28118, and 64118, respectively. While high densities were readily obtained for the high Sr compositions (2828, 28118), it was observed that sintered compacts of these compositions tended to have extensive internal cracking.

Measurements of electrical conductivity as a function of temperature were performed in air on two compositions, 6428 and 64118, using a four-point DC technique. Over the temperature range 25-1100° C, these compositions exhibited maximum conductivities of 400 and 210 S/cm at 540 and 635° C, respectively (See Figure 1). Even though they are excellent ionic conductors, the ionic conduction is masked by the electronic component when measuring overall electrical behavior. In the lower temperature regime, the conductivity was thermally activated; activation energies were 0.08 and 0.17 eV for 6428 and 64118, respectively. These energies are consistent with a small polaron (i.e., localized electronic carrier) conduction mechanism. At higher temperatures, the conductivity decreased with increasing temperature. The explanation for this decrease may lie in the fact that compositions in the $(La,Sr)(Co,Cr,Fe)O_3$ have been reported as experiencing substantial decreases in their oxygen stoichiometry at elevated temperatures.[11] Since these materials are p-type electronic conductors, it is expected that the removal of lattice oxygen would result in the elimination of electron holes according to the defect equation:

$$2h^{\cdot} + O_O^x \Rightarrow V_{\ddot{O}} + \tfrac{1}{2}O_2 \qquad (1).$$

Thus, a decreasing oxygen stoichiometry with increasing temperature would result in a decreasing concentration of electronic carriers (electron holes), causing the conductivity to decrease. From the above equation, it is also clear that the concentration of ionic carriers (oxygen vacancies) should be increasing with increasing temperature, so that the ionic conductivity may increase significantly with increasing temperature, due not only to increasing carrier mobility (ionic mobility is thermally activated) but also to an increasing carrier concentration.

When dense materials are placed in an oxygen chemical potential gradient, a driving force exists to transport oxygen from the high $P(O_2)$ side to the low $P(O_2)$ side. Mixed conducting materials will respond to this driving force by spontaneously reducing gaseous oxygen to anionic oxygen at the high $P(O_2)$ surface, transporting the anionic oxygen through the material via a lattice vacancy mechanism, and oxidizing the anionic oxygen to gaseous oxygen at the low $P(O_2)$

surface. Passive (no applied electric field) measurements of oxygen flux through 2.5 mm thick sintered specimens were obtained using an O_2 (1 atm.)/N_2 (1 atm.) gradient. At 925° C, O_2 fluxes were approx. 0.24 and 0.10 sccm/cm^2 for 6428 and 64118, respectively. As expected, reducing the magnitude of the gradient resulted in decreased O_2 flux. The oxygen flux was highly dependent on temperature (see Figure 2) as would be expected because diffusion of ions in an ionic solid is thermally activated. However, an increasing oxygen vacancy concentration at higher temperatures may also play a significant role. From the flux measurements, it was possible to calculate values for the ionic conductivity. For 6428 at 925°C, the ionic conductivity was 0.215 S/cm, which, when considered with the overall conductivity, corresponds to an ionic transport number of approx. 9.1 x 10^{-4}.

The successful utilization of mixed conducting oxides in oxygen separation applications depends not only on the optimization of materials but also on the development of suitable means to fabricate those materials into appropriate structures, e.g., flat plates, open-end tubes, or closed-end tubes. Several conventional fabrication techniques, including tape casting and cold isostatic pressing, are currently being explored. In addition, a newer technique, tape calendering, is being investigated. In tape calendering of ceramics, the ceramic powders, binders, and plasticizers are mixed together in a high-shear mixer. During the mixing process, the binder-plasticizer system is softened by externally heating the mixing chamber. This softened binder system mixes with the ceramic powder to yield a readily deformable mass, which is then calendered into a thin, flat tape using a two-roll mill with counter rotating rolls. The thickness of the tape is controlled by adjusting the spacing of the two rolls. The resulting tape is flexible and can be laminated or formed before firing. Calendering offers several advantages. The calendering process is solvent-free, so environmental concerns and batch costs are reduced. Since calendered tapes can be readily laminated together by co-calendering individual tapes, calendering is particularly appropriate for fabrication of multi-layer structures.

Calendered tapes containing 6428 have been fabricated and sintered to relative densities greater than 95%. Also, bilayer tapes have been fabricated by co-calendering two 6428 tapes, one of which contained an organic pore forming material. After sintering, the final structure consisted of a thin (approx. 15 μm thick) dense layer of 6428 on a thick (approx. 400 μm thick) porous support layer of 6428 (See Figure 3). The ability to fabricate thin, dense membranes is essential in order to obtain high flux magnitudes; the calendering technique allows these membranes to be co-fabricated on porous support structures having the same composition as the membranes themselves, thereby minimizing problems associated with chemical interaction and mismatch of sintering shrinkage and thermal expansion.

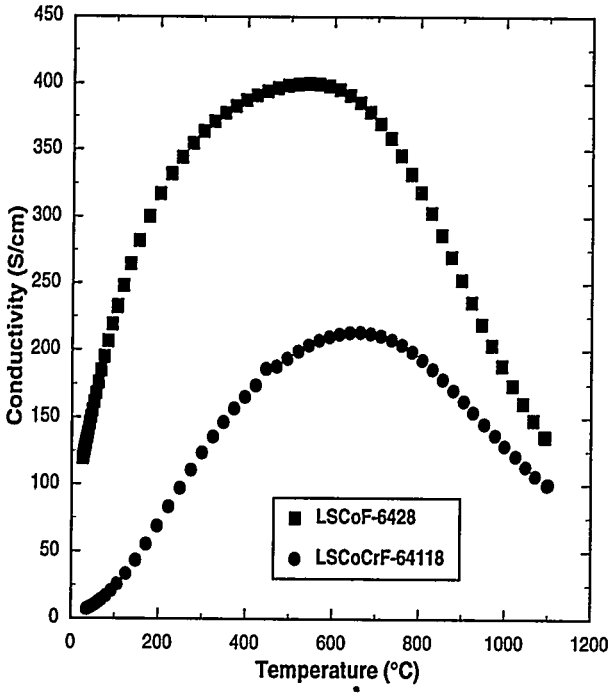

Fig. 1. Electrical Conductivity vs. Temperature.

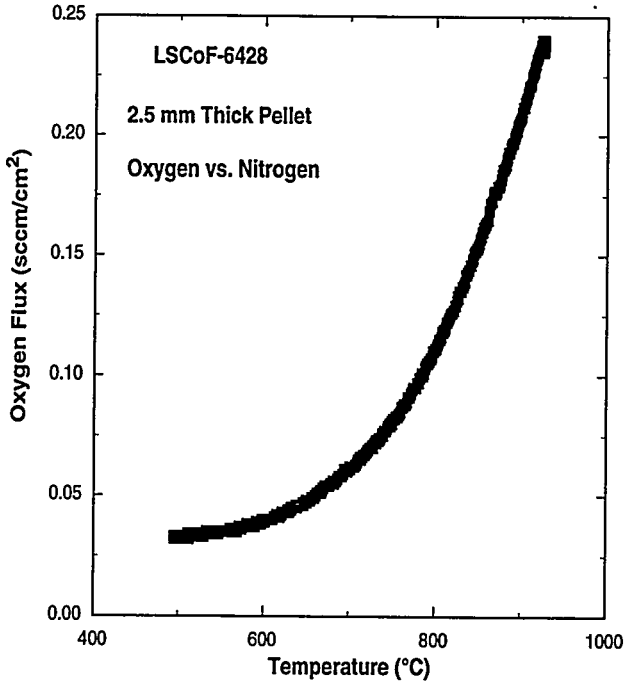

Fig. 2. Passive Oxygen Flux through LSCoF-6428; Oxygen vs. Nitrogen.

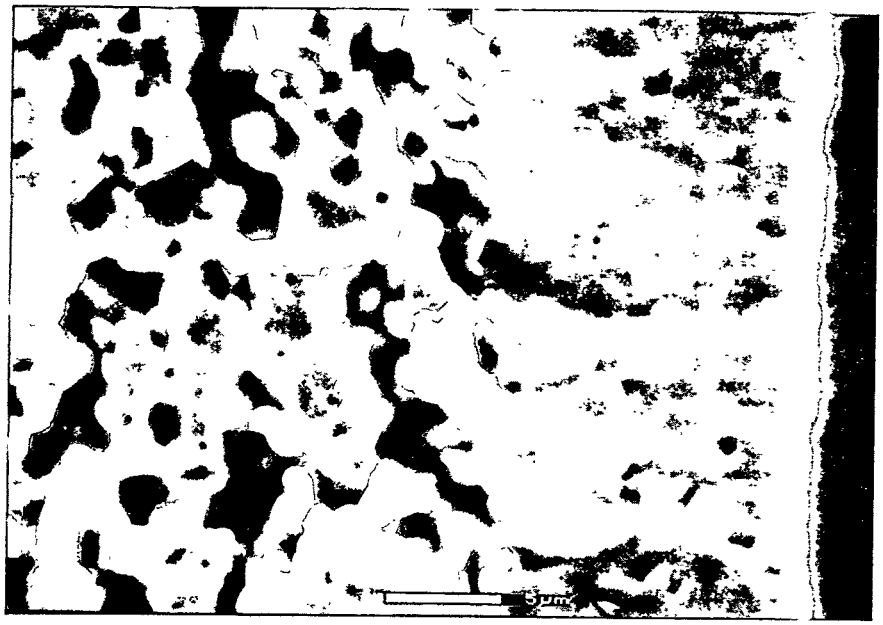

Figure 3. Sintered La0.6Sr0.4Co0.2Fe0.8O3 bilayer structure prepared by calendering.

PROTONIC CONDUCTION IN SrYbCe OXIDES

Fine and homogenous $SrCe_{1-x}M_xO_{3-\alpha}$ (M=dopant ions) perovskite powders were prepared by calcination of combustion derived precursors at <950°C. The precursors of these perovskites were obtained using exothermic redox decomposition of mixtures containing strontium acetate, ceric ammonium nitrate, ytterbium nitrate and glycine at 250°C. The perovskite powders prepared by this technique have been sintered to about 98% theoretical density at 1500°C in 12 hrs.

Four-point conductivities were determined in both dry air and in water-saturated air in the approximate temperature range of 400 to 800°C. Experimental results were fit to the expression:

$$\sigma T = C \exp(-E/kt) \qquad (2),$$

where the pre-exponential, C, is a charge carrier density and material-dependent constant, E is the total activation energy for ionic and electronic migration, k is the Boltzmann constant, and T is the absolute temperature. Activation energies and pre-exponentials determined from the conductivity data are given in Table 1. Based on these results and the data of Scherban and Nowick,[12] the optimal concentration of Yb dopant may be x=0.05 for the $SrCe_{1-x}M_xO_{3-\alpha}$ system. Overall conductivities are slightly higher than obtained previously,[12] which is attributed to higher sintered densities achieved in the present study.

Table 1. Activation Energies, E, and Pre-Exponentials, C, for Conductivity of $SrCe_{1-x}Yb_xO_{3-\alpha}$ Measured in Dry Air and Water-Saturated Air

Atmosphere	Yb Content	E(eV)	C (S/cm)
dry air	x=0.05	0.79	3.3×10^4
water-saturated	x=0.05	0.62	3.4×10^3
dry air	x=0.10	0.85	7.0×10^4
water-saturated	x=0.10	0.64	3.8×10^3
dry air	x=0.15	0.88	3.6×10^4
water-saturated	x=0.15	0.67	2.7×10^3

Transference numbers as a function of temperature were determined by the emf response to known hydrogen and oxygen gradients. Hydrogen ion conduction accounted for essentially all of the conductivity below 400°C, as shown in Figure 4. Above that temperature, oxygen ion and electronic conduction, by inference, grew progressively more important. These results are consistent with those reported previously by Scherban and Nowick.[12]

The kinetics of water uptake by $SrCe_{0.95}Yb_{0.05}O_{3-\alpha}$ was studied over a wide range of temperatures and water partial pressures using thermogravimetry. Water adsorption typically

followed a two-stage process, as is shown in Figure 5. The first, rapid uptake stage is attributed to hydration of the grain boundaries, whereas the much slower, long-term hydration is attributed to hydration of the bulk grains, which averaged 15 μ in diameter in these fully dense samples. In previous studies of water uptake by the cerates, complete hydration of the bulk was reported be reached within a few hours at temperatures even below 600°C; no contribution from grain boundaries was recognized.[6] Changes in resistance as a function of time following introduction of water followed similar trends to water uptake kinetics, indicating that grain boundaries contribute substantially to the observed conductivity. Protonic conductivity from grain boundary phases in the barium cerates have been observed previously, and attributed to a separate grain boundary phase.[13] In the strontium cerates, no microscopic evidence for a grain boundary phase or segregation could be found.

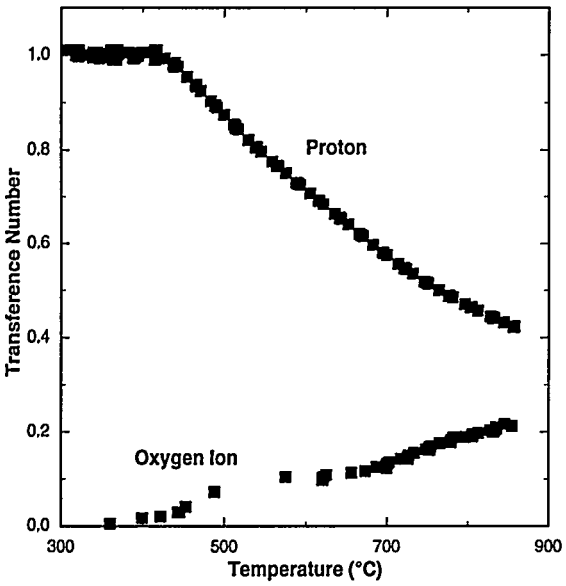

Fig. 4. Transference numbers as a function of temperature for $SrCe_{0.95}Yb_{0.05}O_3$.

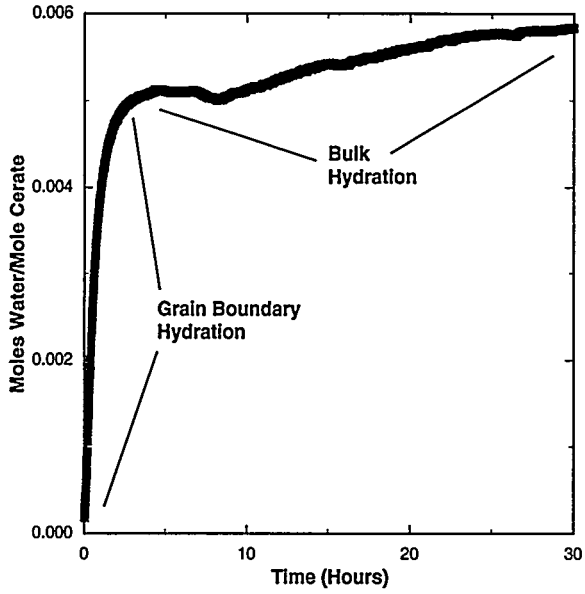

Fig. 5. Kinetics of water uptake at 800° C. for $SrCe_{0.95}Yb_{0.05}O_3$ by thermogravimetry.

By applying a voltage across the $SrCe_{0.95}Yb_{0.05}O_{3-\alpha}$ sample, hydrogen could be pumped through the electrolyte, even at high temperatures where the transference number for hydrogen was smaller than 0.5. Hydrogen flux rates greater than 1 sccm/cm^2 could be pumped through a 2 mm thick disk at 800°C. Introduction of deuterium oxide in the place of water resulted in deuterium labelling of the molecular hydrogen product, even at temperatures too low to result in bulk phase hydration. This behavior again is consistent with grain boundaries contributing a significant share of the total protonic current.

In summary, fully dense, phase-pure $SrCe_{0.95}Yb_{0.05}O_{3-\alpha}$ has been prepared, which is suitable for use as a proton-conducting electrolyte, as a hydrogen pump, and as a hydrogen sensor. Thermogravimetric, permeation, and electrical property characterization results are consistent with the conclusion that the grain boundaries contribute substantially to the protonic current in these materials.

REFERENCES

1. Y. Teraoka, H. M. Zhang, K. Okamoto, and N. Yamazoe, Mater. Res. Bull. 23, 51 (1988).

2. Y. Teraoka, T. Nobunga, K. Okamoto, N. Miura, and N. Yamazoe, Solid State Ionics 48, 207 (1991).

3. W. L. Worrell, Solid State Ionics 52, 147 (1992).

4. U. Balachandran, S. L. Morissette, J. J. Picciolo, J. T. Dusek, and R. B. Poeppel, Proc. 1992 International Gas Research Conference, IGRC 92, CONF-921152-5, 1992.

5. S. Stotz and C. Wagner, Berichte Bunsengesellschaft 70, 781 (1966).

6. H. Iwahara, Solid State Ionics 52, 99 (1992).

7. N. Bonanos, Solid State Ionics 53-56, 967 (1992).

8. J. F. Liu and A. S. Nowick, Solid State Ionics 50, 131 (1992).

9. L.A. Chick, L.R. Pederson, G.D. Maupin, J.L. Bates, L.E. Thomas, and G.J. Exarhos, Materials Letters 10, 6-12 (1990).

10. L.A. Chick, J.L. Bates, L.R. Pederson, and H.E. Kissinger,Proc. 1st Intl. Symp. on Solid Oxide Fuel Cells, Ed. S.C. Singhal, Electrochem. Soc., Proc. Vol. 89-11, 170-187 (1989).

11. L. Tai, M. Nasrallah, and H. Anderson,Proc. 3rd Intl. Symp. on Solid Oxide Fuel Cells, Ed. S. Singhal and H. Iwahara, Electrochem. Soc., Proc. Vol. 93-4, 241-251 (1993).

12. T. Scherban and A. S. Nowick, Solid State Ionics 35, 189 (1989).

13. K. D. Kruer, E. Schonherr, and J. Maier, 14th Riso International Symposium on Materials Science, eds. F.W. Poulson, J.J. Bentzen, T. Jacobsen, E. Skou, and M.L.J. Ostergard, Riso National Lab., Roskilde, Denmark, 1993, p. 297.